CONSORZIO RFX
Ricerca Formazione Innovazione

Activity Report 2018

1. Introduction

This Report describes the activities and the results obtained in the year 2018, developed along the guidelines of the 2018 Activity Programme approved by the Consorzio RFX partners meeting held on 29 November 2017.

In 2018 a fundamental milestone for the Neutral Beam Injectors for ITER was achieved: in mid-May SPIDER went into operation and on 6 June 2018 the first plasma was obtained. The set of implemented diagnostics allowed to characterize the source over a wide range of operational parameters. Some problems have been highlighted: the first one was the Grounded Grid segments of the beam source that was found to be non-conform in terms of vacuum sealing of the hydraulic circuit; moreover SPIDER operation exhibits several occurrences of breakdown outside the plasma chamber. Corrective actions are under way.

In parallel, PRIMA and MITICA activities continued. PRIMA infrastructures realization is going on and several agreements have been signed for the Transfer for Use of plants to Consorzio (in particular for SPIDER systems). As for the of the cooling plant components damaged in the November 2017 flooding, the final technical solution for their recovery has been agreed. In the meantime the system has been used in a temporary setup to allow SPIDER operation. The realization of MITICA power supplies and other auxiliary plant systems proceeded, and the insulation test up to 1.2MV of the transmission line has been successfully completed. In November the MITICA Beam Source procurement has been assigned by F4E with the support of the NBTF team. Hence, all the contracts for procurement of MITICA components are now active. In support of SPIDER and MITICA, the physics of NBI has been studied in the side facilities operating at Consorzio (HVTF, RF laboratory and CATS) and by modelling activities.

The contribution to the ITER project continued also with modelling of disruption scenarios, supported by experimental data from JET and ASDEX Upgrade, and with involvement in the development of the ITER diagnostics Core Thomson scattering and Magnetic Sensors.

The allocation of the funds for the upgrade of RFX-mod in the framework of the POR-FESR 2014-2020 gave start to the realization of the modified RFX-mod magnetic front-end. The main activities have been the design of the modification of the Vacuum Vessel, the Stabilizing Shell and the First Wall (accompanied by the assessment of vacuum tightness, error fields and electric insulation issues), and the adaptation or development of the diagnostic systems for the new machine. In September 2018 the Stainless Steel Toroidal Support Structure has been delivered to the company that is in charge of mechanical modifications. In anticipation of the start of RFX-mod2, the research lines for the first experimental campaigns have been drawn, on the basis of the RFX-mod experience and supported by RFX-mod data analysis and RFP modelling activities.

The participation to ITER Physics Work Packages JET1 and MST1 was affected by the postponement of experimental campaigns in JET and MST devices, so that in most cases only some data analysis and preparation of experiments was done. Consorzio RFX support to DTT project was given both under the EUROfusion Work Package DTT1 with modelling activities, and under direct cooperation with the ad interim project. The well-established collaboration with Stellarators continued, both on LHD and W7-X: in the latter the plasma edge insertable probe designed and procured by Consorzio gave the first results. Involvement in the JT60-SA activities included the drafting of the procurement call of two diagnostics, edge Thomson scattering (TS) and VUV divertor survey spectrometer. In late 2018, EUROfusion assigned to Consorzio RFX the responsibility for the procurement of both. Consorzio RFX researchers have been also charged of coordination responsibilities of EUF activities, with 1 person in the PMU, 6 Scientific coordinators and 1 deputy Task Force Leader in JET, 3 Scientific Coordinators, 1 modeling coordinator and 1 deputy task force leader in MST1. Additionally , WPSA has assigned to Consorzio RFX the responsibility for the Modelling Area coordination.

Activities in support of ITER NBI project, Consorzio contribution to DEMO research under PPPT Work Packages, Socio Economical Studies and the industrial and non-fusion related collaborations continued in line with the previous years. The procurement, under the Broader Approach agreement, of the Power Supply system for RWM control was completed and the system was shipped to Japan in September 2018. Unfortunately, some components were damaged during transportation, despite the supervision of the shipment by Consorzio researchers. An investigation of responsibilities is under way.

The education activities continued, primarily by hosting many students during internships, bachelor and master thesis. In 2018 24 master thesis have been developed at Consorzio RFX, 8 PhD have been awarded and 4 new PhD students have been enrolled.

Many communication and outreach activities have been done, such as the production the production of a promo-video on SPIDER-NBTF shown at a large cinema in Padova, reaching a large audience. The most important event in the year has been the ceremony of SPIDER Inauguration in June, attended by about 360 people.

In 2018, 80 papers have been published in International Journals, including 43 papers submitted by partner laboratories. Consorzio RFX researchers attended 24 National and International Workshops and Conferences, with 5 invited and a dozen oral contributions. In total 131 abstracts have been submitted from Consorzio RFX, other 38 from partners. Approximately 100 contributions will be published on Proceedings or Journal Special Issues.

2. ITER Project

2.1. *Activity for the development of Neutral Beam Injectors for ITER*

2018 was a breakthrough year for the project NBTF.

SPIDER went into operation. After a period of hard work in order to complete the installation and integration of the beam source with the rest of SPIDER, the experimental phase began in mid-year, soon crowned by the first experimental results.

Installation, commissioning and SAT of MITICA power supplies and other auxiliary pant systems were well advanced. In July, after completion of the installation of the HV PS components, the first SF6 gas loading tests, the insulation gas of the components operating at 1MV, were carried out, followed shortly by the first 1.2 MV insulation tests. Furthermore, in 2018 the tender for the procurement of the Beam Source, the core of the MITICA experiment, was also awarded after a long negotiation period. In this way, all the contracts for procurement of MITICA components are in progress.

The main activities performed in 2018 can be so summarized:

- Technical support to the F4E procurement contracts of MITICA plant and components
- Support to installation and tests of components procured by JADA and INDA
- Integration activities for installation and tests of SPIDER and MITICA components and management of the interfaces with PRIMA buildings and plants
- Development of MITICA diagnostics, control and protection systems
- Host activities to support on-site works and safety coordination during installation of equipment of F4E and other DAs
- Management and execution of commissioning and integrated tests
- Start of SPIDER experiments with technical support and scientific exploitation managed and performed by NBTF Team and with the contribution from other parties
- Development of physics modelling in support of SPIDER experiments
- Specific R&D activities in support of design and experiments including: experimental campaigns using the HV Test Facility to validate the electrostatic models and study the voltage holding in vacuum; experimental campaigns in the RF laboratory to study and characterize RF circuit properties of plasma sources in preparation of SPIDER

operation; experimental campaigns using the CAesium ovens Test Stand (CATS) to check and optimize the SPIDER Cs Ovens design and operations.

2.1.1. *PRIMA and host activities*

2.1.1.1. Building and auxiliaries

The NBTF building was finished in 2015 and the formal closure of the procurement contract was concluded in 2017. In 2018 only minor procurements and completions were done. In particular:

- completion of auxiliaries of buildings hosting MITICA PS’s and MITICA bunker
- completion of the special sealed and insulating closures of the penetrations of the MITICA HV transmission line in Building 1
- installation and commissioning of fire extinguish systems around MITICA oil transformers (both step-down and step-up)
- fire-proof cable penetration sealing in all NBTF buildings
- smoke filters (special boxes with smoke control produced in the event of a fire are being installed at the transit doors between the various buildings)
- installation and commissioning of the HVAC equipment for HVH (Building 8); a special HVAC able to guarantee the stringent requirements in terms of number of particles for cubic meter in air.

The integration and interface management work was continued to ensure the coherent integration of the experimental devices by monitoring the construction activities and the full 3D CAD model of the facility, including both the infrastructures and the experimental plant systems and injectors.

Finally, in 2018 the design of the concrete door of MITICA bio-shield was performed and the tender process started. This artefact will be realized and installed in 2019.

2.1.1.2. Cooling Plant

Commissioning and site acceptance tests of the SPIDER Plant Unit were completed and the “Provisional transfer of right to use of the SPIDER cooling plant” signed on 9th March 2018, allowed the use of cooling plant during the first SPIDER operations.

A technical solution was identified and finally agreed to solve the issue of recovering the pumps and equipment affected by the flood occurred at the end of November 2017 in Building 2 at level -4.0 m. A temporary solution aimed at making available the cooling plant for the SPIDER integrated commissioning and operation has been installed: it foresees the use of the primary circuits connected to a temporary and simpler secondary circuit. The SPIDER cooling plant was used in local or manual mode.

Technical documents, procedures and schedule for commissioning and acceptance tests of SPIDER and Shared Plant Units were further reviewed and discussed among the Supplier, NBTF Team and F4E, aiming to prepare the final Acceptance Data Package (ADP) for closure of Stage 1, achieved at the end of September 2018.

Transfer for Use of SPIDER Plant Unit was signed on 10th Oct 2018.

In parallel, hydraulic installation works for MITICA Plant Unit was almost completed in 2018 and continuous activities have been carried out by NBTF Team to support, verify and witness the supplier's activities and commissioning tests on-site. In particular, pressure and hydraulic tests on MITICA Primary circuits were carried out. Follow-up for activities on electrical subsystem and control system development/commissioning was guaranteed. Installation of electrical parts and sensors is to be completed and I&C development is presently in progress/review. Pumps and circuits functional tests are on-going, interleaved with the necessary cleaning process.

A team of engineers and technicians was trained for plant operations, tuning and maintenance. Continuous presence and follow-up during the first SPIDER operations was guaranteed, with particular effort for managing issues about water resistivity degradation and the use of off-line Chemical Control System.

The 3D CAD model of cooling circuits was continuously updated by NBTF Team to allow careful integration checks and to give support to the supplier in the preparation of the detailed drawings of the cooling circuits.

Fig. 2.1 Overall view of SPIDER, MITICA and Shared Plant Units inside Building 2

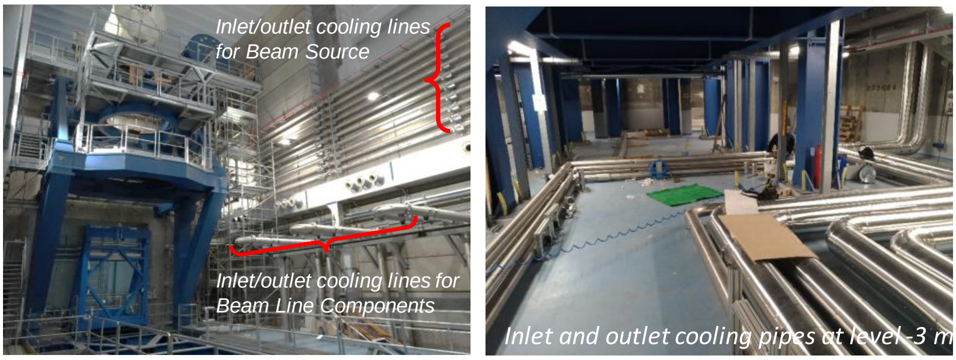

Fig. 2.2 Cooling pipes inside the MITICA Neutron Shield

Overall views of pipes, pumps, heat exchangers and Chemical Control System inside Building 2 are shown in Fig. 2.1. Pictures of pipes installed inside the MITICA Neutron Shield at different levels are presented in Fig. 2.2.

2.1.1.3. Vacuum, gas injection and gas storage for SPIDER and MITICA

The SPIDER and Shared Plant Units were commissioned and tested in 2017. The Transfer of Right to Use was signed and the plant was used for SPIDER operations in 2018. The final Transfer for Use is planned in Q4 2018, after complete check of plant and submitted documentation.

In parallel the review of the MITICA gas injection and vacuum system design progressed in 2018 and is presently on-going. Installation and SAT of the MITICA GVS Plant Unit are planned to be completed in Q3-Q4 2019.

The following activities were carried out by engineers and technicians of NBTF Team as technical follow-up support in 2018: participation to periodic technical meetings, controls and solving of problems due to integration issues, review of documents submitted in F4E-IDM (both for SPIDER and MITICA), preparation of maintenance contracts (with several companies), continuous presence and follow-up during the SPIDER operational period.

2.1.1.4. Host activities

During 2018 significant amount of resources were invested on activities for construction supervision and coordination, mainly concerning installation of experimental plants, integration and conduction of SPIDER experiments. Particular effort was required to manage interfaces between buildings and experimental plant units. Also the management of the interfaces between plant units themselves required large effort: specifically to this end, the interface management structure, run by NBTF Team, worked in a coordinate way with the aim of reducing as much as possible clashes during installation of plants being able to define in real-time the modifications required in any of the plants. A significant activity relevant to integration management between different plants is represented by the component interfacing the MITICA HV Transmission Line (JADA) and the HVD1-TL2 HV Bushing (F4E), named Connecting Piece (CP). In origin this was a missing item and after a long negotiation it was assigned to JADA. The development of an integrated mechanical model to calculate the forces mutually transmitted between TL2 and HV Bushing in normal and seismic conditions and the relevant analyses and verifications have been performed by NBTF Team. On the basis of the obtained results the requirements for CP have been frozen and a special mechanical structure to reinforce the system against seismic event has been designed, provided and installed by NBTF Team.

The NBTF metrology team continued the site and components survey activities, where and when necessary. Just as an example, metrology activities were fundamental during the installation phase of the SPIDER Beam Source in the vacuum vessel and during the installation of the MITICA HV Transmission Line.

The support to F4E and the other Domestic Agencies for the management of the Construction-Erection All Risks insurance contract for the NBTF (CEAR), directly managed by Consorzio RFX, continued. A flooding event in building #2, happened in November the 13th, was claimed to the insurance. Long negotiation was necessary due to difficulties in finding agreement with the Cooling Plant supplier. At the end an agreement was found and the recovery activity started with the support of a company expert on this type of activities.

The NBTF-site management, with reference to “Titolo IV of D.Lgs. 81/08” (Health and Safety on-site), whose structure had been set up through the Implementation Agreement, continued in 2018: the Responsible of Works and the Safety Coordinator continuously monitored and periodically reported the state of the site. Significant resources were spent to assist F4E, in particular by the Safety Coordinator who is in charge for issuing all the Plans for Safety and Coordination (called PSC documents), being the latter an essential part for both the procurement call for tenders and contracts management. RFX personnel (contract Liaison Officer-LO and Deputy Liaison Officer-DLO) closely collaborated with the Safety Coordinator to this end.

With the support of the Coordinator of the Directors of Works (namely CDL) the time schedule for MITICA on-site activities was prepared and discussed among Consorzio RFX and all involved Domestic Agencies during the year. During the July Programme Committee the PM presented a proposal of modification of the schedule in order to reduce the impact on some single procurement contracts in terms of duration and continuity of site works, to the detriment of a partial modification of the purpose of JADA procurement. After internal discussion among IO and DA’s the proposal was accepted and the new MITICA schedule adopted. Furthermore, as a coordination method, more than 30 weekly Site Progress Coordination Meetings (SPCMs) have been held, and the minutes distributed and uploaded in F4E IDM. The SPIDER time schedule has been also managed by preparing, discussing and verifying weekly the activity plan with a visibility of one week, 3 weeks and 3 months.

Several site inspections were performed by nearly all of the Companies and Domestic Agencies that were operating.

General follow up activities were performed for all the companies working on-site and all the companies working under “Balance of Plant” procurements. Further activities were devoted to the follow-up of companies involved into the three signed Framework Contracts (CODAS-Interlock-Safety, Diagnostics, Assembly).

Big effort has been given by the NBTF team to INDA and its suppliers concerning the SPIDER AGPS system. In particular, support during completion of the installation, commissioning and SAT, review of documentation in view of the transfer for use of the system and management of the process to obtain the authorization of the use in the SPIDER experiment.

As for the Licence to operate the two experiments:

- for SPIDER the authorization to use was obtained from the Local Authority
- for MITICA all the radioprotection technical reports have been completed and submitted to the Italian Authorities

In 2018, the Transfer for Use to Consorzio RFX of some plants and components was obtained. In October, the ownerships of SPIDER and of Cooling Plant SPIDER Plant Unit have been transferred to IO and the responsibility for use to Consorzio RFX.

The management of safety and the organization of personnel works on roster for the commissioning and experiment activities prosecuted during the whole year. In particular NBTF Team guaranteed a continuous support in the management of the insulating SF6 Gas in order to fill and empty HV components, also managing a contract of assistance with an external company expert on this kind of activities.

Finally, NBTF Team managed and performed activities on SPIDER plant system in order to guarantee the correct maintenance and intervention to solve troubleshooting and minor faults.

2.1.2. ***SPIDER***

2.1.2.1. SPIDER Beam Source

The delivery of SPIDER Beam Source (BS) occurred in October 2017. Then the BS was tested on-site and installed inside the Vacuum Vessel in February 2018. From April 2018 the BS was used for SPIDER integrated commissioning and experiments, up to the end of 2018. The Acceptance Data Package for the closure of SPIDER BS procurement contract was delivered by the Supplier in Q2 2018, then reviewed by NBTF Team and F4E, and finally approved in September 2018. The contract was then closed and the Final Transfer for Use of SPIDER BS was signed on 10th October 2018.

The NBTF Team gave continuous and timely support with engineers, physicists and technicians directly involved for:

- performing tests and adjustment activities on the BS out of the vessel;
- executing the installation of BS inside the vacuum vessel and connections to service lines (power supply, signals, hydraulics), see Fig. 2.3;
- performing tests after installation;
- applying changes to the BS during short shutdown periods, according to the outcomes from experimental results.

The magnetic field profile has been measured along 384 apertures of the SPIDER beam source, using a Hall-effect Gaussmeter and a 3-axis digitally-controlled supporting structure. The measured magnetic field was generally in good agreement with the design values. However, it was found that the orientation of the Grounded Grid magnets (in segments 1, 3, 4) was not consistent with the orientation of the Extraction Grid magnets. After comprehensive evaluation of the effects in terms of beam optics and heat loads, it was decided to proceed with the first experimental campaign and to postpone the re-orientation of the magnets to the first shut-down period of SPIDER.

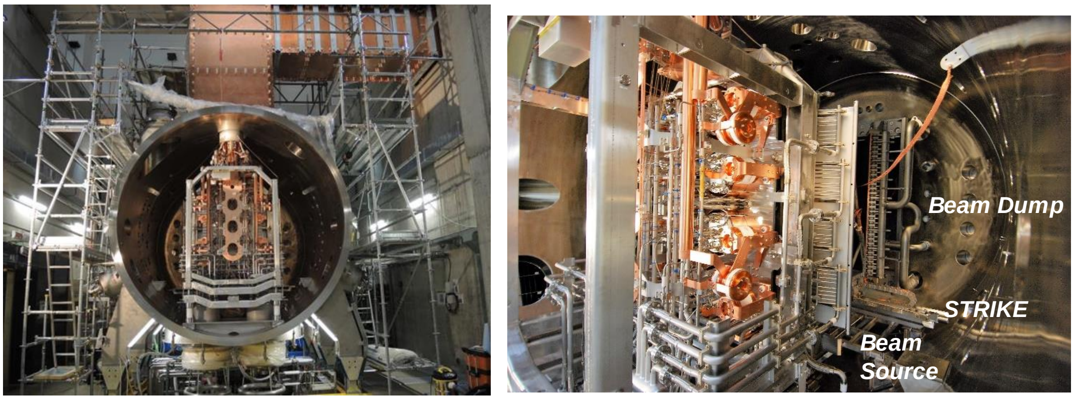

Fig. 2.3 Pictures of SPIDER BS installed inside the Vacuum Vessel.

The tests and relevant activities carried out on the BS during 2018 required a huge amount of resources (engineers and technicians) competent on vacuum and hydraulic technologies, electrical insulation in air and in vacuum, radio frequency circuits, diagnostics, metrology and

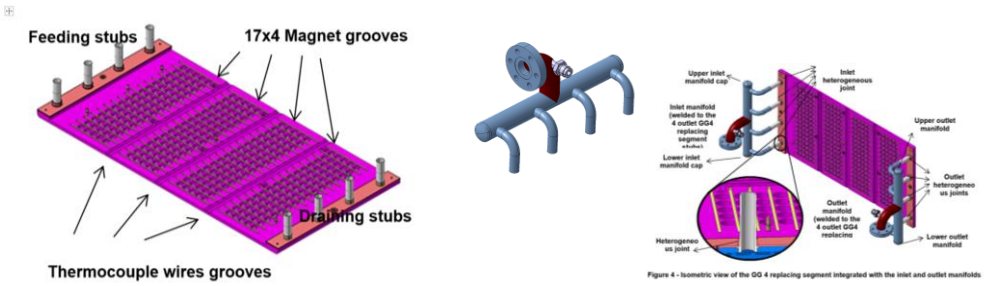

Fig. 2.4 SPIDER Grounded Grid replacing segment n. 4

magnetic measurements [1]. During the period of SPIDER operations a big effort was devoted to investigate the issue of electrical discharges during pulses, both inside the BS and towards the vacuum vessel. Accurate measurements, monitoring and studies were performed investigating the effects of different RF parameters/configurations and of the hydrogen pressure inside the vacuum vessel.

One of the Grounded Grid segments (GG4) was confirmed to be non-conform in terms of vacuum sealing of the hydraulic circuit, so the procurement of a new replacing segment was agreed among IO, F4E and Consorzio RFX. Two different orders were placed in 2018 by Consorzio RFX: order n. 1 for manufacturing and tests of the Cu segment and order n. 2 for manufacturing, welding and tests of two hydraulic manifolds to be connected to Cu segment (see Fig. 2.4).

The procurement order n.1 for Cu segment was awarded in June 2018, kick off meeting was held on 20th June 2018 and works are on-going at supplier's workshop. Delivery on-site is foreseen by mid of March 2019.

The call for tender for procurement order n. 2 (Hydraulic manifolds and welding) was issued on 9th November 2018. The delivery of welded segment after factory tests is foreseen in April 2019. The final tests on-site will be executed by NBTF Team in May 2019.

Technical Specifications and drawings preparation plus management of procurement contracts were entirely carried out by NBTF Team in 2018.

2.1.2.2. SPIDER Power Supplies and modeling

The SPIDER Power Supplies include the Ion Source Power Supply (ISEPS), hosted in a Faraday cage - called HVD - air insulated with respect to ground for -100 kV and the Acceleration Grid Power Supply (AGPS). A Transmission Line connects the HVD to the BS

---

[1] M. Pavei, et al. "SPIDER Beam Source ready for operation", 30th Symposium on Fusion Technology, Giardini Naxos, Italy, 16-21 September 2018, to be published in Fusion Engineering and Design.

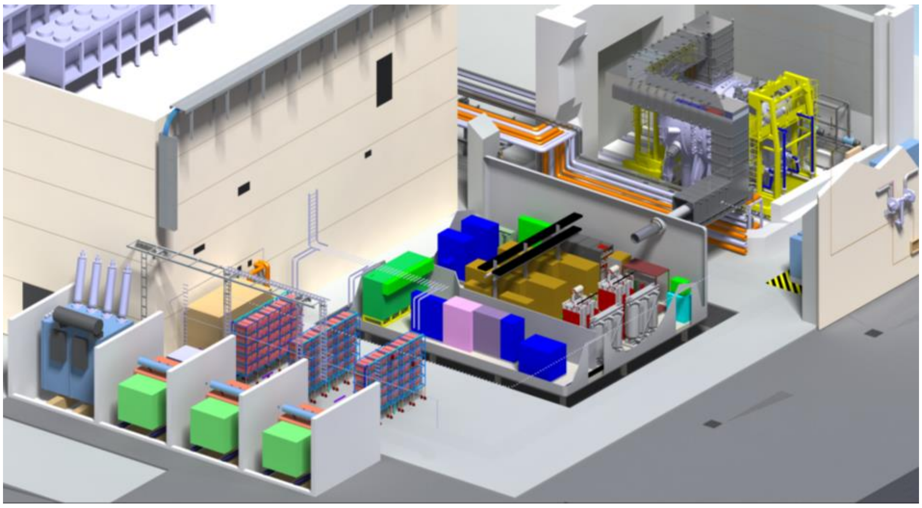

Fig. 2.5 3D view of SPIDER power supply system

through the HV Bushing installed on the Vacuum Vessel (VV). A 3D view of the SPIDER layout is shown in Fig. 2.5 .

AGPS has been procured by INDA, while all the other SPIDER PSs and auxiliary plants necessary to operate SPIDER have been procured by F4E. As of 2018, the SPIDER Power Supplies have been procured and commissioned.

Ion Source and Extraction Power Supply (ISEPS) system

Since 2017 the ISEPS is in operation. Following the installation of the BS, in 2018 ISEPS has been extensively used in SPIDER experimental campaigns for the first time. A large amount of activities has been performed to understand, troubleshoot and optimize ISEPS in order to reach a reliable operation. In particular, the troubleshooting of the RF generators and the characterization of the RF load in different operating conditions required a big effort. In parallel, the activity on the modeling of the SPIDER power supplies progressed in particular for the improvement and validation of the RF circuit models[2], which took advantage from the availability of the experimental data. The chaotic behaviour of coupled RF circuits and oscillators has been reproduced, with results similar to those observed on SPIDER, giving an important contribution to the understanding of the RF source behaviour. Studies have started on the possibility to convert the oscillator to an amplifier (PP ultra-linear), with minor hardware modifications (preamplifier power lower than 300W and efficiency up to 65%). Some effort has been devoted to the general model of the breakdown and to the effects on the RF circuits.

[2] F. Gasparini, et al. "Investigation on stable operational regions for SPIDER RF oscillators", 30th Symposium on Fusion Technology, Giardini Naxos, Italy, 16-21 September 2018, to be published in Fusion Engineering and Design.

Acceleration Grid Power Supply (AGPS) system

SPIDER AGPS components, provided by the Indian Domestic Agency (INDA), have been delivered at Site in April 2016 and installation activities started in July 2016. An overview of the AGPS is shown in Fig. 2.6. Many technical and administrative issues that were faced and solved during 2017 caused significant delays. Main technical issues regarded fire propagation risk, the weakness of some cooling pipes, problems of rust on transformer bolts and some wiring of the control cabinets executed not according to IEC standard. In late 2017 a further delay had been experienced in starting up the rewiring of some parts of the control cubicles, which stopped the commissioning activity. In 2018, the AGPS installation has been finally completed and all pending non-conformities were solved. The Site Acceptance Test has been successfully performed by INDA with the support of NBTF Team. Finally, in late 2018, the integration with SPIDER CODAS and Interlock was also completed.

Fig. 2.6 General overview of SPIDER AGPS

2.1.2.3. SPIDER & MITICA diagnostics

Procurement and installation of a first set of SPIDER diagnostics were completed in 2018 under the Fusion for Energy procurement contract OFC-531-01, ready for start of SPIDER operation in June: thermocouples, emission spectroscopy (Fig. 2.7)[3], electrostatic probes (Fig. 2.8), visible and IR imaging.The same package comprises also the set of more than 90 vacuum windows on SPIDER vessel, for whose installation a special procedure was developed (Fig. 2.9), and the laser absorption spectroscopy, temporarily installed and operated on the cesium test bed (CATS)[4]. he adopted approach that assembly, integration and commissioning of each diagnostic system were carried out by the NBTF diagnostic team has allowed to be flexible, to effectively integrate these activities with the overall NBTF plan.

---

[3] R. Pasqualotto et al., “Plasma light detection in the SPIDER beam source”, submitted to Fus.Eng and Design

[4] M. Barbisan et al., “Design and preliminary operation of a laser absorption diagnostic for the SPIDER RF source”, submitted to Fus. Eng. And Design

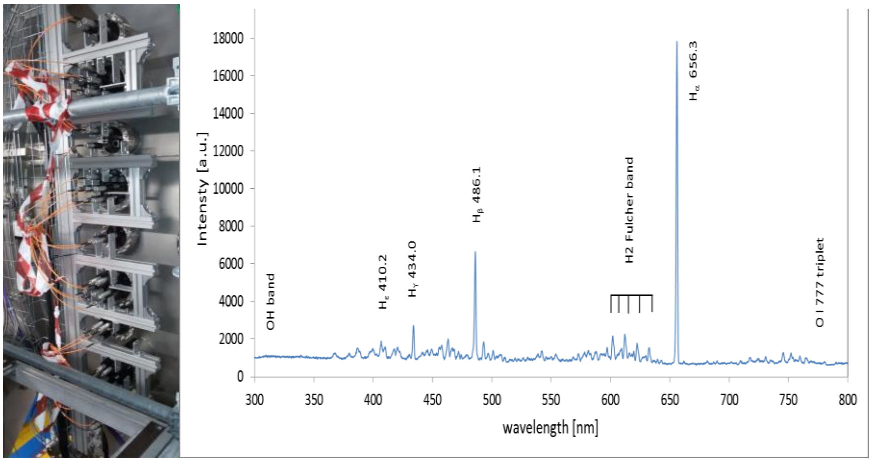

Fig. 2.7 Picture of the spectroscopy optical heads on SPIDER beam source (left) and example of measured spectrum (right)

Fig. 2.8 Pictures of the custom 8 channels electronics module for the electrostatic probes on SPIDER beam source (left) and of the full electronics system in the two dedicated cabinets (right)

The acceptance tests of these diagnostics were passed on 30th May, and then they have been used for SPIDER operation; in particular spectroscopy and visible imaging, that immediately provided valuable results, while thermocouples and electrostatic probes are still being optimised against the induced RF noise.

For other diagnostics, R&D and partial procurement were carried out under F4E contracts OFC-531-01 and OFC-531-02:

- STRIKE procurement progressed significantly with delivery in April of the CFC-1D tiles, which successfully passed the acceptance tests; the remaining components are now being procured, especially for the ex-vessel part, and their installation is being prepared;[5],[6]

---

[5] M. Dalla Palma et al.,“Thermal analysis and high heat flux testing of unidirectional carbon–carbon composite for infrared imaging diagnostic”, Journal of Thermal Analysis and Calorimetry, 2018,

- the neutron diagnostic progressed with procurement of the ex-vessel components, beside repeating the removal and installation procedures of the in-vessel part; [7]
- prototype custom cameras for beam tomography were completed and extensively tested on the bench and on NIO1, also with a dual-camera configuration, and procurement of the complete diagnostic started;
- procurement of Cavity Ring Down Spectroscopy (CRDS) started after acceptance of the final specifications;
- drawings and specifications of the electrostatic sensor prototypes for the beam line components of MITICA were produced (see Fig. 2.10) and will be manufactured in house;
- specifications of fiber optic sensors to perform thermo-mechanical measurements on the beam line components of MITICA

Fig. 2.9 Photo of a typical custom installation for the SPIDER vacuum windows

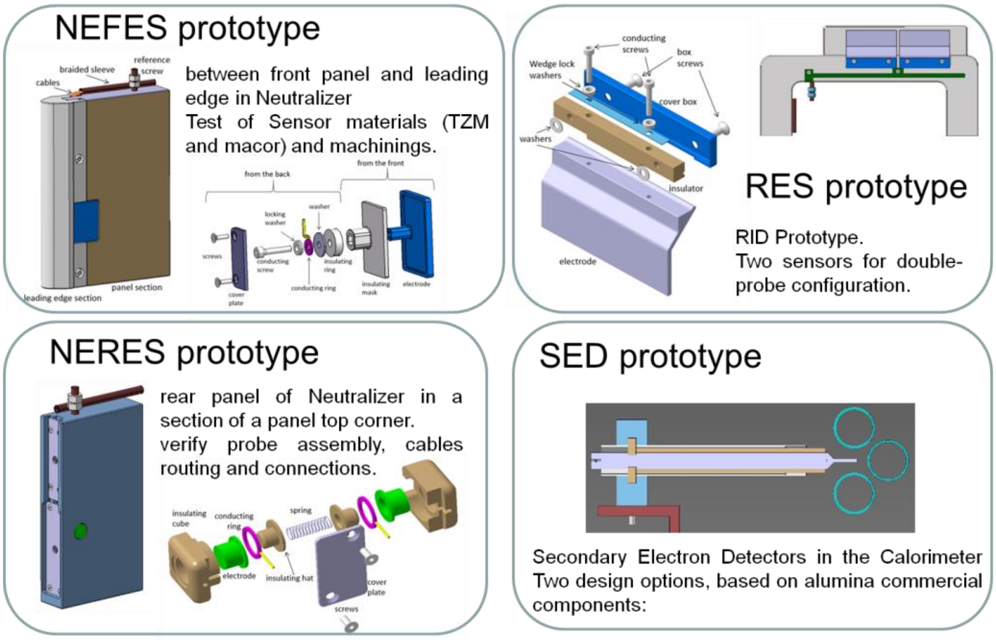

Fig. 2.10 CAD models of electrostatic sensors prototypes for MITICA beam line components

---

[6] A. Pimazzoni et al., "Thermal Characterization of the SPIDER Diagnostic Calorimeter" AIP Conference Proceedings

[7] A. Muraro et al., "Directionality properties of the nGEM detector of the CNESM diagnostic system for SPIDER", Nuclear Inst. and Methods in Physics Research, A (2018)

were produced and procurement procedure started.

The OFC-531-01 contract was closed in October, as scheduled, after acceptance of the full final documentation package.

The OFC-531-02 contract will be extended beyond 2019, to include custom radiation-hard magnetic sensors for MITICA, as prototypes for the ITER HNB.

The collaboration with Milano Bicocca University and IFP-CNR contributed to develop the neutron diagnostic, including a scintillator detector to measure the total neutron yield, and to prepare the final design of the MITICA diagnostics[8] under F4E-NBTF Work Programme 2018.

2.1.2.4. SPIDER CODAS, Central Interlock and Safety Systems

In 2018 the activity on the SPIDER CODAS,Central Interlock, and Central Safety Systems was carried out under the task orders #02 and #03 of the F4E framework contract on the NBTF control systems (F4E-OFC-280).

A set of completion activities were executed, aiming to

- develop and produce the documentation of the interface with SPIDER/Shared cooling and Gas and Vacuum System (GVS);
- develop and debug the Central Interlock System;
- implement the data acquisition systems of the SPIDER baseline diagnostics (source thermocouples, emission spectroscopy, visible and infrared cameras, and electrostatic probes);
- produce the interface sheets and the manufacturing design for the data acquisition of the SPIDER advanced diagnostics (STRIKE, neutrons monitor, tomography, cavity ring-down spectroscopy).

The implementation of the SPIDER Central System was slowly progressed due to the complexity of managing the system life cycle prescribed by the functional safety technical standards, i.e. IEC 61508 for electrical/electronic/programmable electronic systems and IEC 61511 for industrial processes. The hardware architecture design was approved in Autumn 2018 [9] and the Safety Instrumented Functions redefined. The system installation started in

---

[8] M. Dalla Palma et al.,“Simulation of the beamline thermal measurements to derive particle beam parameters in the ITER neutral beam test facility”, Rev. Sci. Instrum. 89, 10J111 (2018)

[9] S. Dal Bello, et al., Safety systems in the ITER neutral beam test facility, 30th Symposium of Fusion Technology, Giardini Naxos, Italy, Sept. 2018.

October 2018 and the Factory Acceptance Tests were executed in mid December. Completion of installation and Site Acceptance Tests are planned for Q1/2019.

2.1.2.5. SPIDER integration and commissioning

The SPIDER integrated commissioning continued in 2018 with the optimization of the operation of SPIDER CODAS, CIS, ISEPS and GVS, and with the integration of the SPIDER Diagnostics[10]. The aim of the commissioning was to start as soon as possible the operation of the SPIDER ion source, that was finally achieved at the beginning of June 2018 with the execution of the first SPIDER plasma pulse[11].

Several SPIDER diagnostics were tested successfully with CODAS, namely the source thermocouples, the diagnostic and inspection imaging system, the emission spectroscopy, and the electrostatic probes. An example of data acquisition from the visible cameras is given in Fig. 2.11.

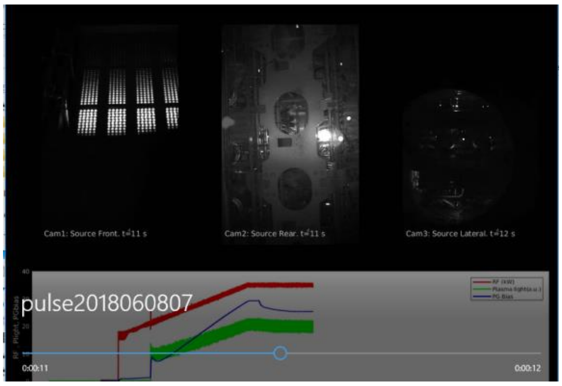

Fig. 2.11 Real-time video streaming of SPIDER visible cameras.

The thermocouples required an ad-hoc campaign to optimize the signal quality that was badly affected by a high-level noise, especially during the operation of the RF. Careful earthing of I&C cubicles, proper connection of signal cable shields and insertion of filters on cables were capable to cancel most of the signal noise injected in HVD.

Integration of SPIDER AGPS with CODAS and CIS was also prepared and the commissioning campaign was carried out, starting from early December 2018.

2.1.2.6. SPIDER experiments: first results and issues

In mid-May 2018 SPIDER operation started.

First of all the following preparation activities were performed:

- the gas injection system and the pumping system were characterised in order to prepare the settings to control the pressure in the source during the pulses (when operating with 8 cryogenic pumps a ratio of 4 is found between source and vessel pressure);

---

[10] A. Luchetta et al., SPIDER integrated commissioning, oral contribution presented at the 30th Symposium of Fusion Technology, Giardini Naxos, Italy, Sept. 2018.

[11] G. Serianni, et al., SPIDER in the roadmap of the ITER Neutral Beams, invited talk presented at the 30th Symposium of Fusion Technology, Giardini Naxos, Italy, Sept. 2018.

- the thermo-ionic current emitted by the pre-ionisation filaments was characterised as a function of the filament heating current;
- suitable protection resistors were inserted in the circuits;
- the plasma initiation sequence was tested by optimising the relative timing of gas injection, application of RF power, start of pre-ioinisation filaments, magnetic filter field.

On 6 June 2018 the first plasma was obtained in SPIDER. The SPIDER control system[12] is very flexible and allows the execution of several parameter scans within single pulses. The first experimental campaigns regarded operation with the ion source and with single RF generators (each one of the 4 RF generators powers one pair of drivers connected in series)[13].

An instance of the light emitted by the plasma as a function of the magnetic filter field current and in different conditions of RF power is shown in Fig. 2.12. A dependence of the plasma light on the magnetic field can be observed as well as a left right asymmetry, which becomes less and less prominent as the RF power increases or the magnetic field decreases; a similar decrease of the left-right asymmetry is found with increasing source pressure. These results are confirmed by spectroscopy.

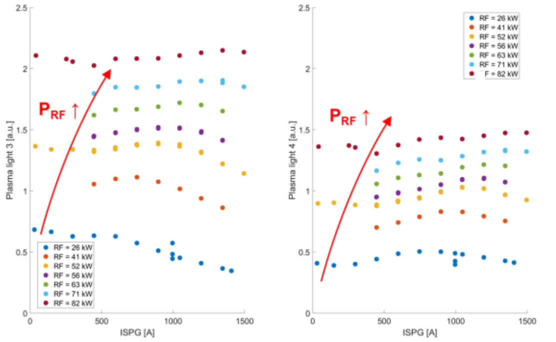

Fig. 2.12 Plasma light collected through the operating drivers.

During SPIDER operation several occurrences of breakdown outside the plasma chamber are detected, due to RF voltages, often leading to premature termination of the discharge and might also result in damages to equipment or cables. To reduce the probability of occurrence of such events, a meshed electrostatic shield was installed, surrounding the RF circuitries and all the other components on the rear side of the ion source. Correspondingly, the range of pressures in which SPIDER can be operated increased and encompassed the whole range explored by the ELISE device (0.3-0.6Pa). Discharges outside the plasma chamber continued occurring; they are also responsible of the difficulties encountered when trying to simultaneously operate more than one RF generator: the discharges detected by one of the RF generators lead to an abort request.

[12] A. Luchetta et al., Fusion Eng. Des. 122 (2016) 928-931

[13] G. Serianni et al., presented at SOFT 2018 and submitted to Fusion Eng. Des.

This was confirmed by masking the apertures of the extraction grid thanks to a stainless steel plate slid on the upstream surface of the grid.

The reduction of the overall conductance, corresponding to a ratio of 20 between source and vessel pressure, allowed to investigate normal source pressure conditions with very low level of vessel pressure: indeed all RF generators worked simultaneously. These experiments gave also preliminary indications about the modifications to be implemented in the pumping speed. The operational space explored during SPIDER operation is shown in Fig. 2.13; in the “blocked” case the higher RF power is obtained thanks to the use of more than one RF generator.

Without the extraction grid mask, a first assessment of DC voltage holding of the SPIDER source was possible by the extraction grid power supply. No breakdowns were detected when applying 12kV between source and vacuum vessel for several tens of seconds up to 0.18 Pa in the vacuum vessel.

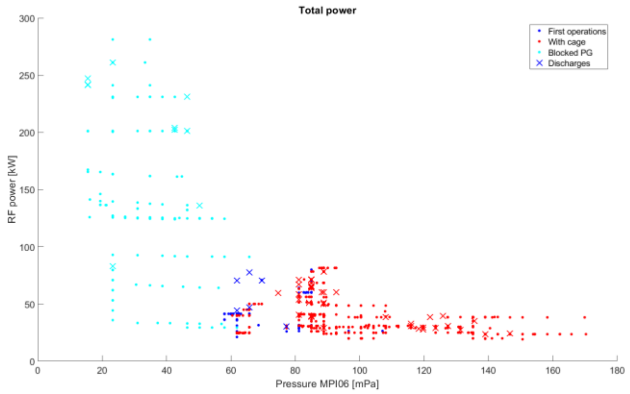

Fig. 2.13 Explored operational space for SPIDER; in the “blocked” case the source pressure is 20 times the vessel pressure; in the other cases the ratio is 4.

2.1.3. ***MITICA***

2.1.3.1. Vacuum Vessel

The MITICA Vacuum Vessel (VV) is composed by three main parts: the VV support structure, the Beam Source Vessel (BSV) (containing the Beam Source and connected to the PS Transmission Line) and the Beam Line Vessel (BLV) (containing the Beam Line Components). The procurement contract is on-going since January 2015 and the Supplier is De Pretto Industrie (I).

The MITICA VV support structure and the Rear Lid Handling System were already manufactured, installed and tested on-site in 2017 (see Fig. 2.14).

The BSV and BLV manufacturing proceeded in 2018 with an effective support given by NBTF Team for technical follow-up. In particular the welding recovery activities on both BSV and BLV were successfully completed, with a huge effort for control of deformations during the execution of critical welding activities.

After welding recovery, the BSV final machining and dimensional controls were completed in Q4 2018 (see Fig. 2.15). Further grinding of weld beads are on-going and will be followed by the accurate cleaning and dry-ice blasting of the internal surfaces, to be carefully prepared for HV holding reasons.

Fig. 2.14 The MITICA VV support structure installed and tested on-site, inside the MITICA Neutron Shield

The tight schedule for BSV foresees the vacuum leak tests in Jan-Feb 2019, the delivery by March and the completion of final installation and tests by mid May 2019.

As regards the BLV, welding recovery and sand blasting were completed in October 2018. Dimensional controls after weld recovery were positively completed and final machining started mid November 2018 ((see Fig. 2.17). BLV delivery on-site is presently expected in September 2019 and completion of tests on-site by mid November 2019.

All these activities and relevant milestones are carefully controlled and verified in order to get an armonized and integrated schedule for MITICA injector installation, considering the parallel on-going activities at PRIMA site for integration and tests of auxiliaries and power supplies.

The NBTF Team guaranteed the technical follow-up during 2018. Frequent meetings and inspections at Supplier's premises (weekly) were necessary for continuous verifications and

Fig. 2.15 The MITICA BSV under machining and ready for dimensional controls.

Fig. 2.17 Pictures of MITICA BLV after welding recovery and under on-going final machining

support during welding recovery activities plus intermediate and final tests. Review of documents and drawings for BSV and BLV were also performed, and support was given for re-organization and updating of the supply quality documents.

2.1.3.2. MITICA Beam Source

The procurement strategy for MITICA Beam Source (BS) manufacturing (see Fig. 2.16) consists in a framework contract divided in three specific stages: stage 1 is the baseline design review, stage 2 is the MITICA Beam Source procurement and stage 3 is ITER HNB Beam Source procurement. Stage 1, involving three companies in parallel, was concluded in 2017; then at the “re-opening of a mini-competition” to assign the BS manufacturing, only one offer out of three companies was received, and it was judged technically not compliant, leading to the cancellation of the procedure.

In 2018 efforts were paid jointly among IO, F4E and RFX to identify the causes for lack of

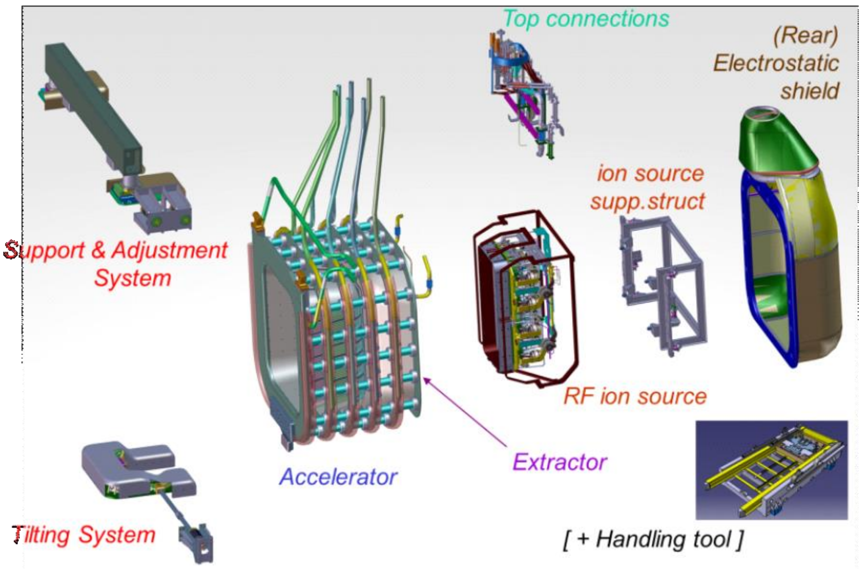

Fig. 2.16 Exploded view of the MITICA Beam Source under procurement

offers from bidders and the best way forward: technical and contractual specifications were revised to take into account risks and difficulties perceived on the bidders' side that impacted the result. The tender was re-issued in June 2018 and three compliant offers were received in August 2018. A thorough evaluation was carried out with the technical contribution by RFX, leading to signature of the contract with Alsyom-Seiv in October and the KoM in November 2018. NBTF Team provided feedback and technical support for checks and review of technical/quality documents and for tenders evaluation.

Discussion over early documentation and preliminary phases has already begun after KoM.

2.1.3.3. MITICA Beam Line Components

A two stages contract was launched: Stage 1 for baseline review, Stage 2 for MITICA BLCs procurement. Three suppliers were awarded for Stage 1: AVS Tecnalia (E), SIMIC (I), De Pretto Industrie – ATT Angelantoni Consortium (I)

Stage 1 Kick-off meetings (one for each supplier) were held in December 2017 and the activities were performed by the three competitors in parallel and carefully followed up by NBTF Team. Stage 1 closure occurred in Q4 2018. Issue of Call for tender, tender evaluation and awarding of stage 2 are planned in Q2-Q3 2019.

Technical support for the follow-up of Stage 1 was guaranteed by NBTF Team with weekly and monthly meetings with three competitors. Substantial amount of resources were involved for review of several documents and follow-up of prototypes manufacturing/testing by three competitors in parallel. Welding processes, machining and assembly sequences, tolerances and metrology for dimensional controls, vacuum compatibility requirements and intermediate and final tests were deeply discussed and optimized together with the three suppliers during stage 1. Pictures of prototypes manufactured during stage 1 are shown in Fig. 2.18.

2.1.3.4. Cryopumps

Two large Cryopumps will be installed inside the MITICA Beam Line Vessel (BLV) to

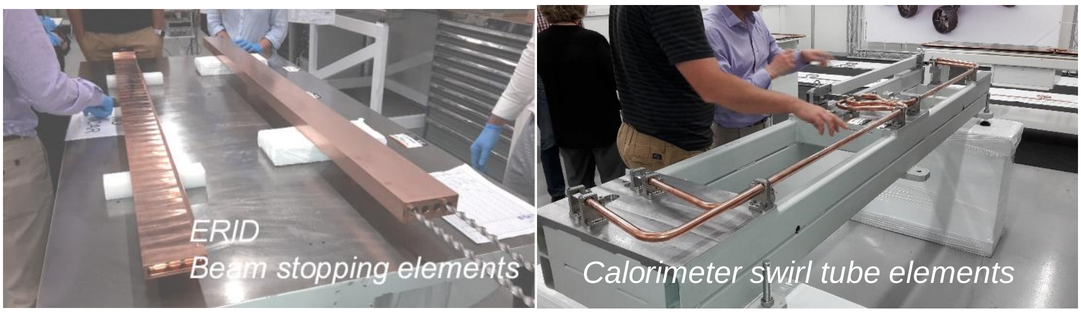

Fig. 2.18 Pictures of MITICA BLCs prototypes for ERID and Calorimeter, manufactured and tested during 2018

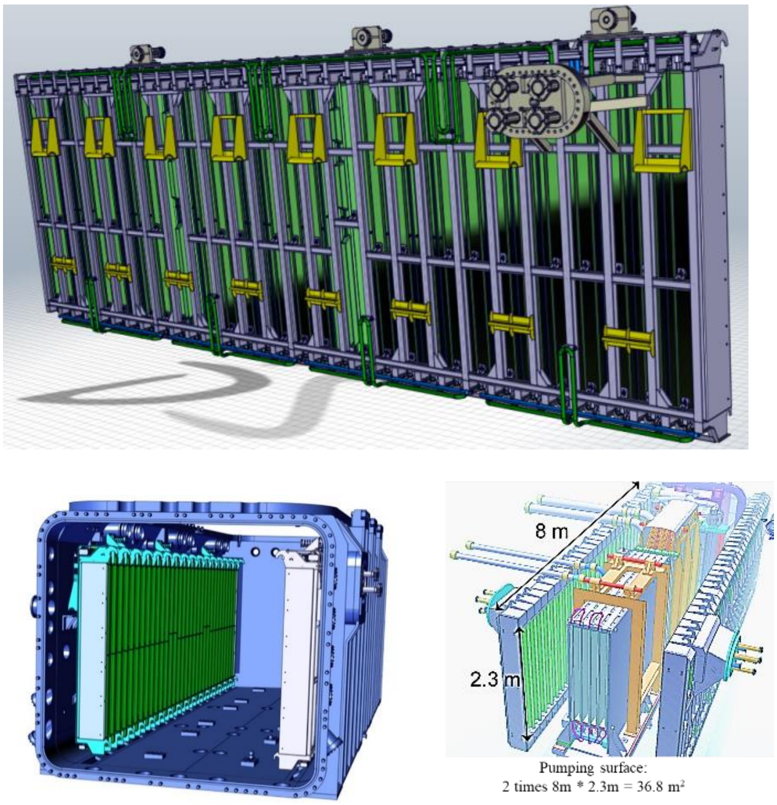

Pumping surface:
2 times 8m * 2.3m = 36.8 m²

Fig. 2.19 CAD views of MITICA Cryopumps

guarantee proper vacuum conditions inside the vessel during MITICA operation (see Fig. 2.19). The Cryopumps are based on adsorption pumping by charcoal coated cryopanels (CPs), 8 m long, 2.8 m high and 0.45 m deep, operated between 4.5 K and 400 K. These cryopanels are surrounded by a Thermal Radiation Shield (TRS) operated between 80 K and 400 K. The CPs will be at the lower temperatures during normal operations, while 100 K or 400 K will be achieved during periodic pump regenerations necessary to remove from the CPs the adsorbed gas (H_2 or D_2). The pumping speed estimated for the two pumps operating in parallel are 5000 m^3/s for H_2 and 3800 m^3/s for D_2.

The complex procurement of Cryopumps is subdivided in three lots, corresponding to specific kowledge and expertise of different suppliers: Lot 1 for support frame and assembly, Lot 2 for expansion profiles and Lot 3 for charcoal coating of pumping surfaces.

The contract for procurement was awarded in Q1 2018: SDMS (F) for Lot 1 and 3, Ravanat (F) for Lot 2. The kick off meeting was held on 15th – 16th May 2018 and the procurement activities are on-going.

During 2018 technical follow-up was carried out by NBTF Team for tender evaluation, awarding of the contract and support during first procurement phases. Participation to bi-weekly and monthly meetings and review of technical documents were guaranteed. In

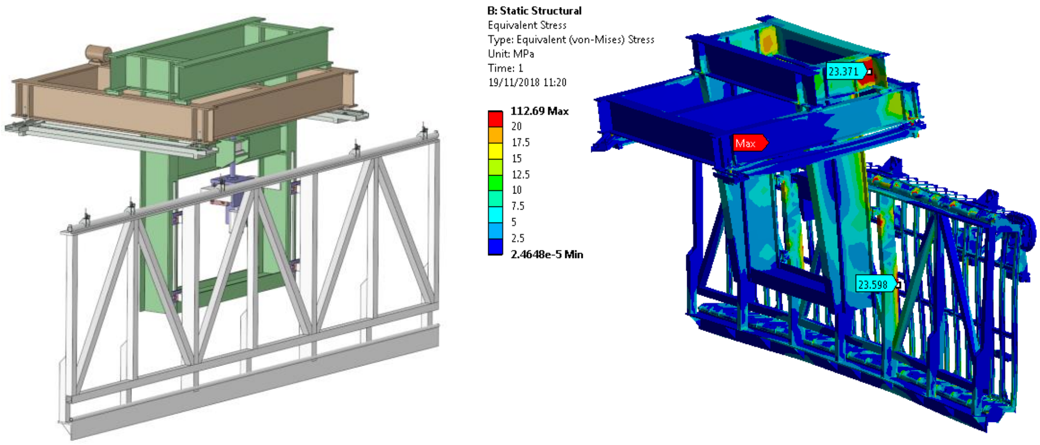

Fig. 2.20 CAD views and results of structural analyses for MITICA Cryopump Assembly Tool

particular material purchase and specific manufacturing processes and prototypes for qualification were thoroughly discussed. First tests for qualification of Aluminium surface emissivity were directly managed by Consorzio RFX.

Further activities in 2018 were addressed to the design of the Cryopump Assembly Tool that will be necessary for the installation of Cryopumps inside the MITICA VV.

The development of a detailed assembly sequence and the Assembly Tool design were carried out (see Fig. 2.20) and Technical Specification for procurement are under preparation. These activities have been managed by NBTF Team and carried out by CCFE as third part under the Work Programme WP2018.

2.1.3.5. Cryogenic Plant

The MITICA Cryogenic Plant is designed to produce supercritical Helium (ScHe) at 4.6K and gaseous Helium (GHe) at 81K and to feed these cryogenic fluids respectively to the cryopanel (CP) and to the thermal radiation shield (TRS) assemblies of the cryopumps. The expected heat loads to be removed in pulse-on scenario are 800 W on CP and 17.4 kW on TRS assembly. The same plant shall also manage the regeneration of Cryopumps at different temperatures.

The procurement contract for MITICA Cryogenic Plant was launched in September 2016 and the supplier is ALAT (Air Liquide Advanced Technologies) (F).

The main equipment, components, warm lines and cryo lines have been delivered.

The installation activities, started in Q2 2018, are still on-going and are planned to be completed by the end of 2018. Almost all of equipment and warm/cryogenic lines have been installed inside Building #2 and Building #4 (see Fig. 2.21) and on the roof of Building #4.

The installation of cryogenic lines inside MITICA Neutron Shield is on-going and completion is foreseen within January 2019.

Fig. 2.21 Pictures of MITICA Cryogenic Plant components and piping inside Building 2.

The electrical part of the plant is still waiting for tests at the factory and approval of certificates before release for delivery and start of installation. In the meanwhile installation of cable-trays is foreseen within January 2019. Completion of assembly, commissioning and Site Acceptance Tests is expected within Q3 2019.

The NBTF Team guaranteed the technical follow-up during 2018. Frequent meetings were necessary for continuous verifications and support during on-site installation activities. Reviews of several documents submitted by the Supplier were also performed. Most of the issues so far identified and solved regarded clashes with other plants, problems at interfaces and details/verifications for fixing of equipment, pipes and cable trays to PRIMA Buildings floors and walls. The effort for this follow-up was much more then foreseen due to lack of preliminary assessment and installation studies on-site by the supplier and sub-supplier in charge for installation.

The procurements of further parts to be integrated with the Cryogenic Plant were also in charge of NBTF Team in 2018: the cooling unit for He compressors and the liquid Nitrogen tanks to be installed out of PRIMA buildings.

Training of NBTF Team engineers and technicians is a major task foreseen in 2019 during commissioning and site acceptance tests. This is necessary to get the proper knowledge and capability for operating and maintaining the MITICA Cryogenic Plant.

2.1.3.6. MITICA Conversion system (AGPS-CS, ISEPS, GRPS)

The MITICA Conversion system includes all the power supplies necessary for the operation of the MITICA experiment, excluding the components for the generation of the High Voltage, i.e. the AGPS Conversion System (AGPS-CS), the Ion Source and Extraction Power Supplies (ISEPS) and the Ground Related Power Supplies (GRPS). Substantial progress in the installation and commissioning of these power supplies has been made. NBTF Team supported all the involved companies during the design, factory tests and activities at Site.

In the following, the progress achieved in 2018 for each subsystem is described.

The MITICA AGPS Conversion System

The AGPS is a special conversion system feeding around 60 MW at -1MV dc to the acceleration grids, and able to interrupt the power delivery in some tens of microseconds in case of grid breakdown, which is a condition expected to occur rather frequently during a pulse.

The ITER AGPS reference scheme consists of an ac/dc stage feeding five three-phase inverters, each connected to a step-up transformer feeding a diode rectifier and a DC filter. The rectifiers are connected in series at the output side to obtain the nominal acceleration voltage of -1 MV dc, with availability of the intermediate potentials.

The AGPS-CS includes two step-down transformers, the ac/dc converter, the dc/ac inverters and the control system. In 2018 the procurement activities progressed very well with the completion of the installation[14]. A picture of the system installed in the main power supply hall is shown in Fig. 2.22.

Fig. 2.22 Picture of the AGPS-CS indoor installation. Ac/dc converters are placed near the west wall. The dummy load cubicles are hidden by the inverter cubicles, on the left side of the picture (south wall).

[14] L. Zanotto, et al., “Acceleration Grid Power Supply Conversion System of the MITICA Neutral Beam Injector: On Site Integration Activities and Tests”, 30th Symposium On Fusion Technology, Giardini Naxos, Italy, 2018, to be published on Fusion Engineering and Design.

Fig. 2.23 Picture of the AGPS-CS Site Acceptance Tests. NIDEC's engineer explaining to F4E, ITER, JADA and Consorzio RFX representatives the result of the tests.

After the installation, the commissioning on the dummy load started around March 2018, and was successfully completed during summer. Each AGPS-CS stage has been tested up to the nominal current and voltage. The breakdown sequence has been proved to be effective.

Fig. 2.23 shows a picture taken during the Site Acceptance Tests. The AGPS-CS system is now ready to be integrated with the rest of the MITICA Power Supply system.

<u>The MITICA ISEPS</u>

The ISEPS design adaptation to MITICA were completed in 2017. In 2018, the follow-up of the contract continued as described hereinafter. The first part of the year was devoted to discuss and prepare the installation activity foreseen for late 2018 and to integrate this activity within the constraints of the overall MITICA schedule. In summer, the installation of the fibre optics from HVD1 (where ISEPS must be installed) to the MITICA local control room were laid down and checked. The review of the documentation was completed and manufacture released for medium voltage and low voltage distribution boards. NBTF Team then attended to FAT in Himmelwerk, IME and OCEM, where all various components and subsystems of ISEPS underwent the contractual factory tests. In late 2018, the ISEPS equipment has been positioned inside HVD1 after the dismantling of one wall of the deck, in view of the bulk of the installation activity foreseen in 2019.

<u>The MITICA GRPS</u>

The MITICA GRPS is actually composed by the Residual Ion Dump (RID) power supply only. This power supply has to provide an average voltage up to 25 kV, plus an ac low-frequency voltage component with maximum amplitude of 5 kV, to spread the power

Fig. 2.24 RID PS during FAT at OCEM premises.

deposited over the RID plates. The nominal output current is 60 A, and the maximum pulse duration is 1 hr.

The selected topology is the Pulse-Step-Modulator (PSM), including a multi-winding dry transformer and 42 water-cooled switching power modules, connected in series at the output.

In 2018, the follow-up of the contract with OCEM progressed with preparation of the installation activities in the first part of the year, followed by FAT at OCEM premises. In late 2018 the installation of the RID PS at Site has been completed and Site Acceptance Tests took place in December.

A picture of the FAT is shown in Fig. 2.24 Fig. 2.25, while a picture of unloading and positioning of the system inside the power supply hall is presented in Fig. 2.25.

2.1.3.7. MITICA HV Components and insulating tests

The installation activities of JADA HV components, started in December 2015, prosecuted till the first half of 2018. All DCG components, the 1MV insulating transformer and 95% of Transmission Line (TL) have been installed. Unfortunately, due to a delay in the delivery of MITICA BS Vessel (BSV), the HV Bushing interfacing BSV and TL and the last piece of TL could not be installed. To limit the delay of insulation tests start, an alternative installation plan was agreed in 2017 and then applied. This plan considers to close the TL end by means of a special cup, without installing the last piece of TL named TL3 bend. In June 2018, after completion of installation activities and preliminary checks and verifications, the HV components have been evacuated, then filled with pressurized Nitrogen to exclude leaks and finally filled with pressurized SF6 gas. In September, AGPS-DCG (step-up transformers, diode rectifiers and DC Filter components) has been submitted to the following insulating tests:

Fig. 2.25 RID PS installation.

- 1.2 MV dc for 1 hour
- 1.06 MV dc for 5 hours, followed by five fast ramps up to 1.26 MV

Tests were successfully passed, see Fig. 2.26, allowing to prosecute the setting up of the plant for the next HV tests.

In November, the second set of HV tests have been performed in order to test the TLs. Also in this case the test was successfully passed allowing to maintain the MITICA schedule without significant delays.

In the last part of the year, after removal of the SF6 gas, the NBTF Team followed the works for installation of the seismic reinforcement and for preparation of the plant for next

1st Step 1200kV - 1 HOUR   2nd Step 1060kV - 5 HOURS

Fig. 2.26 AGPS-DCG insulating tests.

installation of the Connecting Piece. Also in 2018, strong support has been given by NBTF Team to the installation and test of JADA components. The activities were performed under the supervision of QST laboratory of Naka and Hitachi experts, with specific contributions of Consorzio RFX to finalize solutions for different issues encountered during daily operations, with the assistance of a European company (Synecom) for the management of the SF6 gas and assistance during HV tests.

2.1.3.8. MITICA I&C

The design of MITICA CODAS, Central Interlock and Safety Systems progressed with the definition of the interfaces with MITICA GVS, Cooling Plant, Cryogenic Plant, ISEPS, AGPS, and GRPS. miniCODAS was adapted for usage in the AGPS and GRPS factory acceptance tests. The ITER high-performace networks were studied to understand their usability in MITICA CODAS. The Time Communication Network technology was prototyped and the software drivers were prepared and tested[15]. The data archiving network was also tested, but it was considered an immature technology for application in MITICA. The Synchronous databus Network was also tested and eventually considered as a viable and reliable technology for MITICA.

Progress was also achieved in the definition of the MITICA CODAS and Central Interlock system, identifying the ITER-relevant and NBTF-only components.[16]

2.1.4. *ITER Neutral Beam Injector Physics*

<u>MITICA beamlet optics and magnetic deflection compensation experiments</u>

The analysis of the overall results of the 1st and 2nd Joint Experiment campaigns (carried out on the NITS device at QST Naka, Japan in Feb-Mar 2016 and in Dec 2017) has been completed using a new, more precise procedure for fitting the beamlet thermal images on the CFC target. A comprehensive database correlating the beam thermal footprint and the beamlet optics to the operating conditions of NITS and to the transverse magnetic field at the meniscus has been obtained, including all the data collected on NITS experiments (see Fig. 2.27).

The final part of these activities allowed to gain a better understanding on the effect of transverse magnetic field on meniscus shape and therefore an improvement of the 3D optics

---

[15] G. Manduchi, et al., The timing system of the ITER full-size neutral beam injector prototype, 30th Symposium of Fusion Technology, Giardini Naxos, Italy, Sept. 2018

[16] N. Pomaro, et al., Design of MITICA control and interlock systems, 30th Symposium of Fusion Technology, Giardini Naxos, Italy, Sept. 2018.

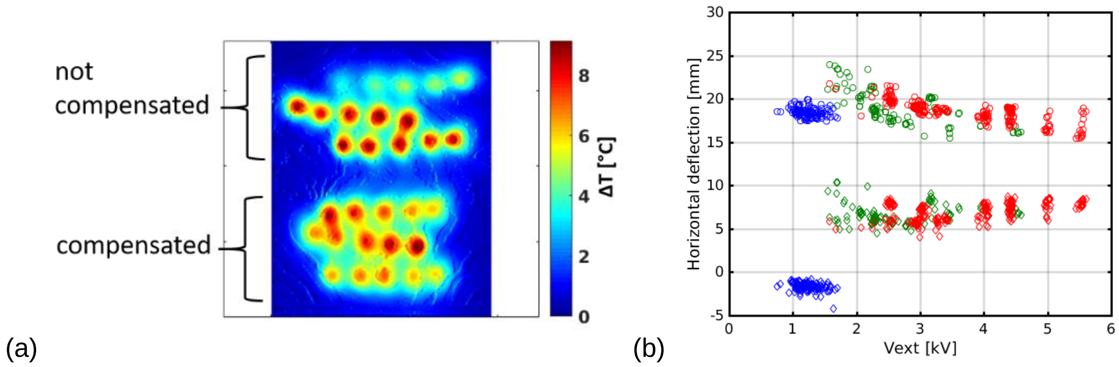

Fig. 2.27 (a) example of IR image on CFC target, (b) horizontal beamlet deflection estimated from the IR image as a function of extraction voltage joint experiments. Different colors and markers indicate different configurations of the magnetic field in the extraction region.

models of the MITICA and SPIDER accelerators [17] [18]. The analysis of these results was discussed and plans for new simulations and experiments to be carried out in 2018-2019 were proposed in meetings with QST personnel.

Since the NITS experiment could only operate at low extraction and acceleration voltage, a proposal for testing the MITICA/HNB optics in the MTF (Megavolt Test Facility) accelerator at QST, with minimal modifications to the existing MTF structure, has been prepared and delivered to QST. Such experiments were intended to validate the MITICA/HNB optics design (already tested at low voltage on NITS) at higher and more realistic voltage levels and to verify the EAMCC calculations of the thermal load on the grids.

The preparation of numerical 3D models of the MTF in support of these experiment has been started, using a newly developed OPERA beam optics model, taking into account a variable meniscus asymmetry, proportional to the local transverse magnetic field. A good correlation with the previous experimental results was confirmed, which allowed to successfully conclude the previous activity.

The application of this model to the MTF experiment at QST Naka was started in order to cross-check the beam optic model at higher acceleration voltage. The results of previous MTF campaigns carried out at QST Naka, Japan, including the thermal images of the beam on CFC target were initially used. New joint experiments on MTF were proposed with QST. The preparation of numerical 3D models of the MTF in support of these experiments has

[17] G. Chitarin, A. Kojima, D. Aprile et al., Improving a Negative Ion Accelerator for next generation of Neutral Beam Injectors: results of QST-Consorzio RFX collaborative experiments, presented at SOFT2018 conference, accepted for publication in Fusion Engineering and Design

[18] D. Aprile, P. Agostinetti, C. Baltador et al., Complete Compensation of criss-cross Deflection in a Negative Ion Accelerator by Magnetic Technique, presented at NIBS2018 conference in Novosibirsk, Russia, accepted for publication in AIP conference proceedings

been started, using both OPERA and COMSOL simulations. Such experiments will also allow to verify the EAMCC calculations of the thermal load on the grids for MITICA/HNB.

<u>Validation of Avocado model with measurements of pressure profile inside the SPIDER accelerator</u>

The loss of negative ions in the accelerator is due to stripping via collision of the beam with the background gas. The pressure profile inside SPIDER accelerator is therefore very important and in 2018 it was directly measured. Such a measurement provided also the assessment of the validity of the simulations performed by the AVOCADO code. The results of the measurements through three accelerator apertures are shown in Fig. 2.28, exhibiting the typical pressure decay in correspondence to the grids. The results are very close to the simulated profiles; simulations allow also the assessment of the conductances of the diagnostic holes of the source and of the gaps between accelerator grids and were employed to compare the throughput of the source also during the operation with masked extraction grid apertures.

During 2018 preliminary activities in view of the simulation of the behaviour of caesium in the SPIDER ion source were performed. The wall processes (both in plasma and vacuum environments) allow the vessel and expansion region into which caesium is injected to reach dynamic equilibrium, where, for a constant flux of caesium emitted from the oven, the adsorption rate is constant. Therefore, caesium vapour is expected to condense on the walls that are at room temperature, whilst for heated walls it is adsorbed with an equilibrium coverage below one monolayer. This knowledge can then be applied to the plasma grid once its temperature and the redistribution of the caesium by the plasma volume is known.

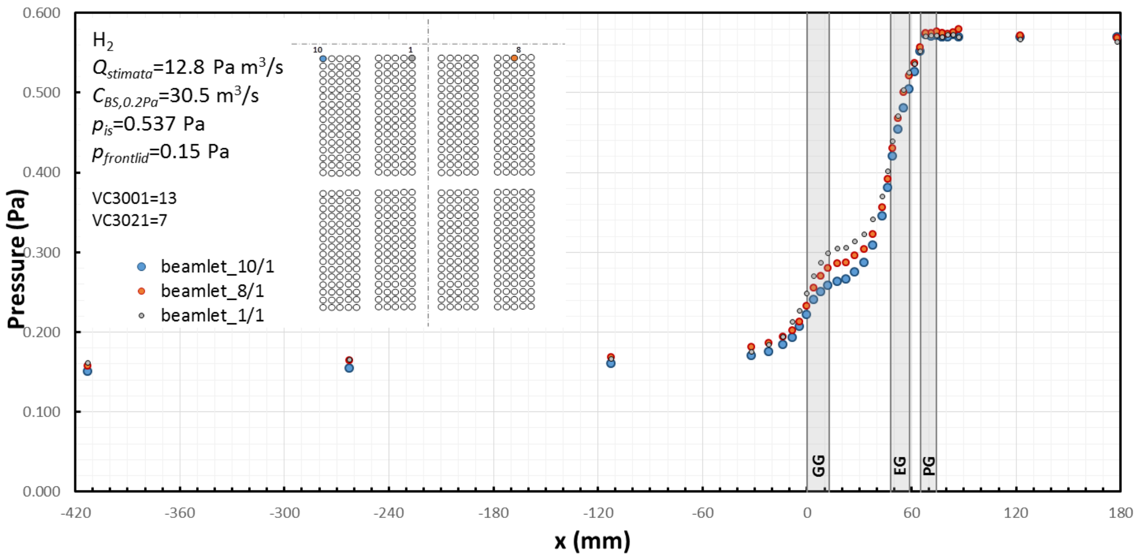

Fig. 2.28 Profile measured inside the SPIDER accelerator (right); colours correspond to the beamlets indicated on the left-hand side.

In the plasma phase, caesium released from the walls by evaporation can be recycled back to the same wall due to the presence of the plasma sheath.

2.1.5. *Vacuum high voltage holding modeling and experiments*

2.1.5.1. HVPTF experiments

An experimental study on the relation between the conditioning process of the surface of the electrodes and the topology of the electric field has been carried out. Using a dual power supply and two electrodes inside a grounded vacuum vessel, one electrode at positive potential and another at negative potential, the electrodes were fully conditioned under a perfectly symmetric electric field configuration. When the voltage of the negative electrode to ground was decreased by few kV, thus creating a lower electric field with slightly different (asymmetric) electric field topology, the occurrence of micro-discharges was regularly observed. These experiments confirmed that small variations of the surface conditions on "facing spots" on the two electrodes are sufficient to trigger a discharge. In order to analyze this phenomenon, a series of numerical analyses has also been carried out considering a mutual exchange of charged particles between electrodes.

An experimental campaign using meshed “transparent" anode (i.e. anode covered by a thin metallic mesh) has also been carried out at HVPTF: a sphere-plane configuration (gap length 37.5 mm) was assumed as reference case to discriminate if the thin metallic mesh can improve voltage holding in high vacuum (see Fig. 2.29).

An Infra-Red camera was also used for monitoring the electrode temperatures during the test. During the campaign, the high voltage conditioning was carried out using an automatic procedure. No voltage holding improvement was observed with respect to the reference configuration constituted by a solid anode. The thermal measurements indicated that the temperature variation of the electrode surface was negligible.

However, a considerable temperature increase was detected on the metallic support sustaining the anode. A specific study allowed to understand the physical phenomenon causing the power dissipation, probably related to an electron cascade regenerative

Fig. 2.29 Meshed (transparent) anode and temperature increase on metallic electrode support

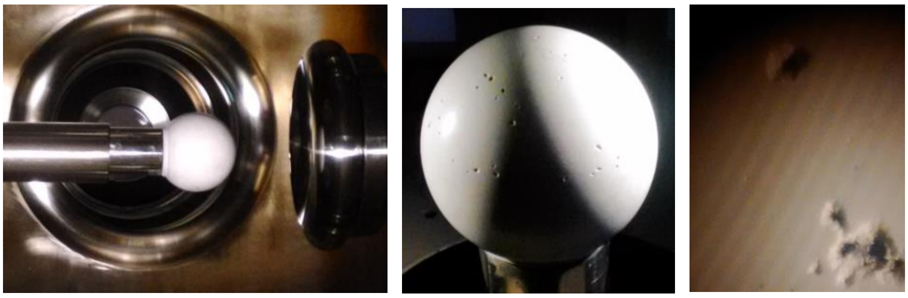

Fig. 2.30 Spherical cathode with plasma-sprayed alumina coating

phenomena [19].

A first experimental campaign was carried out using a spherical stainless steel cathode with plasma-sprayed alumina coating ("lollipop electrode") and a plane electrode (see Fig. 2.30).

The high voltage conditioning was carried out using the automatic procedure. This electrode setup demonstrated a voltage holding up to 440 kVdc. On the other hand, a maximum voltage holding of 430 kV for the same sphere-plane configuration without alumina coating was found. The conditioning required 300-400 breakdowns in both configurations. No substantial improvement of voltage holding has been observed using the alumina coating. After the tests, the alumina coating appeared to be cracked and locally damaged in several locations.

A cross-check of the experimental results has been carried out in order to rule out the effect of small dust and contaminants which were accumulating inside the vacuum chamber, in particular on the surfaces of the support of the negative electrodes.

After thorough cleaning of the vacuum chamber and electrodes, the tests with sphere-plane configuration were repeated. Although the conditioning procedure took a considerably shorter time, in the end the voltage holding capability was similar to the one observed in the previous session.

Additional tests on the 40 mm sphere-plane configuration with gap length of 72 mm were carried out in high vacuum. After more than 140 hours of conditioning and almost 300 breakdowns, a "saturation" breakdown voltage at 580 kV was reached, confirming that the maximum voltage achieved during the previous tests (with gap lengths lower than 72 mm) depended on the electrode configuration under test rather than on the interaction with the vacuum vessel wall; a similar result has been also obtained with a gap length of 148 mm.

[19] N.Pilan, S. De Ambrosis, A. De Lorenzi et al, Evidences of accumulation points in cascade regenerative phenomena observed in high voltage dc devices insulated by vacuum, https://doi.org/10.1088/2399-6528/aaea95

This result confirms the existence, for a single gap in high vacuum, of an upper limit in the hold-off voltage of about 600 kV for vacuum gap length of tens of centimetres.

The beneficial “pressure effect” was also verified experimentally with Argon in sphere-plane configuration with gap length of 30, 72 and 148 mm. When low pressure gas was injected (about 5 10^{-2} Pa) a higher breakdown voltage between electrodes (up to 775 kV for 72 mm gap and up to 800 kV for 148 mm gap) was achieved and a stable hold-off voltage of 780 kV has been kept for more than 10 minutes without breakdowns. The left branch of the Paschen curve in Argon has been also partially investigated.

The High Voltage Short Gap Test Facility (HVSGTF) to measure the Fowler Nordheim emission current has been assembled at Consorzio RFX. The first HV tests in vacuum have been carried out to the maximum voltage (100 kVdc) to verify the X ray biological screen. A further activity aimed to implement a pico ammeter to measure the dark currents has been started.

2.1.5.2. Vacuum High Voltage modelling and preparation of MITICA HV holding tests

The probabilistic model previously developed at Consorzio RFX for the prediction of HV holding in vacuum has been further developed, including the capability to determine the breakdown probability along all possible discharge trajectories between electrodes. The model was validated also on the basis of the experimental results obtained during the tests of the High Voltage Bushing for MITICA [20]. The experimental results obtained at QST on the reduced-size 500 kV voltage holding experiment in vacuum were also used to refine the model. The model has been applied to the design and preparation of first HV holding tests at 1 MV in the MITICA vessel (see Fig. 2.31).

The main objectives of these tests are the following:

- Experimental determination of the HV holding capability in high vacuum in MITICA vessel under realistic conditions with large electrodes (some m^2) and long gaps (up to 0.6 -1.0 m);
- Evaluation of the HV holding improvement achievable by a small increase of the gas pressure (the so called "pressure effect", which typically takes place below 50 mPa);
- Experimental determination of the HV holding capability in presence of an intermediate electrostatic screen at 600 kV, optimization of the shape and

[20] N. Pilan ; A. Kojima ; R. Nishikiori et al, Numerical–Experimental Benchmarking of a Probabilistic Code for Prediction of Voltage Holding in High Vacuum, IEEE Transactions on Plasma Science, 2018, 46, 5, https://doi.org/10.1109/TPS.2017.2775246

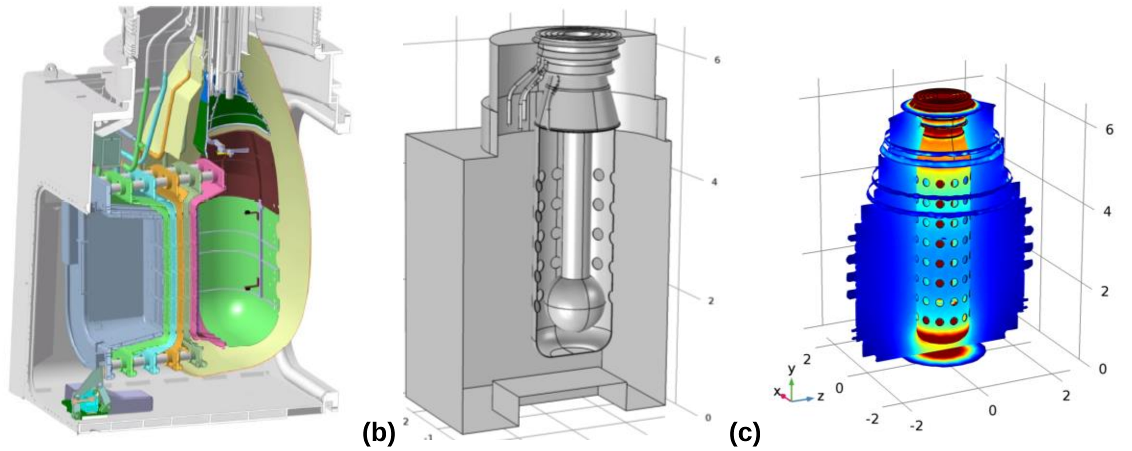

(a) (b) (c)

Fig. 2.31 (a): geometry of the MITICA Beam Source and intermediate electrostatic shield in the vessel; (b) and (c): configuration considered for the first 1 MV tests in the MITICA vessel, including a beam source mock-up and an intermediate electrostatic shield mock-up with holes

number/size of holes in the electrostatic screen, also with regard to the resulting gas pressure distribution;

- Characterization of the behaviour of the HV power supplies and transmission line in case of breakdown;
- Measurement of the currents under realistic conditions during the execution of the tests as well as of the current and the EM noise in case of breakdown.

The test configuration considered for these tests includes a mock-up of the Beam Source (sphere + cylinder), with and without an intermediate electrostatic screen. The intermediate electrostatic screen will be provided with holes for allowing the gas flow. In order to start the tests at low voltage, the distance between the mock-up of the Beam source (sphere) and the ground electrode (plane) shall be adjustable (see Fig. 2.32). Using the above mentioned numerical models, the optimization of the shape of the mock-up and of the screen has been

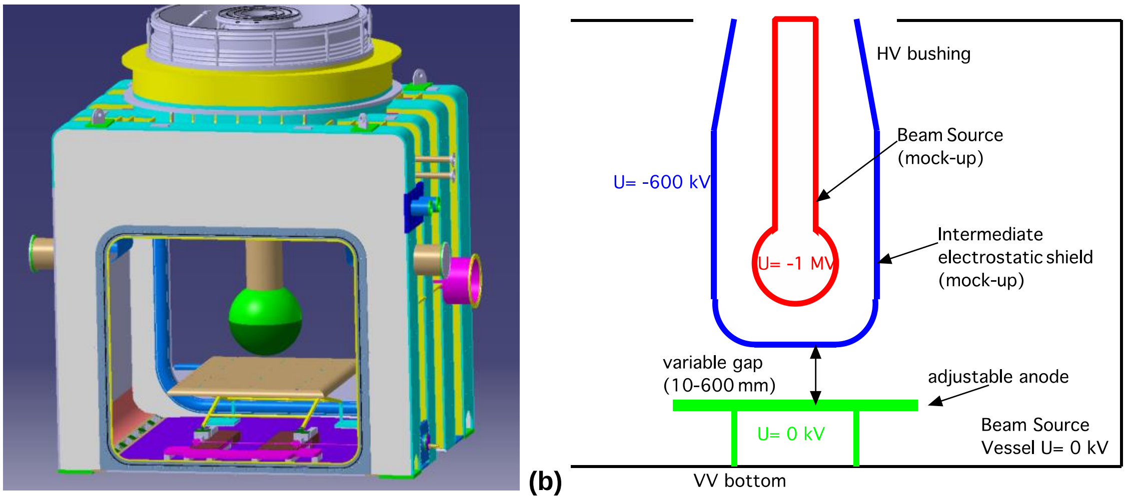

(a) (b)

Fig. 2.32 CAD view (a) and layout (b) of the Beam Source mock-up with the movable electrode inside the MITICA vessel, as proposed for the first 1MV voltage holding tests

carried out, and a first draft of the logical sequence of the HV tests has been discussed. The mechanical design of the mock-ups of the Beam Source, of the intermediate electrostatic screen and of a movable grounded electrode has also been preliminarily defined.

2.1.6. ***RF Research and Development***

To enhance the knowledge in the field of Radio Frequency (RF) driven inductively coupled plasma sources and to investigate possible issues related to the voltage hold off at low pressure of the RF circuit and drivers of SPIDER and MITICA, a RF laboratory was set up at Consorzio RFX, and the first testbed developed is the “High Voltage Radio Frequency Test Facility” (HVRFTF) devoted to the experimental validation of the driver insulation design criteria[21]. The first tests in late 2016 and 2017 on a stainless steel planar circular electrode pair proved the correct operation of the overall plant. The achievement of a voltage of about 10 kV rms with the available RF amplifier and RF circuit components, also allowed validating the circuit models developed during the design phase.

In 2018 a revision of the HVRFTF setup with the installation of fixed safety fences, the preparation of an improved RF circuit and the preparation of technical specifications for a new RF amplifier was carried out. In parallel the procurement of the mock-ups for the drivers (plane – dielectric – sphere is the best configuration worked out so far) was performed and the first tests were carried out for the SPIDER driver configuration (Alumina driver case 8 mm thick, and RF coil touching the driver case) and the improved MITICA driver configuration (Quartz driver case 6 mm thick, and gap of 2 mm between the RF coil and the driver case).

Some pictures of the new driver mock-up are shown inFig. Fig. 2.33.

The results of the experimental campaign showed no clear influence on the breakdown

Fig. 2.33 SPIDER driver cross section (left), mock-up before installation (center) and after installation (right).

---

[21] • A. Maistrello, P. Jain, M. Recchia, E. Gaio, "Studies on the requirements and design of the High Voltage Radio Frequency Test Facility", Fusion Engineering and Design Volume 131, June 2018, Pages 96–104, https://doi.org/10.1016/j.fusengdes.2018.04.086

voltage of the “gap 2” shown in Fig. 2.33. A new driver mock-up is being prepared and will be tested to further investigate the matter.

2.1.7. *Caesium R&D*

Caesium R&D activities on CATS facility started in 2018: the first campaigns for Cs characterization were carried out and simultaneously lots of debugging was done on hardware and software, control and diagnostics. It was possible to start to obtain and characterize the output of Cs flow from the oven prototype procured in 2017, with regard to the control of the oven temperature in the reservoir and the duct. Various SPIDER-relevant diagnostics, like Laser Absorption Spectroscopy and Surface Ionization Detector, were operated in different conditions.

Further tests to characterize the behaviour of the oven at various parameters were then carried out, with particular attention focussed on the valve and on the diagnostics, under different possible conditions in order to give the green light for the production of the series ovens for SPIDER source, which are being delivered at the end of 2018 for testing on CATS before being installed on SPIDER.

Caesium is known to accumulate within the space in which it is injected over successive evaporations when the pump rate is less than the flux of caesium from the oven, which alters the signals obtained from diagnostic techniques. A mobile surface ionisation detector (SID) and a microbalance were employed to measure the equilibrium flux of the vessel, and so to directly measure the increase in the background level of caesium. These measurements can then be applied to the fixed SID to determine which percentage of the flux measured is due to the background level, and which is due to the caesium evaporated freshly from the oven. The mobile SID therefore acts as a reference value, after saturation of the signal is attained. Furthermore, the SID currents are space charge limited, so must be operated with a large enough bias to reach a saturation current, whilst in a single probe configuration connected to ground. The duct and reservoir temperatures of the oven can now be specifically selected to generate the required flux of caesium from the caesium oven.

2.2. *ITER Modelling*

In 2018 the contribution to the ITER modelling activities on disruptions have extended the kind of analysis and simulation results obtained in 2017 with the 3D code M3D for the JET device, to the ITER case, also considering the presence of a finite population of runaway electrons.

In 2017 it was shown for JET disruptions that the electromagnetic horizontal force (i.e. that due to plasma asymmetries) on the vessel increases, as a function of an increasing current quench time normalized to the wall penetration time. This ratio for JET is around 8-10, which maximizes the horizontal disruption forces. In ITER instead, being the estimated current quench of the order of 50 to 150 ms and the wall penetration time of the order of 250-300 ms, the electromagnetic forces are expected to strongly decrease, i.e. forces similar to those in JET could be predicted, even for the highest plasma current and toroidal magnetic field. To confirm this, the ITER reference scenario at 15 MA have been simulated [22]. The main results are given in Fig. 2.34**.** The ITER cases confirm the trend found for JET and the strong dependence of the forces on the above mentioned ratio between the current quench and the wall times. One of the concern for ITER is the role of runaway electrons (RE) that can develop during disruptions, due to the relatively low density (related to the loss of confinement) and the high electric fields (due to fast changes of the plasma current). Since the RE electron current tends to be damped slowly, as it is also verified in experiments, this could change the conclusion about the ITER horizontal wall force. In Fig. 2.34 also cases where a runaway current is present are shown. The RE have been treated as a fluid and the Ohm's law has been modified as[23] :

$$\partial\psi/\partial t = \nabla_{//}\,\Phi - \eta\,(J_{//} - J_{//RE})$$

where ψ is the poloidal flux and Φ is the electrostatic potential, η is the plasma collisional resistivity and $J_{//}$, $J_{//RE}$ are the plasma and RE parallel currents.

In Fig.1 the amount of the RE current varies from to be equal to be 1/2 of the plasma current and accordingly the horizontal force changes. The smaller force is observed for the smaller fraction of RE current. The time history of the relevant quantities is plotted in Fig. 2.35 for the case where the RE brought 1/2 of the plasma current.

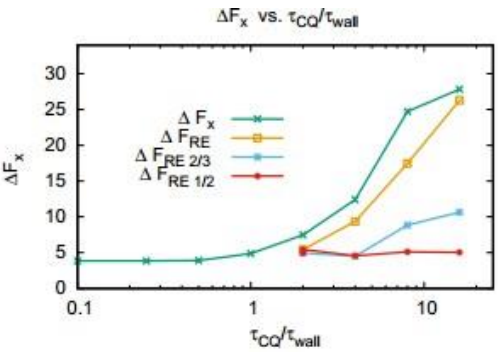

Fig. 2.34 Horizontal force (in MN) vs τ_{cq}/τ_{wall} for ITER cases with no RE and with different RE currents, i.e. I_{RE}/I_p =1, 2/3, ½ .

The model uses some free parameters to describe the time evolution of the RE and plasma current. These results are therefore not self-consistent and have a certain degree of arbitrariness, since the time evolution of the plasma and RE currents is, in practice, imposed. In this model the role of RE is simply to

[22] H. Strauss et.al.,*Reduction of asymmetric wall force in JET and ITER including Runaway electrons*, 27th IAEA Fusion Energy Conference, (Ahmedabad, India 2018), paper IAEA-CN-TH/4-4.

[23] M.N. Rosenbluth, S.V. Putvinski, "Theory for avalanche of runaway electrons in tokamaks", Nucl. Fusion, 37,1355 (1997).

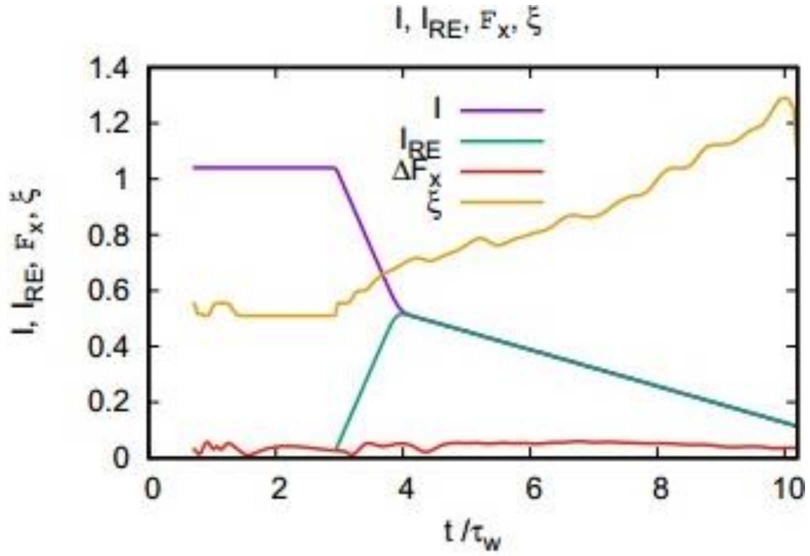

Fig. 2.35 Plasma current (purple), RE current (green), vertical displacemnt (yellow) and horizontal force (brown) vs. time (normalized to the wall time).

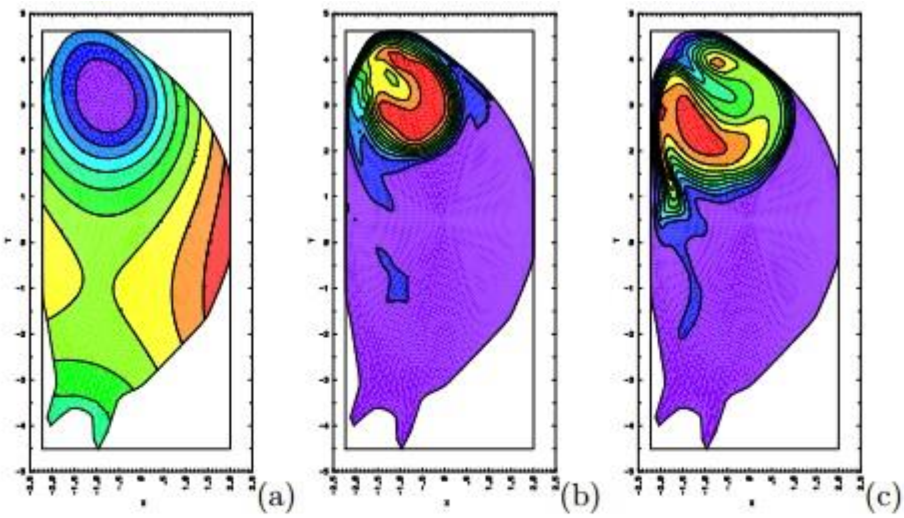

Fig. 2.36 Constant contours in the poloidal plane of (a) poloidal magnetic flux ψ, (b) plasma current and (c) RE current

change to total plasma current. It is clear that for a better assessment of the role of RE during disruptions it would be necessary a treatment able to determine self-consistently the RE time evolution.

In Fig. 2.36 at a given time during the disruption the poloidal flux contours, plasma and RE current contours are shown. It is clear the m=1 structure of both plasma and RE currents.

Finally, it should also be noted regarding the forces, that the decreasing of the horizontal force with the current quench time (for a given wall time) is compensated in real cases by an increase of the vertical force (due to the axisymmetric plasma displacement). In fact the horizontal force is mainly determined by the amount of non axisymmetric plasma deformation during the disruption event, which is related to the evolution of the n=1 mode, while the vertical force is simply related to the evolution of the n=0 vertical axisymmetric plasma movement. The faster this movement, the stronger are the eddy currents induced on the suroounding structures and on the conducting wall and, as a concequence, the resulting vertical force.

During year 2018, the study of the pre-disruption phase of an high density, L-mode discharge of ASDEX Upgrade has been continued. The interest in this type of scenario aims at avoiding/controlling high density disruptions via ECRH heating[24] . This scenario is also a current topic in the MST-1 EUROfusion program and is very important for ITER. These disruptions in ASDEX are believed to be dominated by stochastization due to the superposition of many n=1, high-m harmonics (3≤m≤5) which resonate near the separatrix, coupled to a dominant m=2, n=1 tearing mode (TM), which is braking and increasing in amplitude near the final phase of the disruption[25].

Electron transport was studied via the guiding center code ORBIT[26]. Fig. 2.37 shows co-passing collisionless electron orbits, all with $\mu = 0$, to show the nature of the resonances. Clear resonance islands are seen for each n=1 harmonic, as well as a nonlinearly generated resonance at m/n = 5/2. To study transport 300 eV electrons were launched with a uniform pitch distribution, at a fixed initial flux surface, and a given pitch angle scattering rate, consistent with the temperature and density of the discharge considered. The evolution of the canonical momentum (averaged over a large number of particles)

$$\langle \left(P_\zeta(t) - P_\zeta(0) \right)^2 \rangle = Dt^p$$

was studied as a function of time, to see the behaviour of the electrons in various portions of the chaotic domain (red lines in Fig. 2.37). Within the 2/1 island, transport was found to be superdiffusive, with p=1.23; in the resonance layer near the 5/2 island, transport was strongly subdiffusive, with p=0.2, while particles in the chaotic domain of the m=3—5 islands was mildly

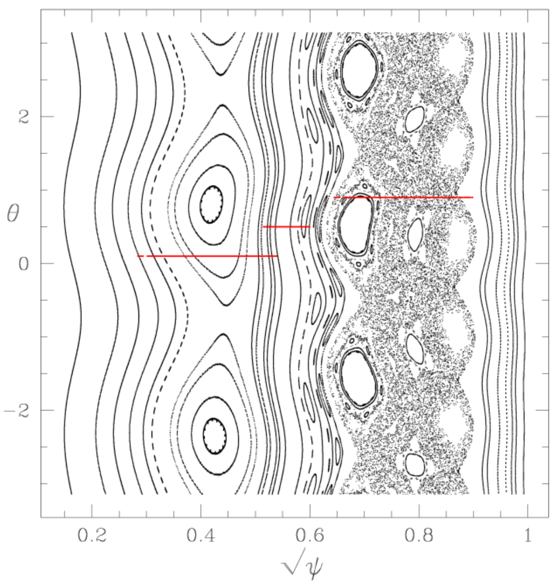

Fig. 2.37 Poincaré of co-passing, collisionless electron orbits during a pre-disruptive phase of ASDEX Upgrade

---

[24] M. Maraschek, et al., Plasma Phys. Control Fusion **60** (2018) 014047

[25] V. Igochine, et al., Nucl. Fusion **46** (2006) 741

[26] R.B. White and M.S. Chance, Phys. Fluids **27** (1984) 2455

subdiffusive, with p=0.5. This result[27] confirms the traditional picture that the 2/1 island has a fundamental role in the thermal quench preceding disruption, since it determines fast electron transport across the island, while the chaotic domain that dominates the outer part of the plasma is characterized by much slower electron transport.

2.3. *ITER DIagnostics*

2.3.1. *ITER core Thomson scattering*

Design activities of ITER core TS were put on hold in 2018 after closure of the IO/16/CT/4300001320 ITER contract by end 2017. Afterwards we have been waiting for the signature, expected early in 2019, of the Procurement Arrangement between IO and F4E to start the procurement, which will be an open call to industry for the full system. Consorzio RFX in the meanwhile has continued the contacts with IO and F4E to be ready for consultancy in the next step and has participated to the design review of the ITER divertor Thomson scattering.

2.3.2. *Diagnostic systems Engineering Services*

During 2018 the two Task Orders launched in 2017 in the framework of the “ITER Diagnostic Systems Engineering Services” contract have been almost completed.

Concerning the task TO#05 (Engineering and coordination for the Outer Vessel Steady-state Sensors, PBS 55.A5/A6) the conceptual and preliminary design of the “in-port-plug steady state sensors” have been completed and approved by ITER-Organization.[28] [29] For this activity, CAD models of the magnetic sensor assembly have been developed in collaboration with ITER Design Office (Fig. 2.39) and FEM thermal analyses have been carried out to assess the most suitable location of installation for the assembly within the Diagnostic Shielding Module (DSM) in order to achieve, in the operating conditions expected in ITER, the same operating temperature relevant for DEMO operations (300°C)

---

[27] G. Spizzo, R.White, M. Maraschek, V.Igochine, G.Granucci, the ASDEX Upgrade Team, 2018 Nucl. Fusion in press https://doi.org/10.1088/1741-4326/aaf07c

[28] P. Agostinetti, G. Gambetta, “Conceptual design of the in-vessel steady state sensors”, <RFX-ITERDES-TN-004>, 27/02/2018

[29] G. Gambetta, N. Marconato, “Preliminary design of the in-vessel steady state sensors”, <RFX-ITERDES-TN-05>, 05/12/2018

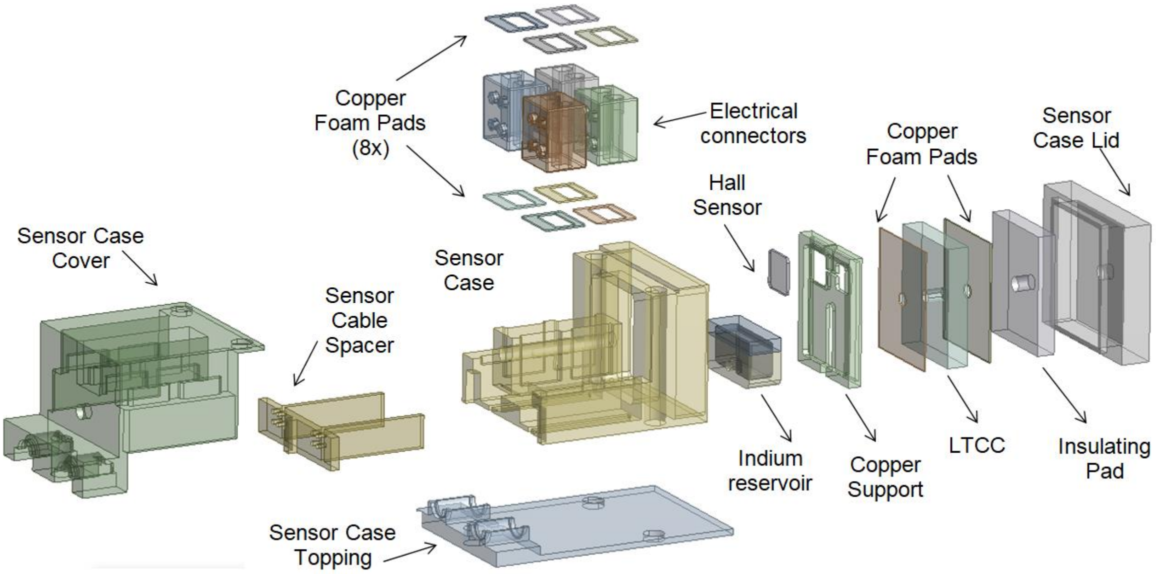

Fig. 2.39 Exploded view of the DSM magnetic sensor case assembly

In the meantime, the manufacture of the sensor assembly for the Hall sensors prototypes to be installed on the WEST tokamak, designed during 2017, has been completed and is now ready for operation (Fig. 2.38).[30]

Concerning the task TO#06 (Update of the design description and requirement documentation of the ITER magnetic diagnostic), the review and update of the "Design Description Document" of the entire ITER magnetic diagnostic system, with particular focus on the system performance assessment and on the definition of interfaces with the diagnostic sub-systems, has been completed in support of the ITER Diagnostic Team.

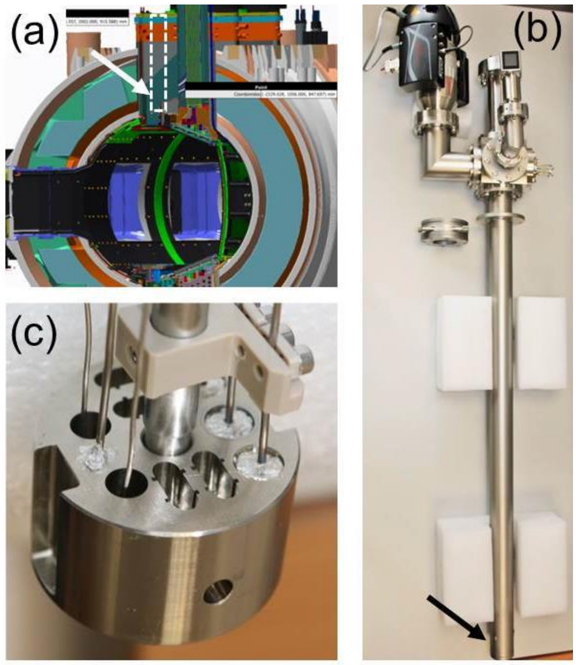

Fig. 2.38 Hall sensors system for WEST tokamak: (a) WEST cutaway view (white arrow indicating the Hall sensor holder); (b) Photograph of the holder assembly (total length ~1.5 m) with black arrow indicating the location of the sensor head; (c) head before the installation of the sensors.

[30] M.Kocan, et al., "Steady state magnetic sensors for ITER and beyond: Development and final design", Review of Scientific Instruments 89, 10J119 (2018); https://doi.org/10.1063/1.5038871

3. EUROfusion Programme

3.1. *RFX-mod: experimental, modeling activities and upgrades*

3.1.1. ***Introduction***

In 2018 the realization of the RFX-mod magnetic front-end modification has started after the award of the industrial innovation project ‘MIAIVO’, granted by Regione Veneto to Consorzio RFX in partnership with 3 companies of the Industrial District “Meccanica dell’Alto Vicentino” (ALCA Technology Srl.; Ettore Zanon Spa.; Sisma SpA) in the framework of the POR-FESR 2014-2020 (Regional Operational Program for the European Regional Development Fund). The progress in the design and implementation of such improvements, in particular related to the modification of the main machine components (Vacuum Vessel, Stabilizing Shell and First Wall) and the adaptation or development of the diagnostic systems, are summarised in Section 3.1.3 and 3.1.6 respectively.

The research activities concerning RFP physics have also progressed developing along the two general lines mentioned in 2018 activity program, i.e.:

- Discussion of RFX-mod2 scientific program and design of new diagnostic systems
- Advancement of RFX-mod data analysis and progress of the RFP modelling activities

Most of planned deliverables have been achieved, except some physiologic re-modulation of the detailed development of few topics. Among them, it is worth mentioning the MHD equilibrium and control, where, as reported in Section 3.1.14, a huge amount of work has been done, though not fully consistent with the planned specific topic; it involves 3D simulation of the effect of plasma-shell proximity on mode amplitude, real time assessment of magnetic diagnostics in RFX-mod2, magnetic equilibrium reconstruction.

3.1.2. ***Analysis of the stabilizing shell gap***

The analysis of the effect of error fields, generated by the unavoidable shell inhomogeneity due to holes for diagnostic access and toroidal and poloidal gaps for the penetration of the electric and magnetic fields, is necessary to provide guidelines for the design and implementation of the shell geometry. A previous study for RFX-mod2[31] assessed that error field reduction in a butt-joint concept with active coils would have been very challenging. A different concept, based on a separate copper sleeve extending over a wide poloidal gap, to guarantee an insulation margin, has been investigated and compared to the RFX-mod

[31] P. Bettini, L. Grando, G. Marchiori, “Feasibility study of a local active correction system of magnetic field errors in RFX-mod”, Fus. Eng. And Des., vol. 96–97 (2015) 649

overlapped one the approximated results provided by Shafranov equilibrium analysis and the results of numerical analyses by the 3D cell method code CAFÉ. Such analysis has shown that though the overlapped gap solution would be adequate from the point of view of error fields, it cannot be just replicated in RFX-mod2 due to both assembly and insulation requirements.

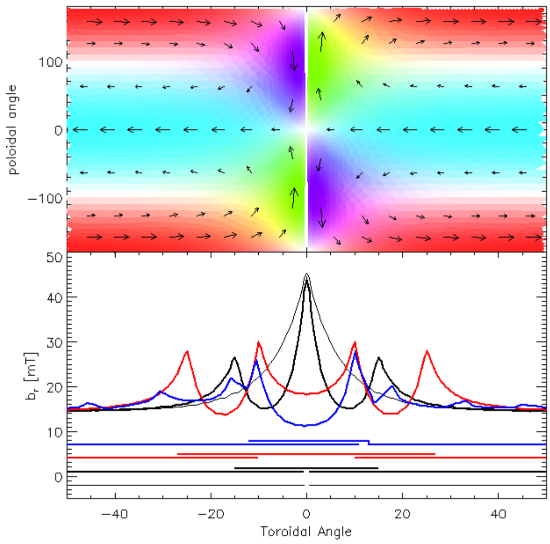

Fig. 3.1 top) Eddy current pattern for a butt-joint shell (color encodes direction, saturation encodes amplitude): bottom) radial error field in the gap region (upper traces) for different shell gap geometries schematically shown in lower traces of corresponding color

Other concepts have therefore been analyzed. Instead of the aforementioned iterative procedure, a time varying uniform vertical field only has been considered to compare the error field suppression of different shell designs. It is assumed that during the startup a vertical field reaching 30 mT in 20ms is applied. Such variation induces eddy currents in the shell which are directed in the toroidal direction except near the poloidal gap edges, where they are mainly poloidal.(upper panel of Fig. 3.1 for a butt-joint shell).

The toroidal dependence of the radial field at plasma radius, for several gap configurations, is shown in the bottom panel of Fig. 3.1. The butt-joint gap concept (thin black curve) is characterized by the highest error field. On the other hand, the RFX-mod overlapped gap solution (blue curve) is the most efficient to reduce error field, which appear in two peaks: one for each shell poloidal edge. In order to compromise between the mechanical simplicity of the butt joint gap and the field reduction properties of the overlapped gap, a concept based on a separated sleeve spanning over a toroidaly widened poloidal gap has been considered. In fact, the addition of the sleeve alone, without modifying the underlying gap, only marginally reduces the main error field (thick black line on bottom panel of Fig. 3.1 and generates two additional error field peaks corresponding to the sleeve edges. The main error field peak can only be reduced if the distance among the shell edges is increased and, correspondingly, the sleeve is widened. By adopting a sufficiently widened poloidal gap, error field peaks of amplitude comparable to the overlapped gap can be obtained, even though their number increases.

Also the Fourier spectrum of error fields plays an important role, not only their amplitude: in particular the m=1 component can be resonant with MHD modes and significantly alter the torque balance. The butt-joint single peak of localized error field is characterized by a monotonically decaying broad m=1 spectrum, both with positive and negative toroidal number n. When multiple error field peaks are present, as for the overlapped gap or the sleeve gap concepts, an interference effect occurs modulating the spectrum according to the distance among error field peaks. Two examples are shown in Fig. 3.2. Lower n (n<7) harmonics correspond to marginally stable or unstable Resistive Wall Modes: even though the plasma response will likely alter the vacuum harmonics spectrum for these helicities (as shown in Resonant Magnetic Perturbation studies performed in RFX-mod: see e.g.[32]), the RFX-mod MHD control system has routinely kept these modes at negligible levels. Higher n harmonics correspond to tearing modes; their effect on plasma is simulated by means of the cylindrical, zero pressure, spectral, RFXlocking code[33].The representation of each m=1/n=7-19 TM eigenfunction is modified in order to include the effect of the corresponding error field harmonics, which is assumed not to alter the mode amplitude at the resonant surface. The error field is kept fixed in order to have a conservative estimate of the effect on tearing mode dynamics in RFX-mod2 and, in particular, of the locking threshold. A parametric study is performed by considering the error field spectrum for the overlapped gap multiplied up to 4 times. The average mode rotation frequencies do not vary significantly unless the error field is multiplied by 4, a value that would imply an unrealistically high applied vertical field during the startup phase.

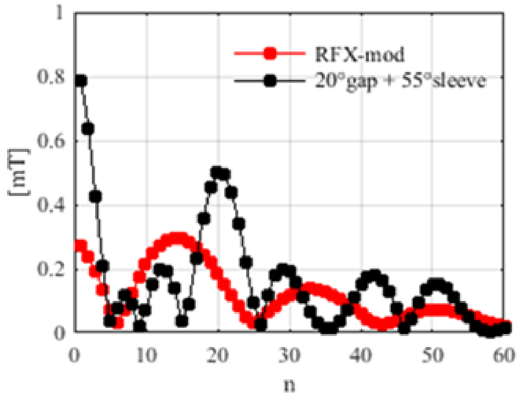

Fig. 3.2 Toroidal spectrum of m=1 error field generated by a startup error field

3.1.3. *Implementation of the machine toroidal assembly modifications*

During 2018 the activities devoted to the modification of RFX-mod experiment have been further progressed with respect to the design developed in 2017[34], focussing on the main components of the machine toroidal assembly, described in the following sub-sections. The activities have been documented in 8 Technical Reports, submitted to the technical

[32] Veranda M. et al., Nucl. Fus **57** (2017) 116029

[33] Zanca, P., et al, Plasma Phys. Control. Fusion **51** (2009) 015006

[34] S. Peruzzo et al., Detailed design of the RFX-mod2 machine load assembly, Fusion Eng. and Design, 136 (2018) 1605-1613, https://doi.org/10.1016/j.fusengdes.2018.05.066

committee or Regione Veneto as deliverables for the first phase of the MIAIVO project, and presented at 3 main international conferences.[35] [36] [37] [38]

3.1.3.1. Vacuum Tight Support Structure (VTSS)

As far as VTSS is concerned, the main issues for the design have been the integration of approximately 150 ports interfaced with other existing components and the implementation of 2 vertical and 2 horizontal vacuum-tight and electrical-insulated joints (Fig. 3.3).

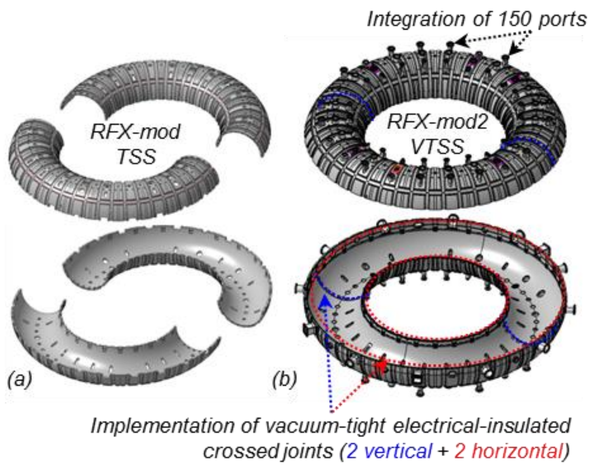

Fig. 3.3 Modification of the 'TSS' of RFX-mod (a) to the 'VTSS' of RFX-mod2 (b)

The integration of ports in the VTSS represents a potential issue due to the requirements of tight geometrical tolerances of the flanges (planarity and parallelism of the order of 0.2 mm) and uneven shape of the port pipe imposed by the existing interfaced components (coils, diagnostics, pumping and fueling). The design has been developed and shared with one of the companies involved in the "MIAIVO" project and verified by means of detailed structural analyses, specification of suitable manufacturing procedures and realization of some representative prototypes (Fig. 3.4).

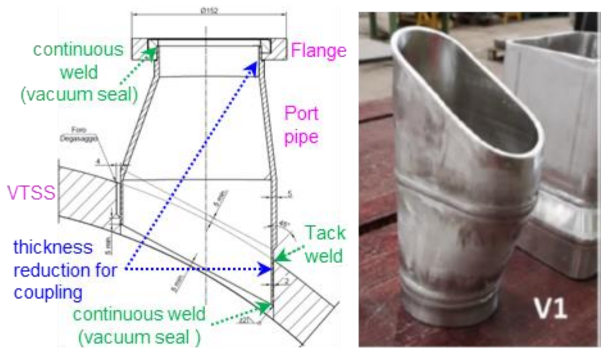

Fig. 3.4 VTSS port manufacturing procedure and prototype

---

[35] M. Spolaore, et al., "Motivations and perspectives of RFX-mod2, the challenge of the upgraded RFX-mod device", 45th European Physical Society (EPS) Conference on Plasma Physics, 2 - 6 July 2018, Prague, Czech Republic

[36] S. Peruzzo, et al., "Technological challenges for the design of the RFX-mod2 experiment", 30th Symposium on Fusion Technology (SOFT 2018), Giardini Naxos (Messina, Italy), 16-21 Sept. 2018

[37] R. Cavazzana et al. "Challenges and Solutions in the Design of RFX-Mod2, a Multi-Configuration Magnetic Confinement Experimental Device", 27th IAEA Fusion Energy Conference (FEC 2018), 22–27 Oct. 2018, Gandhinagar, India

[38] L. Marrelli et al. "From RFX-mod to RFX-mod2: perspectives of the Reversed Field Pinch configuration", 27th IAEA Fusion Energy Conference (FEC 2018), 22–27Oct.2018, Gandhinagar, India

One of the most critical aspects in the VTSS assembly is the requirement to guarantee vacuum tightness and electrical insulation at the present poloidal and toroidal gaps. With the proposed design solution the two lower and higher VTSS quarters are firstly horizontally tight jointed (blue seam in Fig. 3.3), by means of existing stud bolts, with interposed semicircular insulating spacers made of polyether–ether–ketone (PEEK) acting as "half gaskets"; vacuum tightness is provided by proper "CF knife-edge" machined in the extremely narrow room (8 mm) available on the two surfaces of the mating VTSS quarters. The two VTSS halves are then vertically jointed with interposed Viton O-rings, for vacuum tightness, and suitable PEEK and G10 fiberglass spacers for electrical and structural function (red seam in Fig. 3.3). To veriry this design concept a series of tests have been performed on a dedicated reduced-scale VTSS mock-up, which initially provided satisfactory results but unfortunately showed also some failure cases which imply the need of further investigations before freezing the final design solution. In September 2018, after a detailed metrological survey, which will be used as reference to assess possible deformations during the following manufacturing processes, the Stainless Steel Toroidal Support Structure has been delivered to Zanon workshop (Fig. 3.5).

Fig. 3.5 Loading of TSS at RFX on 6th Sept. 2018 (left); TSS at Zanon workshop (right)

3.1.3.2. Passive Stabilizing Shell (PSS)

The PSS for RFX-mod2 must be deeply modified, due to the removal of the present vessel, in order to sustain the new first wall (2016 graphite tiles) and the wide system of in-vessel diagnostics (more than 1000 electro-magnetic and thermo-mechanical sensors, Section 3.1.6.1) and to operate in vacuum conditions. The design of the new support structure has been improved with further CAD and FEM analyses. In order to sustain the electromagnetic loads expected in the worst conditions (plasma fast termination) the thermoplastic support rings have been reinforced with additional fastening bands and stiffening ribs, which still provide the suitable electrical discontinuity of the shell along the poloidal direction (Fig. 3.6).

The overlapped gap of the PSS spanning 30° along the toroidal direction, necessary to minimize magnetic error fields (Section 3.1.2), represents a potential risk of arching between

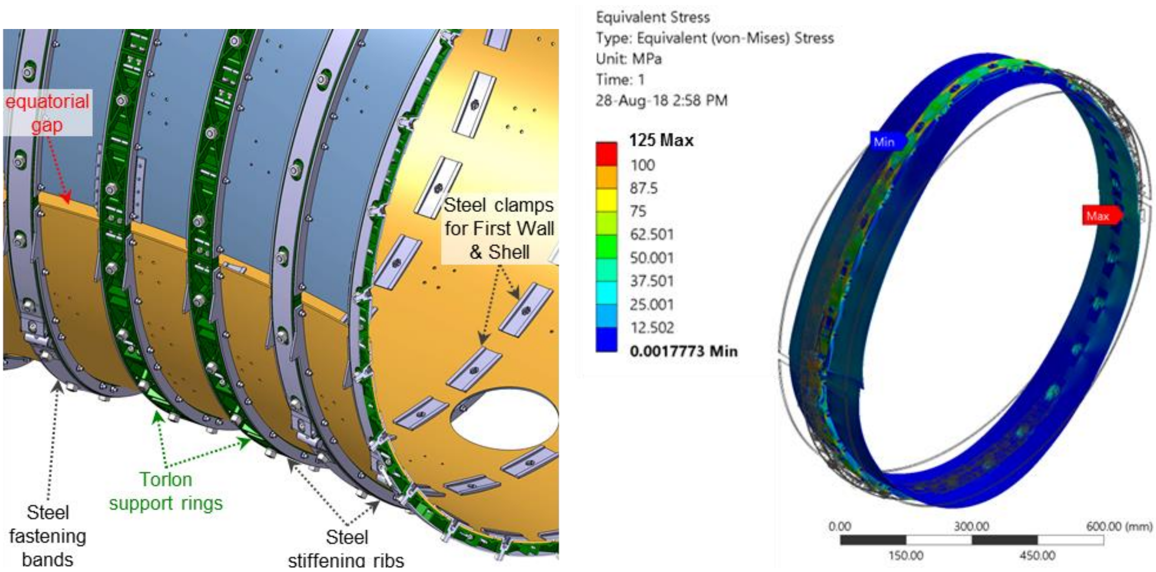

Fig. 3.6 Detail of the components of the PSS assembly (left); Equivalent stress in the PSS assembly in the worst expected condition (1/72 model of the torus) (right)

facing edges of the shell, being in contact with weakly ionized gas at the plasma boundary and potentially exposed to overvoltage of the order of 1 kV during plasma operation[39]. To minimize the risk of arching a feasibility study has been carried out aimed at obtaining an insulating Al_2O_3 coating on a wide surface of the Cu shell. Among different thermal spray coating processes, Detonation Gun Spraying (DGS)[40] has been selected, for its potential excellent bond strength, low porosity and cost effectiveness, and it was tested with a facility available at ENEA Brasimone.

The results obtained on small samples coated with different layers of alumina (Fig. 3.7) proved the capability to withstand overvoltage up to 2 kV in the operating conditions expected at plasma boundary during RFX-mod2 operation. To assess the actual reliability of the process, further tests have been planned, consisting in thermal cycles and mechanical stress. In the meantime a market survey has been started to assess the availability of suppliers for the execution of the coating on the entire RFX-mod2 shell with DGS or Air Plasma Spray as an alternative.

[39] R. Cavazzana et al., Design constraints on new vacuum components of RFX-mod2 upgrade using electrical modeling of reversed field pinch plasma, Fusion Engineering and Design, 136 (2018) 1209-1213, https://doi.org/10.1016/j.fusengdes.2018.04.103

[40] S. Lakhwinder et al., A Review on Detonation Gun Sprayed Coatings", Journal of Minerals & Materials Characterization & Engineering, 11 (2012) 243-265

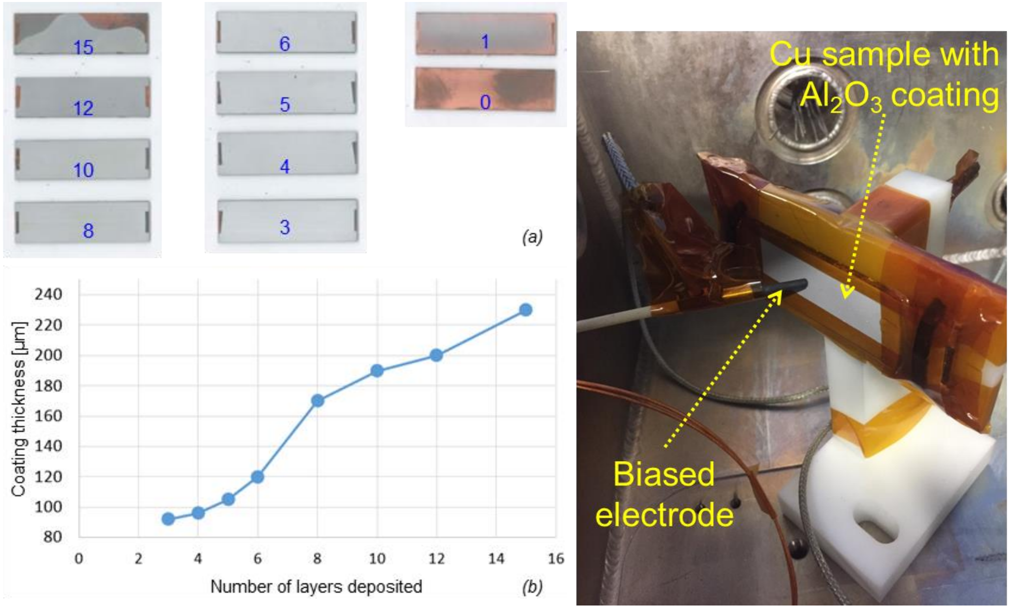

Fig. 3.7 (a) Cu samples (100 x 30 x 3 mm) with different number of coating layers deposited; (b) coating thickness as a function of number of layers (left); experimental setup for electrical insulation withstand tests (< 3kV) in weakly ionized plasma (ne~ 10^{15} m-3; Te ~ 1eV) (right)

3.1.3.3. First Wall (FW)

The new First Wall for RFX-mod2 derives basically from the existing RFX-mod FW, characterised by the same locking system compatible with the existing remote handling system and with modified geometrical dimensions to protect the wider surface of the shell and to minimise the plasma wall interaction. The design of the FW thas been almost completed with the overall CAD modeling (Fig. 3.8) and suitable structural verification of the tiles in standard and abnormal operating conditions. Minor modifications are still under refinement to meet the interface requirements with the in-vessel sensors and viewing diagnostic systems.

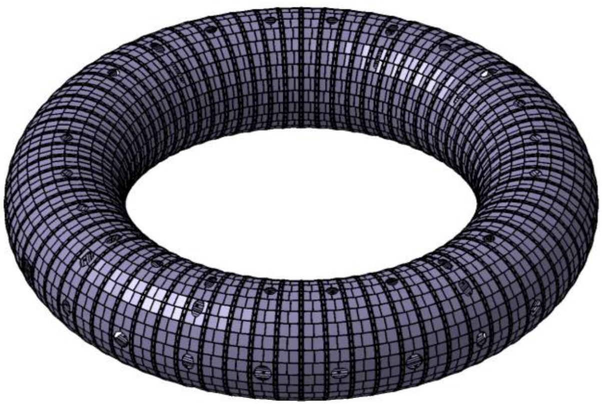

Fig. 3.8 First Wall assembly

3.1.4. *Design of the Glow Discharge Cleaning (GDC) system*

After a dedicated analysis carried out in 2017, and though possibly in the first campaigns the same system operating for RFX-mod will be available, some guidelines for the design of a more efficient glow discharge plant for RFX-mod2 have been assesed[41]. Total anodes area as large as possible should be foreseen, in order to mitigate the deformation of the profile of teh ion current density at the wall. Small anodes are indeed related to larger non-uniformity and also require more electric power to sustain the current. The most favourable pressure is close to the threshold value below which the voltage to sustain the discharge rises. It has also been found that anodes can be integrated into the first wall tiles without affecting the ion current distribution..

3.1.5. ***Development of the RFX-mod2 scientific programme***

In 2018 a group of physicists has analysed the research lines to be proposed for the first experimental campaigns in RFX-mod2, on the basis of the RFX-mod experience and, mostly, to explore as soon as possible the effectiveness of the modifications and the potentialities of the new device. The main topics enatiled where: extension of experimental scenarios, energy and particle transport in QSH, edge and SOL physics, Tokamak plasmas, theory and modelling developments. An internal note is being produced to be shared and discussed with the laboratory in a dedicated series of meetings. After the completion of the scientific discussion (in 2019), the final document will be released.

3.1.6. ***Design of new diagnostic systems for RFX-mod2***

3.1.6.1. Internal Magnetic and Electrostatic sensors

The final layout of an extended set of in vessel magnetic probe is still to be finalized, being a study of different arrangement still undergoing. The current baseline design is summarized in Table 3.1[42]. The toroidal arrays for toroidal and radial field will improve the reconstruction capability of the time evolving helical structure, resolving m=1 modes with n number up to 36, and estimating the amplitude and phase of m=(0, ±1,±2) at each n. This will allow not only more precise field and Poincare map reconstruction with respect to RFX-mod, but also an improved mode control capability. The 12 poloidal arrays of three-axes probes are placed in a checker-board configuration, so that the equivalent expected resolution is roughly equivalent to 6 arrays of 28 sensors aimed at measuring the total plasma current and at resolving modes and structures in the range n=1,2; m=-13..+14. This latter feature is mainly devoted to the reconstruction of the LCFS in shaped tokamak configuration, where the

---

[41] A. Canton et al.,"designing high efficiency glow discharge cleaning systems" 23rd PSI Conference, Princeton, NJ, USA (2018), submitted to Nuclear Mat. And Energy

[42] R. Cavazzana et al.,"Challenges and solutions in the design of RFX-mod2, a multiconfiguration magnetic confinement experimental device", Proc. 27th IAEA FEC Conference, Gandhinagar (2018, to be submitted to Nucl. Fus.)

MEASUREMENT	PROBE TYPE	LAYOUT
Local field B_r, B_t, B_p + plasma current	Three axes pick-up	12 poloidal arrays x 14 probes
Local toroidal field B_t	Single axis pick-up	6 toroidal arrays x 72 probes
Average radial Field B_r	Saddle loop	8 toroidal arrays x 72 probes
Toroidal loop voltage and poloidal flux	Single loop	8+8 loops
Poloidal loop voltage and toroidal flux	Single loop	12 loops

Table 3.1 Layout of magnetic measurements

toroidal periodicity is of low order. The pick-up coils are designed with a reference area of 0.025 m^2, which ensure enough signal for good signal integration and with a final bandwidth at the transmission line end of 200 kHz to allow the study of a broad range of magnetic modes and fluctuations, such as tearing modes, sawtooth crashes and reconnection events.

A wide layout of poloidal and toroidal arrays of langmuir probes embedded in the First Wall tiles (Fig. 3.9) has been defined for a total of 400 electrostatic sensors aimed at monitoring plasma density, particle and energy fluxes, plasma potential, electron temperature and other related quantities. The finalization of the design is still undergoing with the details of the interface with the copper shell and cabling up to the feedthrough.

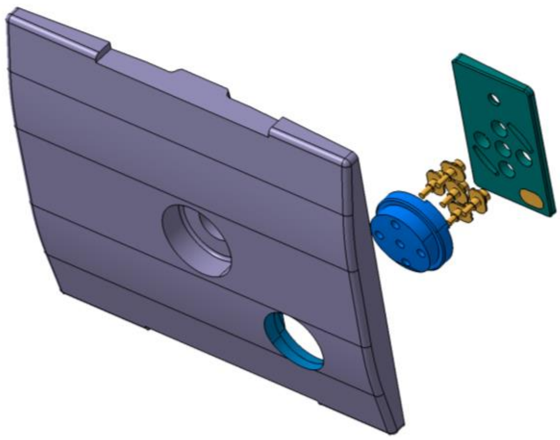

Fig. 3.9 exploded view of the Langmuir probe (5 pin balanced configuration) embedded in a FW tile

3.1.6.2. Neutron and γ-ray detectors

A neutron and g-ray detector has been developed (2017) and installed (2018) on the MST Reversed Field Pinch. The diagnostic has been successfully installed and calibrated. First results have been presented at 2nd Asia-Pacific Conference on Plasma Physics (sec. 3.1.12) [43]

3.1.6.3. Fast reciprocating manipulator (FaRM)

No specific activity was needed in 2018, the design of the system is ready for procurement, once budget is assigned

3.1.6.4. Crystal spectrometer

A crystal spectrometer used in the past on FTU[44][45][46][47] (where a large experience on this diagnostic is available) will be installed on RFX-mod2, to provide core ion temperature and possibly rotation velocity- measurements by observing lines from Neon and Argon (to be puffed/injected into the plasma). The system is based on a Johan scheme. In 2018 a preliminary study of the layout has been done. Crystals have been obtained via the on-going JET Dispersal of Assets procedures, while the choice of the detector will be defined in 2019.

3.1.6.5. Temperature and SXR diagnostics

A new beam dump for Thomson scattering laser has been designed, to double the laser path thus improving signal-to-noise ratio. New Multi Pixel Photon Counte (MPPC) detectors combined with organic scintillators have been characterised for the RFX-mod2 SXR diagnostic[48]. Such detectors proved to work in geometries and energy ranges of interest for RFX-mod2 (3-10 keV), though the energy discrimination of incident photons is challenging. To increase the photon budget, a double detector layout could be adopted.-

3.1.7. ***Loan of the AIST 1MW neutral beam***

The 1 MW neutral beam injector on loan from AIST, Tsukuba, will be applied to RFX-mod2 (in addition to the diagnostic Neutral Beam already installed in RFX-mod) in order to measure ion temperature and flow and to address the study of the fast ions confinement. In agreement with our Japanese colleagues the system has been lent free of charge to Tokamak Energy Ltd, Cullham Innovation Center for a period of three years. The system has

---

[43] L. Cordaro et al.,*Neutron-gamma measurements at the Madison symmetric Torus* presentation at 2nd Asia-Pacific Conference on Plasma Physics, 2018, Kanazawa, Japan

[44] R. Bartiromo, F. Bombarda, R. Giannella, Nucl. Instr. And Methods in Physics Res. B9, 679 (1985)

[45] R. Bartiromo, F. Bombarda, R. Giannella, Phys. Rev. A, 32, 531 (1985)

[46] D. Pacella, M. leigheb, M. Mattioli, Phys. Scripta 57, 265 (1998)

[47] R. Bartiromo, et al., workshop for Diagnosis of Contemporary Fusion Experiments, Book Series: International School of Plasma Phys. piero Caldirola, vol. 9, pag. 959

[48] A. Fassina, P. Franz, 45th EPS Conf. on Plasma Physics, Prague, p. P5.1004 (2018)

been shipped in July, and is presently being installed with some modification on the spherical Tokamak. This will allow to get acquainted with the injector and anticipate any required adaptation before the installation on RFX-mod2.

3.1.8. *Theory, modelling and data analysis related to RFP helical states*

Advancements in the study of magnetic chaos reduction and transport barrier formation in helical topology have been achieved during 2018 in collaboration with Pisa University (Prof. Pegoraro), Istituto Sistemi Complessi CNR (Dr. Grasso) and ENEA-Frascati (Dr. Falessi). A refined technique has been developed and then applied to first RFP numerical cases

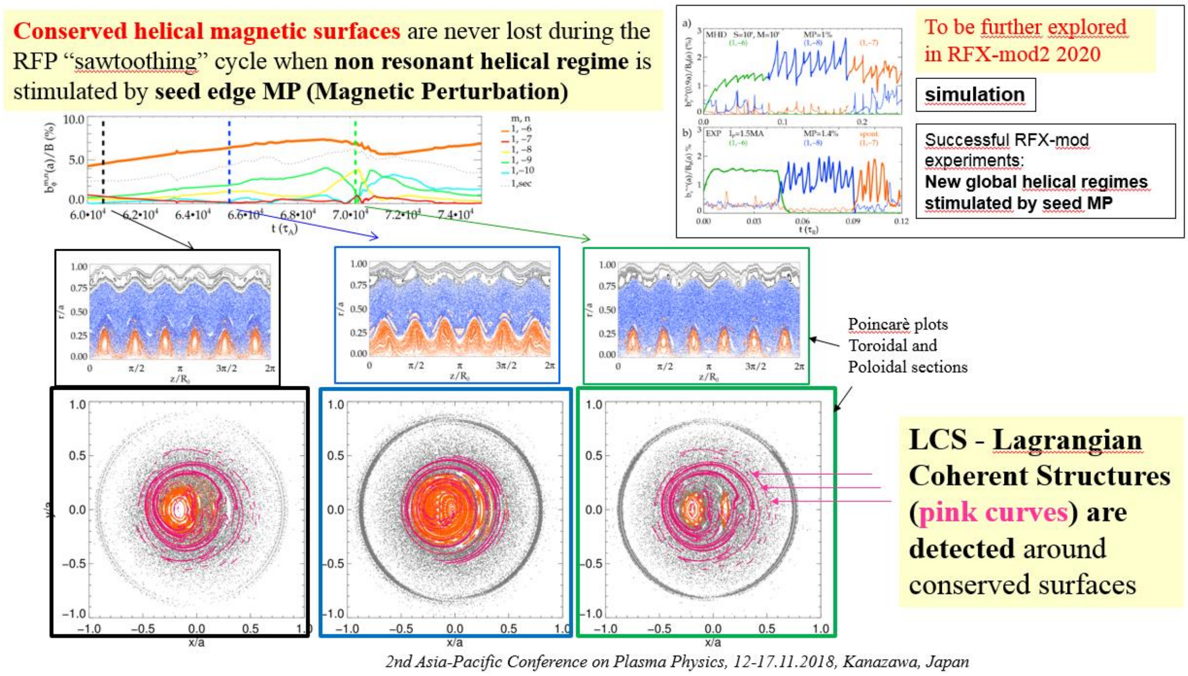

Fig. 3.10 Magnetic chaos healing and formation of Lagrangian Coherent Structures provide a possible explanation for the formation of transport barriers observed in RFX-mod helical regimes

(obtained in 3D nonlinear MHD modelling) aiming to detect Lagrangian Coherent Structures, i.e. small leakage surfaces acting as confining structures hidden in the chaotic sea of weakly chaotic regimesa shown in Fig. 3.10 [49,50,51,52,53] -.

---

49 G. Di Giannatale, M.V. Falessi, D. Grasso, F. Pegoraro and T.J.Schep Physics of Plasmas 25, 052307 (2018); https://doi.org/10.1063/1.5020164

[50] G. Di Giannatale, M.V. Falessi, D. Grasso, F. Pegoraro and T.J.Schep Physics of Plasmas 25, 052306 (2018); https://doi.org/10.1063/1.5020163

[51] G. Di Giannatale, M.V. Falessi, D. Grasso, F. Pegoraro, T.J.Schep, M. Veranda, D. Bonfiglio and S. Cappello Journal of Physics: Conf. Series 1125 (**2018**) 012008 doi:10.1088/1742-6596/1125/1/012008

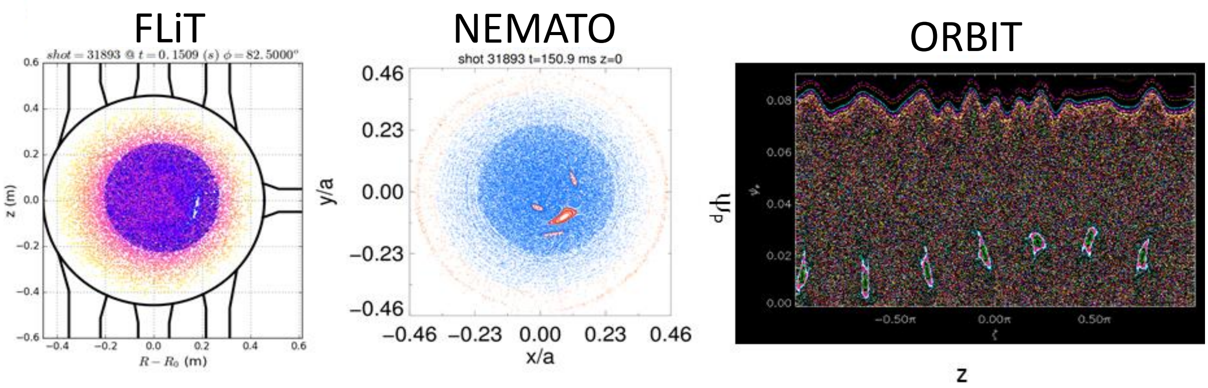

Fig. 3.11 Comparison of magnetic equilibrium reconstruction obtained by different codes in a stimulated QSH

The inclusion of an *ad hoc* momentum source has been recently implemented (3D nonlinear MHD modeling codes SpeCyl and PIXIE3D). A first sistematic study shows that plasma rotations (with experimentally relevant amplitude) can facilitate the transition to helical regimes; in addition, a thorough analysis of experimental-like numerical simulations revealed the transient excitation of Alfvénic waves after the sawtooth crashes, which characterizes both numerical and experimental transition (dithering) to helical regimes[54], [55]. The comparison with experimental observations is described in the following

A thorough comparison of the new helical regimes[56] obtained both in 3D nonlinear MHD modeling and in RFX-mod first experimental tests has been carried on. In particular, during 2018, the experimental magnetic field reconstructions have been elaborated in order to be analized with the NEMATO volume preserving code (which together with PIXIE3D is available at RFX thanks to the longstanding collaboration with Dr. Luis Chacon – LANL). As a first step, NEMATO reconstructions are being compared with those from other numerical tools (example in Fig. 3.11, work presently in progress).

The analysis of temperature profiles in discharges with seed perturbations inducing helical states with different helicities has progressed: an example is shown in Fig. 3.12, comparing

---

[52] Pegoraro, Bonfiglio, Cappello, DiGiannatale, Falessi, Grasso, Veranda, submitted PPCF

[53] Cappello et al “Negotiating with magnetic self-organization in confined plasmas ” invited presentation at 2nd Asia-Pacific Conference on Plasma Physics, 2018, Kanazawa, Japan

[54] Bonfiglio et al,” Alfvén waves in RFP plasmas: nonlinear 3D MHD modeling and comparison with RFX-mod”, http://meetings.aps.org/Meeting/DPP18/Session/UP11.9V APS-DPP (**2018**)

[55] Veranda et al http://ocs.ciemat.es/EPS2018PAP/pdf/P2.1060.pdf EPS p2.1060 (**2018**)

[56] Veranda et al “Magnetohydrodynamics modelling successfully predicts new helical states in reversed-field pinch fusion plasmas” Nucl. Fusion 57 (**2017**) 116029

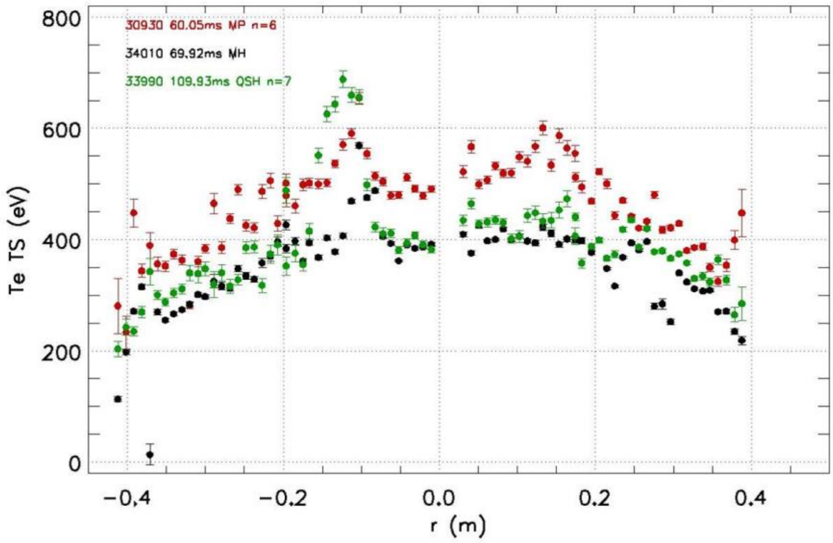

Fig. 3.12 Electron temperature profiles from Thomson scattering in a Multiple Helicity (black), n=7 QSH (green) and n=6 QSH (red)

a Multiple Helicity profile with n=7 and n=6 QSH's in discharges at the same current (1.2MA) and density (4 $10^{19}m^{-3}$); however, this analysis is still in progress and conclusions about a comparison among different helicities cannot be drawn yet : the analysis will proceed in 2019.

By using Hamiltonian neo-adiabatic theory, it has been shown in a simpified geometry applicable -for the moment- to Solar Corona heating issue, that, in contrast with standard views, an irreversible energy transfer from a low frequency Alfvén wave to a charged particle can take place, and that a single low-frequency Alfvén wave can provide a relevant heating of this corona [57].

In addition, the contact established in 2018 with experts of the JOREK team at the *Course on non-linear extended MHD code JOREK*, in view of our contribution on modelling of JET-Mitigation of the disruption (section), offered the opportunity to perform a more general comparison with the 3DMHD codes available at RFX. In fact, first steps were performed toward a comparison/benchmarck of the SpeCyl and PIXIE3D codes with the code "Discontinuous Galerkin Spectral Element Method for nonlinear resistive MHD in 3D geometry" (under development by Florian Hindenlang and Eric Sonnendruecker at the MPI-IPP Numerical Methods in Plasma Physics (NMPP) division)[58].

---

[57] Escande, Gondret, Sattin; "A single low-frequency Alfvén wave can provide a relevant heating of the solar corona", submitted PRL ; preprint available HAL: https://hal.archives-ouvertes.fr/hal-01929112 (**2018**)

[58] F. Hindenlang visit 2018/10/15-19 - RFX seminar 2018/10/16 (**2018**)

3.1.9. ***Assessment of RFP scaling laws***

RFX-mod database has been further analysed as a basis for a preliminary design of a hybrid reactor with a RFP fusion core. In particular, a scaling of electron temperature with current density as $T_e \propto J^{1.1}$ has been assessed. From such relation, and assuming Spitzer-like resistivity dependence ($T_e^{5/2} \propto J\tau_E$) and no dependence of τ_E on minor radius, the following loop voltage scaling is obtained: $V \propto R\, I_p^{-0.65}\, a^{-0.35}$.

Based on such scaling, a preliminary design of a FFH reactor wibased on a RFP magnetic configuration shows on the electromagnetic side the possibility to reach 20 MA plasma current with presently available technologies, which can be combined to the relatively simplicity of this solution both as construction and for remote maintenance[59].

3.1.10. ***Transport studies***

Microturbulence studies. In 2018 the activity in microturbulence was planned to be basically on the relation between microtearing modes and electron transport barrier. Actually the studies have been focused on the behaviour of microtearing (MT) and also electron temperature gradient (ETG) driven instabilities in helical states[60],[61]. Helical states in the RFP have positive impact on the performance, including the occurrence of electron transport barriers with strong temperature gradients. However, in presence of such strong gradients, which are related to reduced stochastic transport, radially localized microturbulence is likely to devolop becoming important as transport driving mechanism in the region surrounding the helical core. In fact, in previous years it was found that in helical states the ITG microturbulence growth rate is higher than in axisymmetric states[62]. In 2018 the gyrokinetic GENE code applied too the magnetic equilibria calculated by VMEC+GIST has been used to focus on ETG instabilities at $\beta \neq 0$ and $\nu \neq 0$ with realistic magnetic 3D equilibria. Both MT and ETG modes have been found to be unstable only across the barrier.

Compared to the axisymmetric case, as for ITG it has been found that both MT and ETG modes have higher growth rates (with ETG particularly stabilized in the axisymmetric case), see an example in Fig. 3.13, where solid lines corerspond to MT and dashed lines to ETG.

---

[59] R. Piovan et al., 3th Int. Conf.on fusion Neutron Sources and Subcritical fission systems (FUNFI), Hefei, anhui, China (2018), invited talk

[60] Predebon I. et al., Asia-Pacific Conference on Plasma Physics, Kanazawa, Nov.12-17 2018 (2018)

[61] Predebon I. et al.,Joint Varenna-Lausanne Int. Workshop on Theory of Fusion Plasmas, Varenna,Aug.27-31 2018 (2018)

[62] M. Zuin et al., Nucl. Fusion 57 102012 (2017)

Transport in presence of magnetic islands. MT modes have also been experimentally measured in RFX-mod. Recently, an interpretation based on such measurements has been proposed for the results obtained by the MAXs transport code[63] comparing DAx (Double Axis) and SHAx (Single Helical axis) plasmas. MAXs is a code based on a Multiple Domain Scheme which allows the description of transport in presence of magnetic islands. It has been applied both to RFX-mod and LHD plasmas. More specifically, the thermal diffusivity corresponding to the temperature gradient region in DAx and SHAx plasmas have been compared (see Fig. 3.15 for the temperature profiles in the two regimes). The result is shown in Fig. 3.14, indicating a lower thermal diffusivity corresponding to DAxs. Correspondingly, different MT spectra are measured in the two configurations, with SHAXs related to a more peaked spectrum. A sound interpretation will require dedicated non linear gyrokinetic simulations.

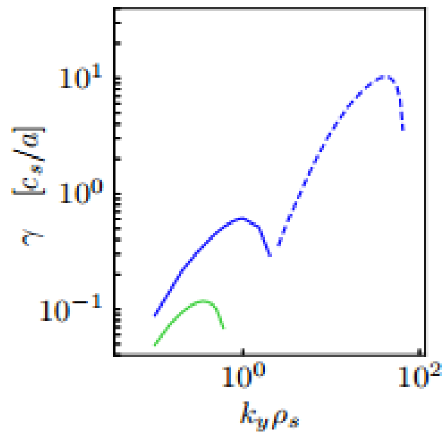

Fig. 3.13 Growth rate of MT (solid) and ETG (dashed modes in 3D helical geometry (blue) and axisymmetric geometry (green) at the barrier.

Fig. 3.13

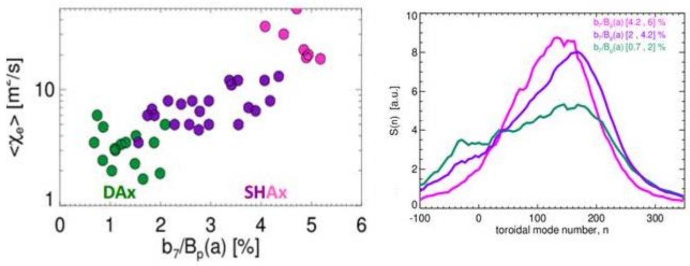

Fig. 3.14 Thermal diffusivity in DAx and SHAx RFX-mod plasmas and, for comparison three experimental MT spectra (green DAx, violet & pink SHA

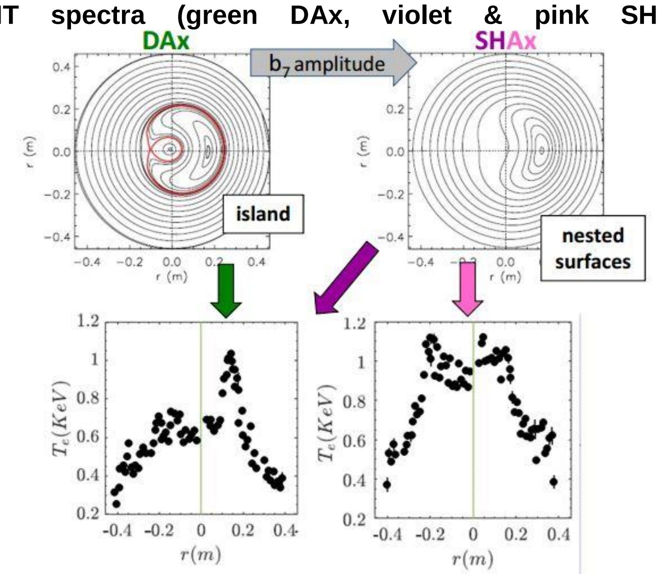

Fig. 3.15 Comparison of DAx and SHAx magnetic surfaces with the corresponding temperature profiles

3.1.11. *Impurities*

In the perspective of performing impurity studies in RFX-mod2 exploiting the TESPEL (Tracer Encapsulated Solid Pellet) diagnostic by the injection of heavy impurities in the plasma core, a modelling activity has

[63] F. Auriemma et al., Nucl. Fus.58 096037 (2018)

started in 2018. Impurity simulations are currently caaried out by 1D codes (with the usual radius or with the helical flux as radial coordinate). Such codes are now being modified in order to include an internal source term. In the meanwhile, an extensive benchmark and updating of the atomic physics is in progress, comparing ADAS database with data used in the ITC code.-[64]

3.1.12. *Edge physics and Plasma-wall interaction: 2d filaments dynamics in tokamak plasmas*

Filaments propagation from the edge to the SOL and vice versa couples the turbulence of these two regions which might enhance the Scrape-Off-Layer (SOL) fluctuation and the interaction with plasma-facing components. In addition, the intensification of cross-field transport provided by filaments might compete with parallel transport and so impact the heat flux width at the divertor. On the other hand, ExB shear regulates perpendicular velocity, inhibiting the turbulence growth and decoupling edge-SOL turbulence[65]. The aim of this work was to study turbulent filaments in different plasma conditions in the RFX-mod running as a tokamak; from the regular ohmic L-mode to H-mode: ELMy and free-ELMs (both induced by biasing technique). Results reported here were presented at the EPS conference 2018 [66][67]and preliminary results on 2D features of ELMy bursts observed in RFX-mod tokamak were reported in[68] . The 2D filament dynamics was captured through measurements with the U-probe by applying conditional average in the extreme events of an ion saturation current signal (I_s) considered as reference. Fig. 3.16 shows the I_s blob dynamics in different radial position (at the top) and the floating potential (Φ_f) map at different time slices (at the bottom), both showing outward propagation. 2D cross-correlation was applied to obtain their 2D

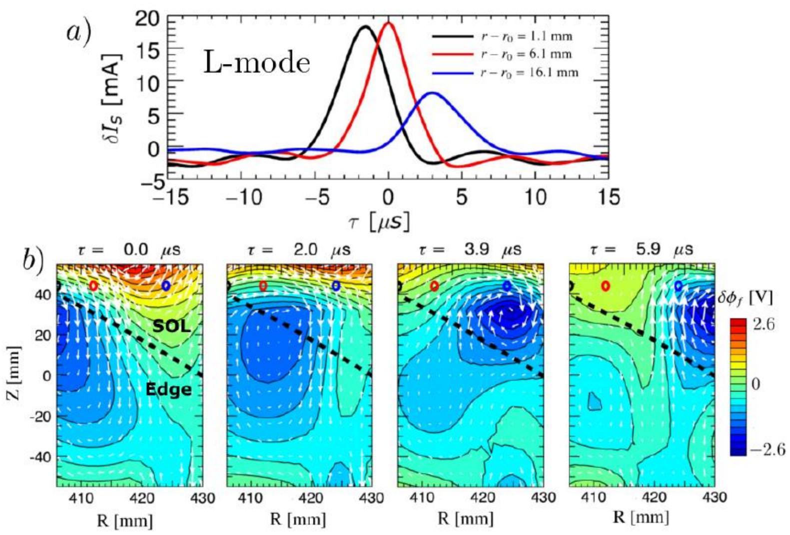

Fig. 3.16 The conditional average of filaments detected with the threshold criterion seen by a) the ion saturation signals (the redline is the reference) and b) 2D floating potential map in four frames (#39136). The white arrows represent the ExB flow

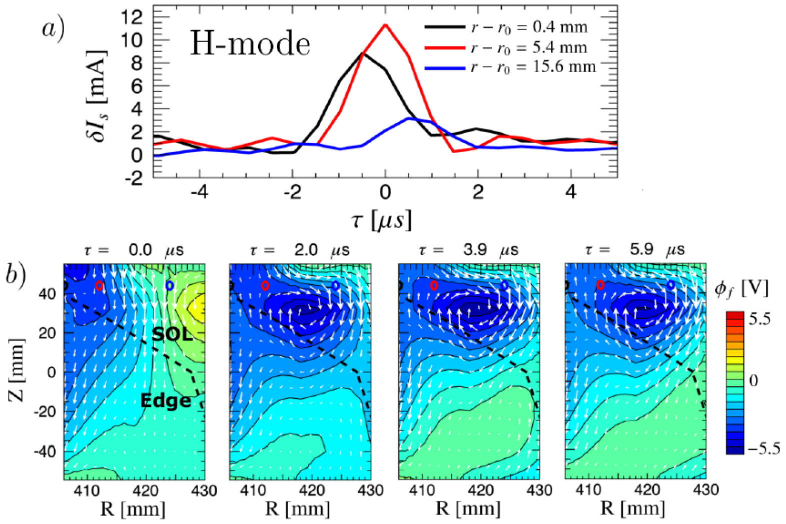

Fig. 3.17 Same as previous figure but for the H-mode regime induced by electrode biasing

velocity and size, as well as other relevant parameters . In H-mode, filaments are trapped and dissipated at the shear layer location (Fig. 3.17), while they travel freely into the far SOL in L-mode, with typically radial velocity of 2.5 km/s. In the ELMy phase, the relaxation of the transport barrier allows bigger and/or slower structures to endure the background flow shear and then reach outer regions.

Effect of high n mode locking in helical plasma-wall interaction The effect of toroidal harmonic m=1 with 7<n<23 (secondary modes) in QSH plasmas has been analysed in detail[69]. The secondary modes develop an interfernce pattern which produces a deformation of the the magnetic field lines in large poloidal lobes. The latter hit the plasma facing components, resembling the toroidal "homoclinic lobes" observed in the Tokamak divertor with RMP application.

The local parameter $S_k=\Delta_{sec}/\Delta_{1/7}$ (with Δ_{sec} and $\Delta_{1/7}$ displacements related to local secondary and dominant modes respectively) has been assumed as a good estimator of the PWI strength. It has been found to be very well correlated with the global parameter $b_{sec}/b_{1/7}$, which is in turn related to core diffusivity[70], but in addition also contains information on the mode phase.

As shown in Fig. 3.18, the condition $S_k<0.7$ corresponds to $b_{sec}/b_{1/7}<0.3$ that was found to be a threshold for the development of electron temperature transport barriers. The relevance of

[69] P. Scarin, M.Agostini, G. Spizzo, M. Veranda, "Helical Plasma-Wall interaction in the RFX-mod: effects of high-n mode locking", Proc. 27th IAEA FEC Conference, Gandhinagar (2018, to be submitted to Nucl. Fus.)

[70] F. Auriemma et al., Nucl. Fus. 55 043010 (2015)

the S_k parameter has been investigated in terms of magnetic topology by evaluating the connection length to the wall L_{cw} (calculated by the ORBIT code) in a QSH state as shown in Fig. 3.19. In the locking region the connection length $(L_{cw,hole})$ is always about one order of magnitude smaller than average value, moreover it is also lower than the Kolmogorov length L_k. Therefore, using the RMP terminology, transport in the locking region is laminar $(L_{cw,hole} < L_k)$, while outside a well-formed, ergodic SOL is present $(\langle L_{cw}\rangle > L_k)$.

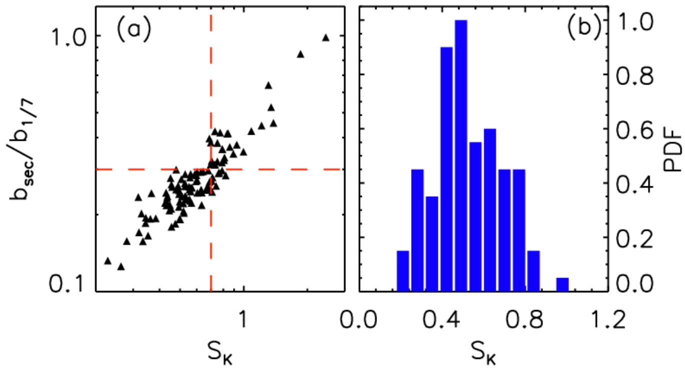

c

Fig. 3.18 (a) Linear trend of global parameter linked to the experimental core diffusivity $b_{sec}/b_{1,7}$ toward the local one S_k indicating the level of radial locking deformation; (b) Probability Dendity Function of QSH frames with electron transport barrier toward S_k

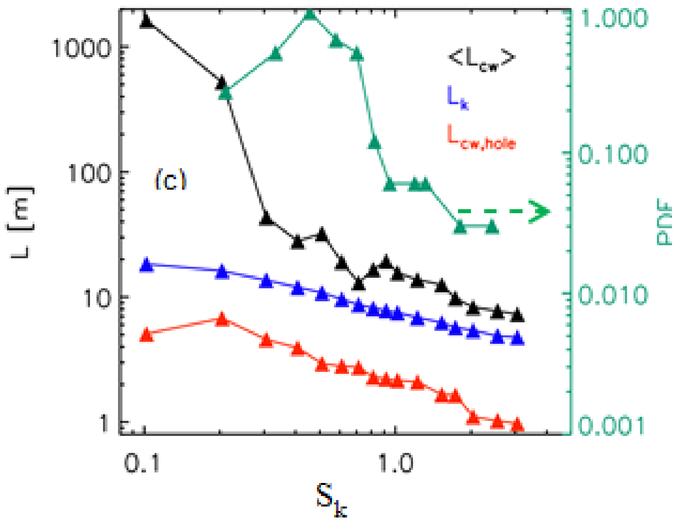

Fig. 3.19 Full scaling of L_{cw} parameter with S_k

The connection length L_{cw} has a threshold-like behaviour,increasing by an order of magnitude below S_k~0. This threshold indicates that, by decreasing the amplitude of the secondary modes, one could in principle gain one order of magnitude in the value of $\langle L_{cw}\rangle$. In the upgraded RFX-mod2, a decrease of the magnetic field deformation of about a factor 2 is expected that would be equivalent (for the same $\Delta_{1/7}$ of RFX-mod) to reach S_k<0.3 with an associated increase of $\langle L_{cw}\rangle$ and a better edge ergodic region outside the locking.

3.1.13. *Fast particles*

Alfvenic activity studies In the RFX-mod device, long wavelength high frequency (>400kHZ) modes have been detected, whose amplitude is found to be enhanced during the spontaneous reconnection processes characterizing the RFP dynamics[71]. The Alfvénic nature of such fluctuation has been deduced by the linear dependence of the associated frequency on the Alfvén velocity in a variety of experimental conditions, with different plasma current and electron density values and isotope masses. Moreover, a lower frequency branch of discrete coherent Alfvén eigenmodes has been observed to be destabilized in RFX-mod when the spontaneous transition from an axysimmetric to a single helical equilibrium occurs at high plasma current levels (above 1MA).

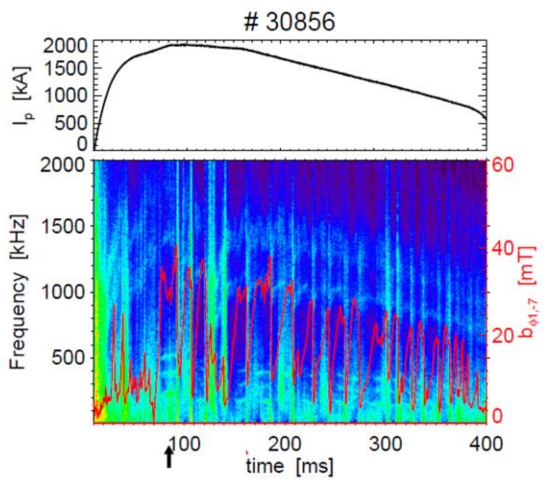

Fig. 3.21 (top) time trace of the plasma current in a RFX-mod shot; (bottom) spectrogram of dBp/dt signal. In red, time trace of the amplitude of the toroidal component of the m/n=1/7 dominant mode

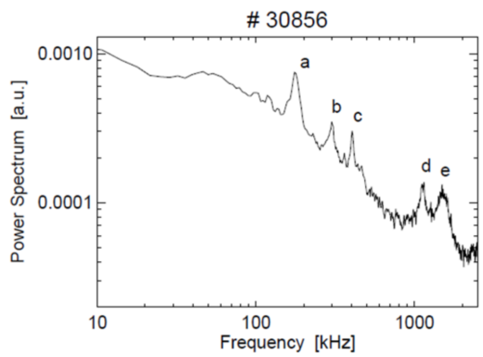

Fig. 3.21 Power spectrum measured around t=85ms (black arrow in fig. 3.4), showing 5 coherent modes

In Fig. 3.21 an example is shown of a color-coded contour spectrogram, i.e. the frequency power spectrum resolved in time, of a signal from a single magnetic probe, measuring the time derivative of the poloidal magnetic field fluctuation collected in a high plasma current RFP discharge. The red overplotted curve is the time behavior amplitude of the amplitude of the toroidal component of the dominant m/n=1/7 mode. The power spectrum at a given time interval, indicated in Fig. 3.21 with a vertical arrow, exhibit five clear coherent peaks, named a-e, as shown in Fig. 3.21. The first three, at lower frequencies (normally below 500 kHz) are the ones emerging when the helical axis states form, while the two at higher frequency are almost ubiquitously present in RFX-mod spectra.

The long wavelength nature of the observed modes has been deduced by applying the two-point analysis technique to signals coming from high-frequency in-vessel magnetic coils located in various poloidal and toroidal positions at the edge of the plasma column.

The spectral properties of such instabilities have been compared to those predicted by dedicated numerical simulations performed with the 3D MHD nonlinear visco-resisitive code

---

[71]] S. Spagnolo et al., Nucl. Fusion 51, 083038 (2011)

SpeCyl. The modeling results suggest that reconnection processes, which almost cyclically occur in the RFP plasmas, can destabilize long wavelength Global Alfvén eigenmodes, not damped at radial locations where a minimum of the Alfvén continuum occurs, as well as compressional modes, whose dispersion relation is a solution of the magnetosonic Alfvén waves. It is interesting to note that the compressional branch of the Alfvén spectrum is normally disregarded in Tokamak plasmas, because of the associated very high frequency.

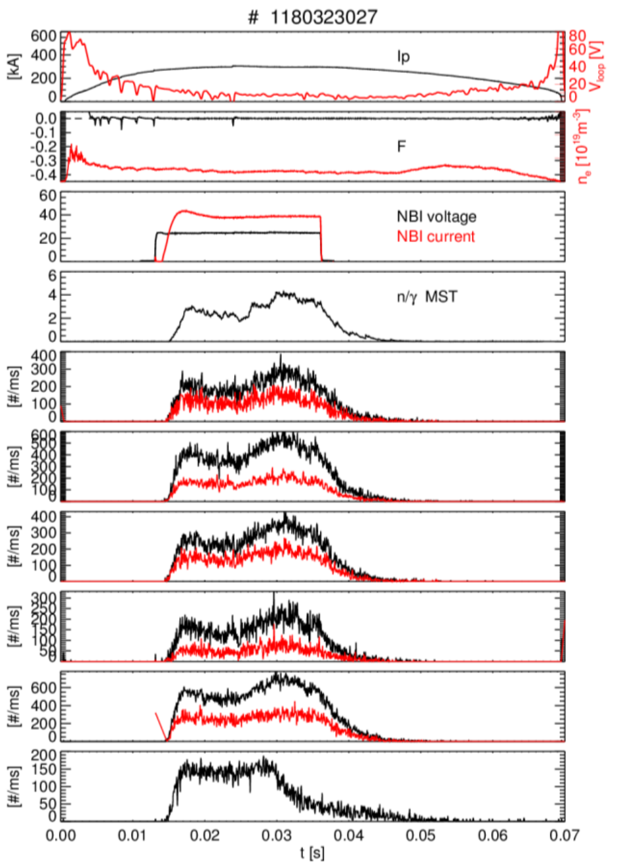

Fig. 3.22 MST plasma discharge, from top to bottom: plasma current (black) and loop voltage (red); reversal parameter (black) and electron density (red); beam voltage and current;signal from the low rtime esolution neutron-gamma detector; 6 channels (corresponding to 6 lines of sight) from the new fast system, showing neutron (black) and neutron + gamma (red) signals

Preliminary results from neutron-gamma-rays measurements in MST. The system installed and calibrated in MST has been operated in a wide range of operation conditions, both with and without the injection of a neutral beam (25 keV, 40 A). As an example, Fig. 3.22 MST plasma discharge, from top to bottom: plasma current (black) and loop voltage (red); reversal parameter (black) and electron density (red); beam voltage and current;signal from the low rtime esolution neutron-gamma detector; 6 channels (corresponding to 6 lines of sight) from the new fast system, showing neutron (black) and neutron + gamma (red) signalsshows the time traces from the six channels of the new detector in a plasma discharge with beam injection, highlighting the strong improved time resolution with respect to the previously used detector (also shown).First preliminary analyses show an excellent time resolution and the capability of the diagnostic of withstanding high neutron and gamma-rays flow, up to several Mcounts/ms[72]. The evaluation of the signal decay time after beam switching-off allows the estimate of the fast particle confinement time.Thanks to the very high time resolution, very

[72] L. Cordaro et al., .,"Neutron-gamma measurements at the Madison symmetric Torus" presentation at 2nd Asia-Pacific Conference on Plasma Physics, 2018, Kanazawa, Japan

fast processes as those occurring at reconnections can be studied, when transient peaks of both neutron and gamma rays are detected.

3.1.14. *MHD equilibrium and control*

3D simulation of mode amplitude dependence on plasma-shell proximity. In order to predict the m=1 mode scenario for RFX-mod2, a set of SpeCyl simulations have been performed with Lunquist number $S=10^5$, Prandtl number P=10 and different values of the plasma-shell proximity b/a starting from the reference case b/a=1 (corresponding to the standard version of the SpeCyl code) up to b/a=1.2. RFX-mod value for shell proximity is 1.11, while RFX-mod2 design corresponds to 1.04.[73] It is conservatively assumed that temperature and loop voltage remain the same throughout the scan. The resistivity of the wall at plasma radius is very high (more precisely the ratio between the wall time and the Alfven time $\tau_w/\tau_a=10^3$) so that eddy currents induced into it are negligible on the relevant simulation time scales.

The simulations are characterized by quasiperiodic sawtooth cycles with reconnection events: the resonant m=1, n=-7,,-20 are the most active modes whose amplitudes spike at the reconnection times. It is found that the time averaged edge value of the radial field associated with these modes grows with the ideal shell distance, starting from zero for the reference case in which the ideal shell corresponds to the plasma edge (b/a=1). Fig. 3.23 shows the scaling of normalized edge and volune integrated amplitude of m=1 modes as obtained by Specyl as a function of plasma-shell proximity. Also predicted (and shown in the same figure) is a reduction of overall mode energy of about 30% for RFX-mod2 compared to RFX-mod suggesting a decrease of internal transport

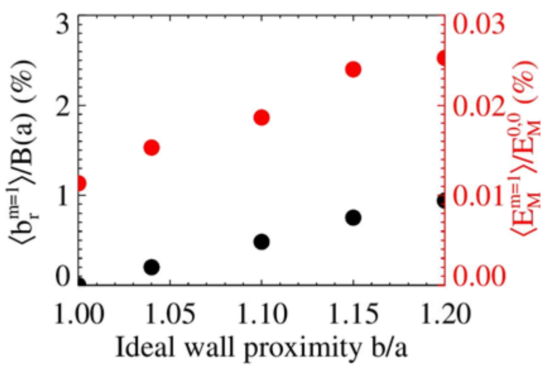

Fig. 3.23 scaling of normalized edge and volume integrated amplitude of m=1 modes as obtained by Specyl as a function of plasma shell proximity

Real time assessment of the magnetic diagnostics in RFX-mod2. The magnetic diagnostic system in fusion devices plays a critical role in both real time plasma control and off line in-depth analysis as it provides the most relevant information for the reconstruction of the plasma shape and position. The failure or malfunction of one or more components can

[73] L. Marrelli et al., Proc. 27th IAEA FEC Conference, Gandhinagar (2018, to be submitted to Nucl. Fus.)

cause negative consequences in several applications, including plasma equilibrium and stability control.

Usually their assessment is carried out by suitably operating the devices in dry discharges or in well controlled plasma conditions and suitable calibration coefficients are introduced. This procedure was applied to RFX-mod for both reverse field pinch and tokamak discharges in order to set a reliability flag to magnetic measurements after each discharge. This system is presently applied only to Bt measurements using the expected waveforms applied to the system before the plasma is actually produced. However this leaves to the operator the assessment of the coils measuring other components of the magnetic field.

In the paper from Chiariello[74] a new procedure has been proposed able to provide a check up of all the main magnetic diagnostics (e.g. local probes, saddle coils and flux loops), to identify the probes to be investigated, to provide each component with a reliable confidence coefficient and, finally, to suggest reasonable corrections of the actual measurements. In this approach a complete description of the plasma behavior is not needed in order to reduce the computational burden, a linear plasma model can be adopted based on the equivalent plasma currents model[74-75-76]: an equivalent current density on a suitable toroidal surface is introduced, and its density is expressed as a truncated Fourier Series. The methodology is based on a "mirror" operator performing two main actions; a first, inverse action models the unknown sources including the plasma equivalent currents, and a second, direct action reconstructs the magnetic field in the region of interest. The capability of the representation in the first inverse step can be suitably calibrated to bring out, in the second direct step, the discrepancies to be interpreted as faults or malfunctioning.

First test have been done for some RFX-mod discharges in order to test the feasibility of this approach and possibly consider a future implementation in real-time

Equilibrium reconstruction for a shaped tokamak. The computation of plasma equilibrium at RFX is addressed with different codes assuming a fully numerical or semi-analytical approach. In the framework of the latter situation in the case of Reversed Field Pinch discharges, the NCT code was developed[77] providing a reconstruction based on a perturbative approach in toroidal geometry. A similar procedure was devised to provide

---

[74] A.G. Chiariello, A. Formisano, F. Ledda, R. Martone and F. Pizzo, *IEEE Transactions on Magnetics* **54** (3) (2018) 1-4

[75] J. Luo, Plasma Science and Technology **4** (2) (2002)

[76] P. Bettini, A.G. Chiariello, A. Formisano, F. Ledda, G. Marchiori, R. Martone, F. Pizzo, D. Terranova, *Fusion Engineering and Design* **123** (2017) 546-550

[77] P. Zanca and D. Terranova, *Plasma Phys. Control. Fusion* **46** (2004) 1115

equilibria for the tokamak configuration taking into account a parametric representation of a coordinate system suitable for describing a shaped tokamak in toroidal geometry[78]:

$$R(r,\omega)=R_0+\Delta(r)+[r-E(r)]\cos(\omega)+\delta(r)\cos(2\omega)$$

$$Z(r,\omega)=[r+E(r)]\sin(\omega)-\delta(r)\sin(2\omega)$$

Where R and Z are the usual coordinates, E and δ are representative of plasma elongation and triangularity, and δ is poloidal angle. As in previous work, parallel current density is modelled with a two-power representation providing an adequate solution to represent shaped configurations with up-down symmetry.

Given that this approach is based on a perturbative analysis, the work addressed also the range of values that can be allowed to the free parameters (E and δ) before the starting assumptions are broken. An example for a test case is presented in Fig. 3.24 representative of a JET discharge.

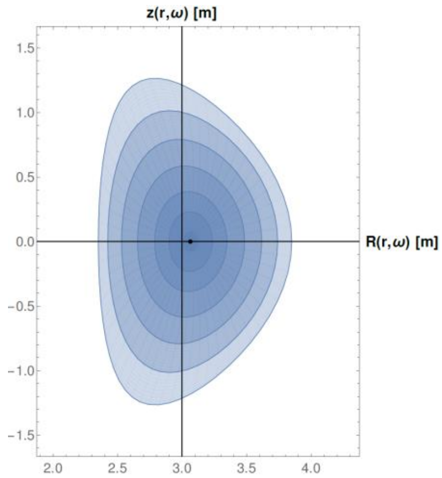

Fig. 3.24 Reconstructed equilibrium for some representative JET parameters.

Magnetic equilibria reconstruction in the RELAX RFP. Experimentally measured states in the low aspect ratio (R/a=2) RELAX device have been compared with a cylindrical relaxation theory79. the experimental states have not been found to be consistent with the theoretical predictions, in particular in plasmas with large reversal of the edge toroidal field. Further investigations, in collaboration with KIT, should clarify these points in 2019.

---

[78] R. Fitzpatrick *et al.*, *Nuclear Fusion* **33** (1993) 10

[79] R. Paccagnella, S. Masamune, A. Sanpei, Phys. of Plasmas **25** 072507.(2018)

3.2. *ITER Physics Work Packages*

3.2.1. *Introduction*

The shift to 2019 of the whole JET experimental campaigns and an analogous postponement of three months of the AUG ones have significantly affected our programmed contribution to the Eurofusion acivities. TCV campaigns have also been curtailed, but with somewhat less consequences. JET activities have nonetheless continued with the analysis campaigns, including 40% of the foreseen work at home, and with the preparation of the experiments (detailed pulse plans, machine parameter specifications, request of diagnostics and request of scarse resources) , whose approval procedures have been anticipated. WX7 has completed the campaign Op1.2, in which the plasma edge probe designed and built by CRFX has been successfully employed, yielding results useful for future analysis. The activity for JT-60A has continued as planned with the increment of preparatory work to launch diagnostics procurement projects. DTT has seen modelling activities under the EUROfusion work package but also work within the ad interim DTT project organization that has been launched. Coordination responsibility has been shared by CRFX with 1 person in the PMU, 6 Scientific coordinators and 1 deputy Task Force Leader in JET, 3 Scientific Coordinators, 1 modeling coordinator and 1 deputy task force leader in MST1. Additionally , WPSA has assigned to CRFX the responsibility for the Modelling Area coordination.

3.2.2. *MST1*

3.2.2.1. Extension of the operating space of fully non-inductive scenarios on AUG and TCV. Topic 16

The experimental plan of MST1 Topic 16 could not be completed in 2018 on TCV due the unavailability of the required ECRH power. Nonetheless, data analyses and modelling of the 2017 experimental sessions were carried out. βN values up to 1.4 and 1.7 were obtained in lower single null L-mode (H98(y,2)~0.8) and H-mode (H98(y,2)~1) TCV plasmas, respectively, at zero time averaged loop voltage and q95~6. Fully non-inductive operation could not achieved with NBI alone, whose injection can even increase the loop voltage in the presence of EC waves. A strong contribution to the total plasma pressure of bulk and Fast Ions (FI) from NBI is experimentally evidenced and confirmed by interpretative ASTRA and NUBEAM modelling, which further predicts that FI charge-exchange reactions are the main loss channel for NBH/CD efficiency. FI losses have been confirmed to localize mostly on outer midplane using ASCOT code.[80] It was confirmed that internal transport barriers, which are expected to maximize the bootstrap current fraction, have not been formed in either the electron or the ion channel in the plasmas explored to date, despite a significant increase in the toroidal rotation and FI fraction with NBI, which are known to reduce turbulence. CRONOS modeling is being carried out to investigate this evidence. The results of this work was presented at the 27th IAEA FEC conference[81].

3.2.2.2. Density Limit

The power-balance density limit (DL) model presented in [82] has been compared to high-density disrupted L-mode discharges perfomed in TCV within the T-25 campaign. The model is compatible with the experiments, but the comparison is not definitive due to doubts about the Z_{eff} signal provided on these shots [83]. A similar analsyis has been carried out on JET high-density disrupted L-mode discharges: the model describes fairly well the maximum observed densities, much better than the empirical n_G criterion, by including radiation losses from impurities and edge neutrals Fig. 3.25 [84].

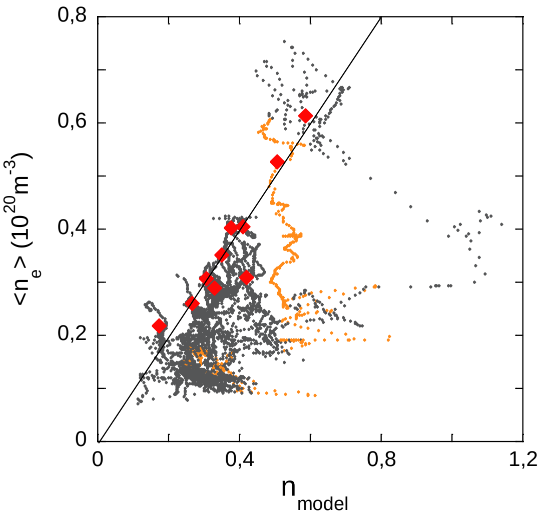

Fig. 3.25 Experimental densities versus modeled DL, for JET, C-wall discharges. Red diamonds mark the disruptions. Grey: D shots. Orange: He shot.

3.2.2.3. Filamentary transport in high-power H-mode conditions and in no/small-ELM regimes to predict heat and particle loads on PFCs for future devices- Topic 21

The investigation of filamentary transport in high density regimes in MST1 devices has continued during 2018. The experimental activity has been limited to TCV tokamak, due to the shifting of the corresponding programme on ASDEX-Upgrade. On TCV a series of NBI assisted H-Mode discharges, shown in Fig. 3.26, were performed where plasma conditions

---

[80] M. Vallar et al., Nonlinear contribution of neutral beam injection in TCV EC-heated advanced tokamak scenarios, 45th EPS conference on plasma physics, Prague, 2018

[81] C. Piron et al, Extension of the operating space od high-βN fully non-inductive scenarios on TCV using neutral beam injection, 27th IAEA Fusion Energy Conference, Gandhinagar, India 2018

[82] P. Zanca et al, A unified model of density limit in fusion plasmas, Nucl. Fusion **57** (2017) 056010

[83] P. Zanca et al, L-mode density limit analyses in JET and TCV, internal document NT-FC/91, RFX, Padova (2018)

[84] P. Zanca et al, 27th IAEA Fusion Energy Conference, Gandhinagar, India, TH/P5-22

were varied through gas puff or Nitrogen seeding with the aim of reaching a detached plasma. Despite the attempt and the observed increased of Divertor collisionality Λ_{div} no modification of the upstream profiles has been observed, consistently with the fact that the divertor remains attached in all the explored conditions. In the meantime the analysis of the database collected on both TCV and AUG during 2017 continued during 2018.

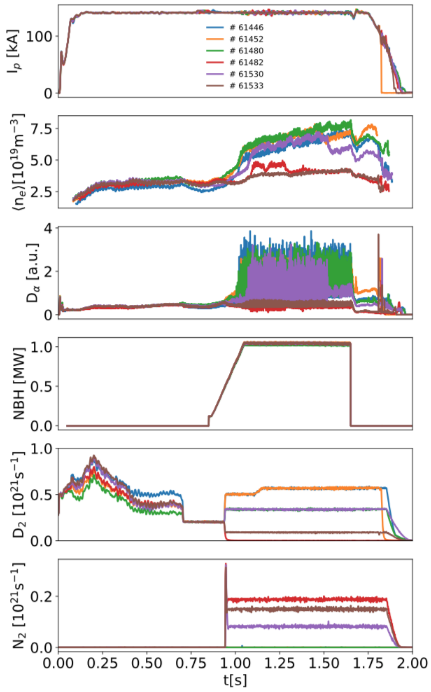

Fig. 3.26 From top to bottom. Plasma current, central density, Dalpha, NBH power, Deuterium fueling and N2 seeding during the H-Mode operation in TCV D shots.

An investigation has been done in order to determine the dependence of shoulder formation on current by performing current scan in L-Mode both at constant toroidal field and at constant q_{95}. In ASDEX-Upgrade it has been clearly demonstrated that the observation of the onset of shoulder occurring earlier in density at lower current can be well reconciled, both for the upstream and for the target density, in terms of edge Greenwald fraction (i.e. edge density from interferometer divided by Greenwald density) and this is true for both the scans as seen Fig. 3.27. The behavior is similar for TCV for the current scan at constant B_t whereas during the scan at constant q_{95} no clear shoulder has been observed at lower current levels. This has been attributed to the lack of detachment at lower current and toroidal field which is presently under investigation. Concerning the blob behaviour no dependence on plasma current has been observed nor in AUG neither on TCV.

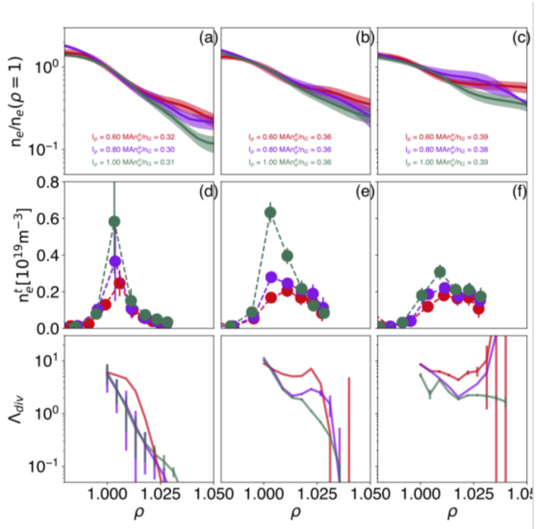

Fig. 3.27 Top: SOL density normalized to the value at the separatrix Middle row: Outer target density Profile. Bottom row: Divertor collisionality. The color code refer to different current levels, the different columns refer to different value of edge density normalized to Greenwald fraction.

It is confirmed that Divertor collisionality is not a qualifier for the increasing of blob-size or flattening of upstream profile on TCV. The investigation of shoulder formation in H-Mode has continued on AUG with discharges with up to 5.8 MW of heating power. A clear dependence of shoulder amplitude has been observed on mid plane pressure, with flatter

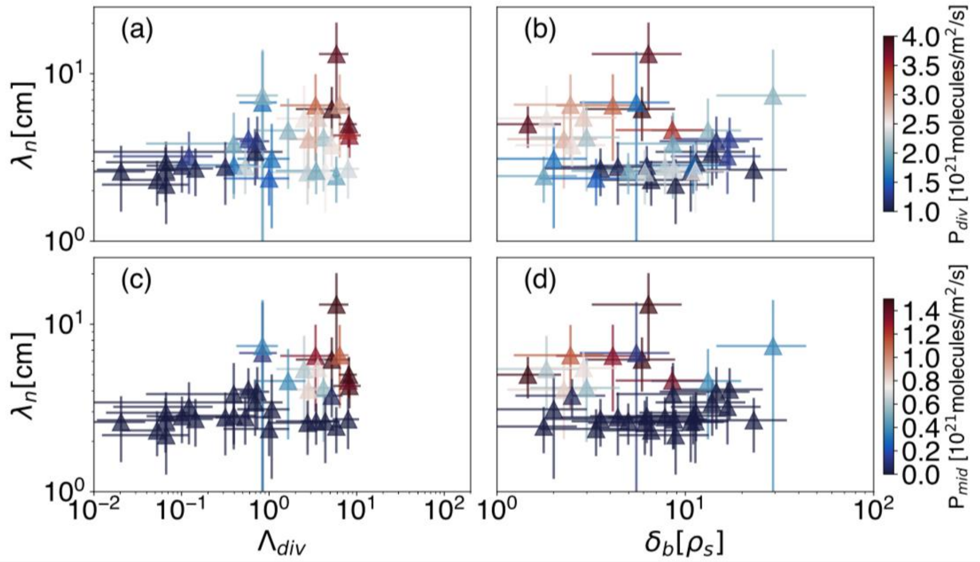

Fig. 3.28 E-folding length as a function of Λ_{div} (frames on the left) and as a function blob-size (frames on the right). In frames (a) and (b) color code refers to divertor neutral pressure, whereas in (c) and (d) to midplane neutral pressure

profile observed when higher mid plane neutral pressure is observed ((see Fig. 3.28). An intensive work has been done also for measuring the emission of neutral deuterium in the divertor region, using two visible cameras with two filters for Dα and Dγ. They observed the divertor region from the outboard midplane and they are absolutely calibrated. Since they observe along lines of sight (LoSs), they measure integrated signals, and in order to obtain a 2D map of emissivity ε, a tomographic algorithm has been developed. In order to introduce as little as possible a-priori constraints, the pixel method is used, and the inversion is performed with an iterative algorithm. So far it was possible to observe the movement of the D_alpha radiation from the inner to the outer target with enhanced radiation in the main SOL as soon as the shoulder develop.

3.2.2.4. Edge modeling studies in alternative configurations and with varying flux expansion Topics 24 & 25

Edge modeling has been performed with the SOLEDGE2D-EIRENE code on pulses of experimental campaigns Topic-24 and Topic-25. For Topic-24 Double Null (DN) divertor configuration pulses both in L-mode and in H-mode have been analyzed. The main aim was the evaluation of the transport parameters of DN in different regimes. Modeling evaluation and validation of transport profiles was done by means of comparison with up-stream, divertor and spectroscopic measurements. Transport profiles were used to infer density and/or seeding requirements to achieve detachment. Estimated density and seeding values will be used in next Double Null experiments. Part of the analysis of double null pulses have been devoted also to the study of drift effect on the observed top/bottom asymmetries, this is one of the first assessment of SOLEDGE ability to deal with drifts. For the same Topic-24 a modeling activity also started trying to understand why a clear dependence of detachment threshold on flux expansion was not observed experimentally, differently from what predicted by simple edge models. For Topic-25 it was continued the effort to model Snow Flake configurations to assess their advantage with respect to the standard Single null configuration in terms of lower power load at target and easier detachment.

3.2.2.5. International collaboration

International collaboration missions at General Atomics (USA) have been carried out for studies of global MHD stability in presence of 3D geometries and kinetic effects. The tools developed and the expertise gained can be applied to RWM stability/control, plasma response studies with 3D structures and fields in particular. A special focus has been set on stability studies of high beta Advanced Tokamak scenarios, with applications ranging from present day experiments to forthcoming devices e.g. JT-60SA.

An international collaboration has also been exploited for developing a new coupling strategy between linear MHD plasma response (MARS-F) and 3D boundaries (CARIDDI). This strategy can account for non-ideal effects for plasma stability.

3.2.3. ***JET1***

3.2.3.1. LH Transition

A contribution to the study on the role of the ion heating channel in the L-H transition in JET, has been given in terms of numerical simulations (JETTO+PENCIL/ASCOT withing JINTRAC suite) within the analysis and modelling task T17-08 *L-H transition physics* merged into the task M18-14 *Isotope effects on L-H transition power threshold*. The work has been presented first at TTF 2018 meeting[85] and also with an invited contribution at APS conference 2018[86]. The JET power balance analysis at the L-H transition will be also presented in a dedicated paper. The current understanding is that the presence of a minimum in plasma density of the L-H power threshold cannot be fully explained by the direct ion heating and the thermal exchange between electron and ions.

3.2.3.2. Impurity transport studies Task T18-03 and Exp. M18-07

In the context of the task T18-03, the analysis of the impurity behaviour has been extended from the core to the edge by using the suite of codes COCONUT that couples JETTO for the

---

[85] E. R. Solano, E. Delabie, P. Vincenzi, C. Bourdelle, J. Hillesheim, C. Maggi, P. Carvalho, A. Huber, *Power balance analysis at the L to H transition in JET-ILW*, TTF, Seville, Spain, September 11-14

[86] E. Delabie, et al., Reconciling L-H threshold dependencies on JET-ILW with the ErxB shear mechanism, 2018, APS Conference invited

core and EDGE2D for the EDGE, including models for he ELMs, in such a way that core transport studies can be carried out using meaningful boundary conditions. Particular work has been devoted to test of gyrokinetic models in JETTO. Fig. 3.29 shows a sample result of the W flux at the divertor simulated by COCONUT. Preliminary results on the ELM imapct on W and on the rimpurity penetration across the pedestal layer have been presented at the EPS conference in Prague[87]. In parallel the preparatory work for the experiment M18-07 (Impurity transport), shifted to 2019, has been completed and the technical approval obtained.

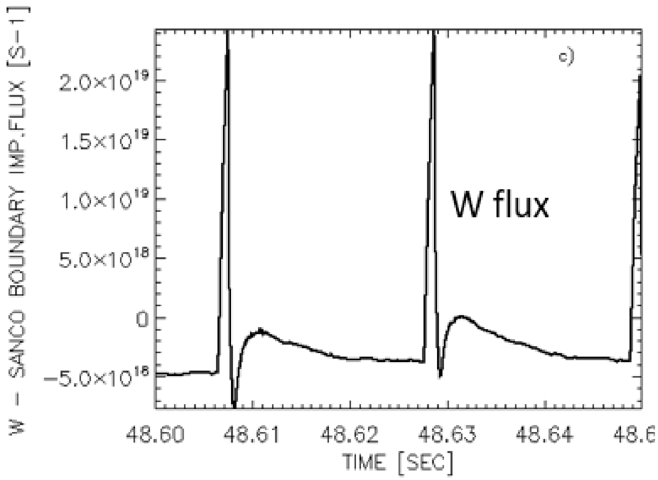

Fig. 3.29 Simualtion of W flux at the outer divertor simulated by COCONUT in a 32 MW JET discharge

3.2.3.3. M18-06 experiment preparation

In the contest of scientific coordination for experiment M18-06 “Impact of inner leg flux geometry on W influx” pulse design activity has been done. The experiment is recognized to be very important for the definition of the two JET reference DT scenarios: the baseline and the hybrid ones, for this reason a detailed and well agree experiment preparation was required. Experiment definition has been already done for the baseline scenario by selecting the appropriate reference pulse to be used as starting point for geometry study. In collaboration with Tuscia University various equilibrium with different flux expansion have been generated with CRETE-NL code trying to keep fixed in the best way strike point positions and plasma shape to be ovoid spurious effects. In figures Fig. 3.30 it is show as is

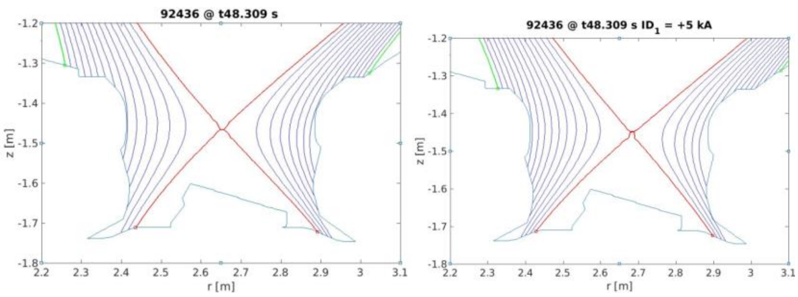

Fig. 3.30 Flux surfaces (spaced 3.6 mm at outer mid plane) in divertor region of reference pulse and with reduced flux expansion (ID_1=+5kA).

87 M Valisa L Carraro FJ Casson et al http://ocs.ciemat.es/EPS2018ABS/pdf/P2.1096.pdf

possible to compress flux surfaces toward separatrix with respect the reference pulse to reduce heat flux on top targets (tanks to a higher distance from separatrix in terms of magnetic flux). Edge modeling have been performed on the reference pulse and with the same parameters on generated equilibrium to evaluate the reduction on heat load at the top divertor target which was recognized to be an important source of tungsten core contamination. The same activity is presently foreseen for the hybrid scenario also.

3.2.3.4. Real time control tools M18-09

The development and the integration of the RAPTOR suite of codes in the MARTe2 framework on JET was advanced in 2018. The upgrade of the real-time equilibrium reconstruction EQUINOX code was completed, good agreement is achieved with EFIT equilibrium modeling for a reference JET baseline discharge, a systematic comparison is being carried out on a wider database. The integration of EQUINOX in MARTe2 was also started. A real-time algorithm was implemented to map the diagnostic profiles from geometric to normalized magnetic coordinates. Furthermore RABBIT, a code capable of evaluating in real-time the Neutral Beam heating, current drive and fast ion radial deposition, was integrated in the suite. Data I/O interfaces between the codes of the suite were developed. Data exchange, storage and visualization is supported by the MDSplus software.

3.2.3.5. Pedestal gyrokinetic stability T17-05

In the framework of task T17-05, deliverable D3 (linear and non-linear gyrokinetic modelling of pedestal transport; assess whether results are consistent with inter-ELM evolution, pedestal structure, and limitations on pre-ELM pedestal pressure), the activity related to the investigation of the isotope effect on pedestal micro-instabilities has further proceeded. Three discharges have been considered for this purpose, with the aim to compare the influence of the main gas species in two couples of discharges characterized by the same stored energy and the same input power. In order to disentangle the isotope effect from profile effects, we have artificially changed the main ion mass (D to H, and vice versa). An extensive analysis has been carried out with the gyrokinetic code GENE, from low to high poloidal wavenumbers (KBM/ITG to ETG range), at different radial wavenumbers (i.e., different ballooning angles), across the whole pedestal (i.e., differentiating top and steep gradient region). In the cases investigated here, electrostatic instabilities turn out to be dominant, KBMs being marginally unstable at very low wavenumbers. A mixing length estimate of the resulting transport shows a moderate isotope effect across the steep gradient region, yielding higher conductivities in H than in D in gyro-Bohm units. Further analysis is required in 2019, extending our previous analysis to nonlinear simulations.

3.2.3.6. 3D equilibrium reconstruction . Task T17-15

Non axi-symmetric configurations are observed in JET on a limited extent during operation with EFCC, when snake structures appear and in extreme conditions during a disruption when the plasma undergoes a global 3D distortion. In the latter case in order to sort out possible asymmetries, attempts of equilibrium reconstuction were done running EFIT++ with separate octants information. This approach cannot provide a self-consistent view while the VMEC[88] code can address correctly (though with some limitations) this situaiton. This analysis is presently ongoing along with the improvements in the benchmark with EFIT++ and the modelling of experimental measurements. In this respect, the main issue being addressed involves the role of passive structures that close to disruptions play an important role and impose some limitations in the modelling of magnetic data in a straight forward way using the V3FIT[89] code.

3.2.3.7. Isotope effect Exp. M18-23

Isotope effect on transport is one of the key topic in recent years JET activity, with the foreseen campaigns in pure Trituim (TT) and Deuterium and Tritium mixture (DT). The transport properties are ruled by many ingredients, one being the plasma rotation: numerical simulations with TRANSP and NUBEAM have been performed (as part of M18-23 experiment) to assess the NBI injection geometries which provide similar plasma rotation in plasma with different isotopes and mixture.

3.2.3.8. Prediction of high current performance. Task T17-07

Within M18-01 and M18-02 experiments (baseline scenarios and hybrid scenarios) interpretative simulations of performing on pulses with the highest neutron yield of the last campaign (92436 and 92398) hav ebeen carried out to predict the plasma performance at higher current, field and heating power. TRANSP prediction of the plasma performance for medium β_N = 1.9 plasmas has been done, as an alternative route to reach the highest fusion power in DT plasma. The predictive capability of the Trapped Gyro Landau Fluid (TGLF) code on hybrid discharges of JET has been investigated. TGLF is coupled to the predictive version of TRANSP. TRANSP+TGLF have been used to predict the evolution of the hybrid Deuterium shot 92398, which is the hybrid shot where the highest neutron rate has been measured. The work is still ongoing since a only a subset of available TGLF options has been used. In the reference discharges the T_i measurements are not available, hence T_i =

---

[88] S.P. Hirshman and J.C. Whitson, *Phys. Fluids* **26** 3554 (1983)

[89] J.D. Hanson, S.P. Hirshman, S.F. Knowlton, L.L. Lao, E.A. Lazarus and J.M. Shields, *Nucl. Fusion* **49** 075031 (2009)

1.25 T_e has been assumed. Simulations have been done using the settings agreed on the wiki page https://users.eurofusion.org/tfwiki/index.php/TGLF_recommended_settings, in particular Saturation equal 1 is used. When the experimental rotation profile is included, density and ion temperature are well reproduced, while the electron energy transport is overestimated, hence too a low electron temperature is calculated. This activity has been performed within in the T17-07 modelling task.

3.2.3.9. Disruption mitigation: shattered pellets JOREK simulations.

In 2018 a new JET modelling activity started at Consorzio RFX with the participation of D. Bonfiglio (from the CRFX Theoretical Physics group) to a training course organized by EUROfusion for the use of the nonlinear 3D-MHD code JOREK. The specific topic proposed when applying for participation to the JOREK training course was modelling of disruption mitigation with Shattered Pellet Injection (SPI) in JET. After the training course, D. Bonfiglio joined the team of JOREK modellers working on this topic, composed by D. Hu (ITER), E. Nardon (CEA) and A. Pau (Cagliari University). After considering deuterium shattered pellets [90], in 2018 the effect of impurity pellets was studied [91]. This modelling activity will continue in 2019 with the study of mixed pellets as planned for the upcoming JET campaigns.

3.2.4. ***DTT***

Following the constitution of an ad interim project structure, CRFX has been involved in the process of DTT cost estimates validation, the definition of the day 1 diagnostics package, the dimensionning of the neutral beam injection, the specification of the power supplies, the qualification of the pysics targets and the revision of the overall project that should end up in a new project document in early 2019. Modelling activities of the efficacies of different divertor solutions have been carried out withing the WP DDT1 workpackage.

3.2.4.1. Beam losses estimation

A rather comprehensive evaluation of fast particle losses of the DTT NNBI has been undertaken during year 2018. Evaluations have been carried out to support the choice of the most suitable beam energy and injection angle[92]. In particular, a set of simulations have

---

[90] D. Hu *et al.*, Nucl. Fusion **58,** 126025 (2018) https://doi.org/10.1088/1741-4326/aae614

[91] D. Hu *et al.*, "Study of full impurity Shattered Pellet Injection by non-linear 3D JOREK simulation in JET", APS-DPP 2018 http://meetings.aps.org/Meeting/DPP18/Session/TP11.76

[92] P.Agostinetti, T. Bolzonella, M. Gobbin, P. Sonato, G. Spizzo, M. Vallar, and P. Vincenzi, in 30th Symposium on Fusion Technology (SOFT), Giardini Naxos, Sicily, 2018, poster P1.019

been carried out using the METIS[93] code, considering the reference single null (SN) scenario[94] with two tangential NNBI systems. These simulations show that a beam energy around 400 keV allows central heating with enough beam penetration (see Fig. 3.31a and Fig. 3.31b) and that large injection angles give a more balanced heating distribution and increase current drive (see Fig. 3.31c and Fig. 3.31d) while decreasing the shine-through losses (see Fig. 3.31e).

Another important issue when designing a high-energy NBI system, is the rapid loss of fast particles in presence of toroidal magnetic field ripple[95].

The expected ripple in DTT is 0.22% in the low-field side (normalized to the field on axis B_0), not a large number, if compared e.g. with standard values expected in ITER[96]: the expected fraction of lost particles (monoenergetic and collisionless) has been calculated with the Hamiltonian, guiding center (GC) code ORBIT[97] using as input the single-null equilibrium for DTT (with ripple) and the initial ion positions calculated with the above mentioned METIS code.

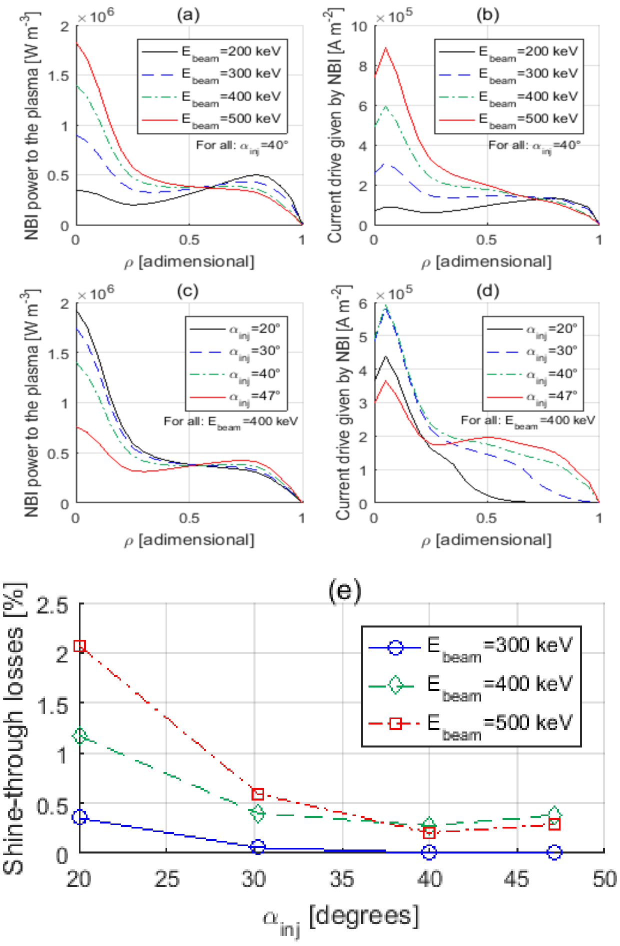

Fig. 3.31 (a) NBI power and (b) current drive released to the plasma as a function of the injection angle; (c) NBI power and (d) current drive as a function of beam energy; (e) shine-through losses as a function of angle and energy

The result is that collisionless losses (without shine through, which is not accounted for in ORBIT) amount to ~4% of injected particles, for energy E = 400 keV and tangency radius Rt

[93] J.F.Artaud, et al., Nucl.Fusion **58** (2018) 105001

[94] R. Albanese, Nucl. Fusion **57** (2017) 016010

[95] R. B. White, et al., in Fusion Energy Conference (Proc. 12th Int. Conf. Nice), vol. **2** (1988) p.111

[96] V.Kiptily, et al., Nucl.Fusion **49** (2009) 065030

[97] R.B. White and M.S. Chance, Phys. Fluids **27** (1984) 2455

= 1.77 m. This radius corresponds to an injection angle $\alpha_{inj} = 40°$, measured w.r.t the first wall: this result is shown in Fig. 3.32(left). These collisionless losses can be divided in prompt losses (particles lost in less than 10 toroidal turns, black) and ripple losses (red trace, loss time > 10 turns). The contribution of ripple losses is rather modest, ~0:5%, and decreases with the injection angle, meaning that trapped particles are the main channel of losses when ripple is switched on. To see this, one can plot the loss time, expressed in toroidal turns, as a function of the pitch parameter, which is the velocity parallel to the field, divided by the total velocity: $\lambda = v_{\parallel}/v$. While prompt losses are insensitive to pitch, ripple losses are localized at $\lambda = 0.65$, corresponding to particles injected with $\alpha_{inj} \sim 40°$ (see Fig. 3.32, right panel). These results indicate that we are in presence of the resonance between trapped particle precession and ripple periodicity, a collisionless mechanism which in principle can determine the rapid loss of all high-energy, trapped particles, as found in the 1980's on TFTR and TORE-SUPRA[98]: for this reason, for a beam energy of ~400 keV it is safer to design the beamline with an injection angle $\alpha_{inj} \gtrsim 40°$.

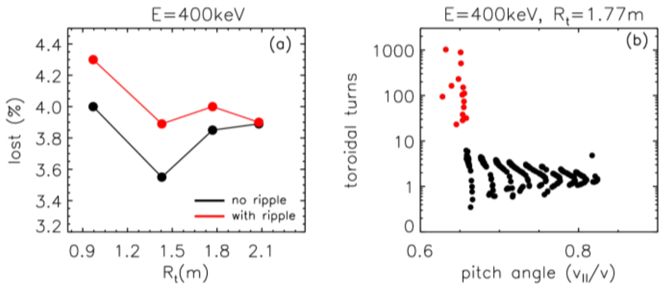

Fig. 3.32 (left) fraction of prompt losses (black) and same quantity plus ripple losses (red) as a function of injection angle; (right) loss times, expressed as toroidal turns, as a function of the pitch parameter (normalized parallel velocity)

As a consequence of the physics evaluation, the energy of 400 keV was chosen and the injection angle was increased up to the mechanical limit (considering the presence of the toroidal field coils) of 39.65° with respect to the direction perpendicular to the first wall. This angle corresponds to a 30° angle measured with the radial direction *at the vacuum vessel*.

3.2.4.2. Conceptual design of the Neutral Beam injector for DTT

The main purpose of the Divertor Tokamak Test (DTT) is to study solutions to mitigate the issue of power exhaust in conditions relevant for ITER and DEMO. The key feature of such a study is to equip the machine with a significant amount of auxiliary heating power (45 MW) in order to test different divertor solutions. The experiment shall be able to study different divertor magnetic configurations and reach a reactor relevant power flow to the divertor. The proposed mix of heating power foreseen to achieve the target value of 45 MW delivered to

[98] R.B.White, Phys. Rev. E **58** (1998) 1774

the plasma will be provided by Electron Cyclotron Resonant Heating (ECRH), Ion Cyclotron Resonant Heating (ICRH) and Negative-ion-based Neutral Beam Heating (NNBH).

In this framework, during 2018 a conceptual design of the DTT Neutral Beam Injector has been developed at RFX in collaboration with ENEA-Frascati and IFP-Milano.

The design development was driven by integrated physics and engineering evaluations, aiming at optimizing all the main critical aspects at the same time. Flexibility has been considered as the main design guideline, following the needs of the DTT experiment. Efficiency and RAMI have also been considered as guidelines. Most of the adopted technologies are ITER-like, the main differences from the design of the ITER NBI being the adoption of a modular beam source and of a hybrid cryogenic-plus-NEG pumping system. The former solution is foreseen to obtain an easier manufacturing of the grids, to permit a higher flexibility of the beam and to allow for a smaller testbed facility. The latter one aims at increasing reliability and availability of the injector, while decreasing the costs.

3.2.4.3. Definition and design of the Divertor Tokamak Test facility

The activities devoted to the design of DTT divertor have performed with three main aims: to assure that DTT design will allow the installation of the divertor selected by EUROfusion in 2022, to provide the input for the design of the divertor pumping system and finally to contribute EUROfusion in selecting the divertor configuration that provides the better results in the power exhaust. To the first aim the various proposed magnetic configuration have been verified in terms of compatibility with the proposed vessel and wall structures. In particular to provide the maximum performance with presently foreseen magnetic and technological solution some modification to the initially proposed vessel and toroidal field coils shapes have been requested and decided. Uno of the critical aspects of DTT design is the requested flexibility in terms of compatibility with many divertor configurations and also liquid metals targets. One element affected that is affected from this requirement is the divertor pumping system. To design a system with the requested flexibility a collaboration has been setup with the KIT laboratory, to find the optimum divertor configuration in terms of high pumping efficiency they will use the results of our edge modeling simulation and their DIVGAS (Divertor Gas Simulator) code. To last aim of help EUROfusion in selectin the best divertor configuration a first comparison of the three main divertor configurations SND, DND and SFD+/SFD- in term of power exhaust have been done with the SOLEDGE2-EIRENE code. Comparison was performed in pure deuterium and with Neon or Argon seeding. Without impurity seeding a power scan at high separatrix density has shown that SFD- and con operate in detached condition at a power about 50% higher than this allowable in SND see Fig. 3.33). SFD configurations when attached reach higher temperature at strike points than other configurations (related to higher temperature at separatrix). Neon seeding

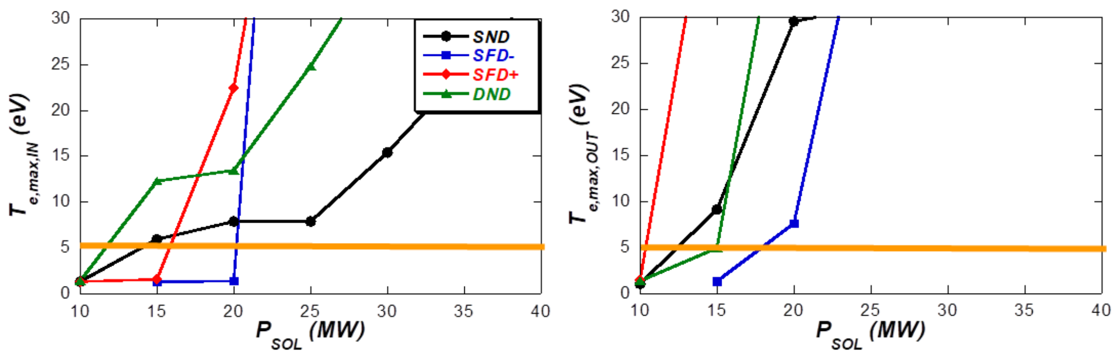

Fig. 3.33 Maximum target temperature at inner and outer target for considered divertor configurations

confirms the advantage of SFD configuration in term of a lower Zeff to reach detachment at maximum P_{SOL}. As observed in DEMO-ADC modeling SFDs require higher pumping speed than SND and DND probably related to the more open divertor geometry, this suggest that a better divertor geometry could further improve this configuration.

3.2.5. *WPDTT-AC*

The coordination of the DTT1-AC4 “Power exhaust modelling" has been continued together with the modelling of the alternative DEMO configurations. With the SOLEDGE2D-EIRENE edge code have been modeled all the alternative divertor configurations proposed for DEMO. In particular modeling has been done for Snowflake plus and minus (SFP and SFM), X-Divertor (XD), Super-X divertor (SXD) and Double null divertor (DND) configurations. In pure deuterium PSOL power scans have been done for all previous configurations and reference single Null (SND) one at two density levels using transport parameters ($D_{\perp}$=0.42 m^2/s and $\chi_{\perp}$=0.18 m^2/s) corresponding to a parallel heat flux decay length of ≈3 mm. At middle separatrix density (nsep=$2.4 \cdot 10^{19}$ m^{-3}) detachment was achieved up to P_{SOL}≈50 MW in all alternative configurations this can be compared to the much lower value of PSOL≈30 MW allowed to the SND case. Alternative configurations outperform SND one also in term of peak heat flux providing a lower one at PSOL values close to detachment. Results are similar at high separatrix density value y (nsep=$4.0 \cdot 10^{19}$ m^{-3}), in this case detachment was achieved up to PSOL≈85 MW in all alternative configurations and up to PSOL≈75 MW in SND case. The smaller relative difference between alternative configuration and SND at high density can probably be attributed to the neutrals effect and the better divertor closure with considered divertor geometry is probably better in SND case.

3.2.6. ***WPSA***

3.2.6.1. Enhancement projects: Thomson scattering and VUV spectrometer

Within the collaboration between EU and QST-Japan for the procurement of components for the JT-60SA experiment, C RFX has contributed in 2018 to drafting the procurement call of two systems: the core and edge Thomson scattering (TS) diagnostics and the VUV divertor survey spectrometer. Regarding the TS system, the activity has also been a first step towards the provision of four subsystems: the collection optics with their mechanical structure and the laser of edge TS system, the fibers and polychromators for both core and edge TS systems. In particular CRFX has developed optical design studies of the collection optics, has coordinated the design of the the mechanical structure, performed by the Romanian Institute of Atomic Physics (IAP), has performed preliminary design of the prolychromators, agreed with QST the technical specification of the optical fibers and proposed a dedicated laser for the edge system. On the front of the VUV spectrometer, the activity consisted in the definition of possible solutions for the spectrometer and the related optical coupling compatible with the geometrical and environmental constraints, with the suggetion to enhance the diagnostic potential from a generic survey to an imaging system.

Late in 2018 Eurofusion has appointed CRFX responsible laboratory for the procurement of of both TS and VUV spectrometer, partly funded by Eurofusion, partly procured directly by F4E. The contracts will start in 2019 and are due to be completed in 2020 for the VUV spectrometer and 2021 for the TS system .

3.2.6.2. Resistive wall modes studies

Extending activities started between 2016 and 2017, Resistive Wall Mode stability studies have been carried out for the high beta JT60-SA Scenario 5 with the linear codes MARS-F and MARS-K. With the latter in particular, stabilization of the most unstable n=1 RWM at low plasma rotation has been found. The stabilizing mechanisms is identified with precession drift resonance with thermal ions. The effect of plasma flow on kinetic-RWM stability has been studied with a rotation profile calculated consistently with the JT-60SA beam geometry. A work summarizing the latest developments on this topic, as well as on active feedback stabilization, has been presented at the IAEA Fusion Energy Conference[99].

[99] L Pigatto et al :27th IAEA FEC , Gandhinagar, India, 22-27 October 2018, paper TH/P5-23

3.2.6.3. Neutral Beam injection studies

Simulations of NBI injection have continued from 2017, with applications of the ASCOT code to the JT-60SA reference scenarios (2,3,4,5 as from the Research Plan)[100]. Activities related to the evaluation of fast ion losses with the effect of external 3D fields (and plasma response) have started in 2018 and will be continued in 2019.

3.2.7. *WPS1*

3.2.7.1. LHD campaign: transport in magnetic islands and isotope effects

Participation to the LHD Deuterium experimental campaign has been addressed to the study of the heat and particle transport properties in plasma with islands and to enhance the comprehension of the isotope effects in stellarators. The later topic is still controversial, since no strong evidences have been found in previous smaller devices. To study the transport properties in LHD, heat and cold pulse experiments have been performed in plasma with 2/1 RMP islands. The analysis is ongoing.

The analysis of 2017 experiments, where iced pellets were injected in LHD plasmas with (1,1) RMP island, have been presented at the 2nd AAPPS-DPP conference, as an invited talk. In particular a MAxS particle transport analysis has been shown, highlighting that also for particles the island acts as a low diffusivity region surrounded by a 10 times higher diffusivity plasma. Fig. 3.34 shows the temporal evolution of the density radial profile measured by the Thomson Scattering (stars) compared with the MAxS predictive simulations (solid line). The transport coefficients are shown in the lower panel, where the important decrease of the diffusivity inside the island is evident.

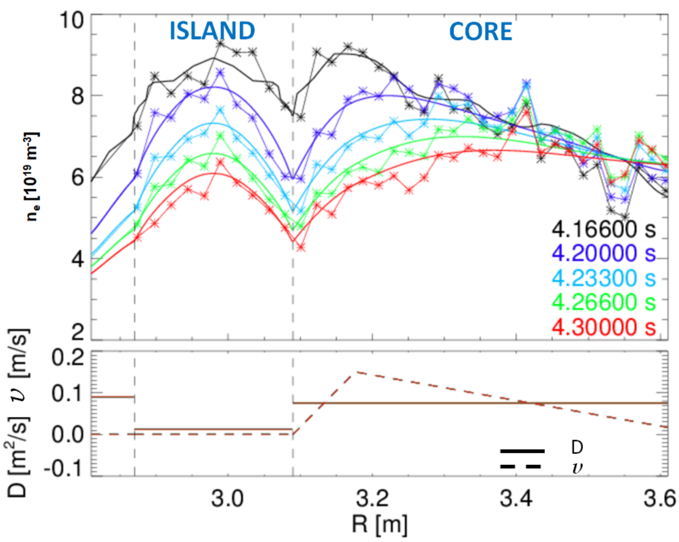

Fig. 3.34 Temporal evolution of the density radial profile measured by the Thomson Scattering (stars) compared with the MAxS predictive simulations (solid line

3.2.7.2. Procurement Installation an first use of insertable probe

During 2018, following the final approval of the Consorzio RFX design [101] by the IPP Greifswald team, the

---

[100] M Vallar, PDH Thesis

[101] P. Agostinetti, et al. "Design of a High Resolution Probe Head for Electromagnetic Turbulence Investigations in W7-X." IEEE Transactions on Plasma Science (2018).

High Resolution Probe Head (HRP) to be installed on the W7-X experiment, was built and finally assembled in Padova, then delivered to W7-X in Greifswald. In particular the aim was to provide information on parallel current density associated to L-mode filamentary turbulent structures as well as on ELMy structures in H-mode[102,103,104,105]. Furthermore the possibility to measure the time evolution of radial profiles of flow was considered as a further interesting part of the study, given the strong interplay expected between the turbulent fluctuation and the average flows. Special attention was devoted to the design of a shield for magnetic sensors embedded into the probe head, which would allow the magnetic fluctuation measurements ($f_{meas} \leq 1$ MHz) and at the same time the shielding from ECRH (f_{ECRH}=140GHz) used for additional heating. The probe head was then installed on the W7-X Multi-Purpose fast reciprocating Manipulator (MPM) and successfully commissioned. The HRP probe was then exploited during the OP1.2b W7-X experimental campaign in July and October 2018. As an example the spectrograms of different magnetic field component fluctuations exhibiting a bursty behavior is shown in the right panel of Fig. 3.35. This phenomenology is consistent with the presence of the localized electromagnetic filamentary structures [[105]].

3.2.7.3. Thomson Scattering

In 2018, following previous informal contacts with W7-X researchers, a formal collaboration has been established between the Thomson scattering teams of RFX and W7-X Teams, with the purpose of carrying out in W7-X a test the dual-laser, self-calibrating Thomson scattering technique, proposed for ITER. These experiments will use a new Nd:YAG laser system operating at 1319 nm, under development for W7-X. In the framework of this collaboration one CRFX post-doc visited the W7-X group at IPP-Greifswald during the summer 2018 and collaborated to the TS measurements during the OP1.2b experimental campaign.

3.2.8. ***WPISA***

In 2018 the new version Universal Access Layer (UAL) has been finalized and is currently being released. In this context, the activity carried out at RFX has been related to the low level layer, i.e. the layer that provides direct access to the backend components actually reading and writing data. In particular two backends have been implemented: MDSplus

[102] M. Spolaore,et al. Phys. Rev. Lett. 102, 165001 (2009)
[103] N. Vianello et al. Nucl. Fusion 50, 042002 (2010).
[104] Furno I., Spolaore M., Theiler C., N. Vianello, et al., Phys. Rev. Lett. 106, 245001 (2011).
[105] Spolaore, M., et al. Nuclear Materials and Energy 12 (2017): 844-851.

backend for reading and writing data to/from MDSplus pulse files, and Memory backend, for caching in memory data used in simulation.

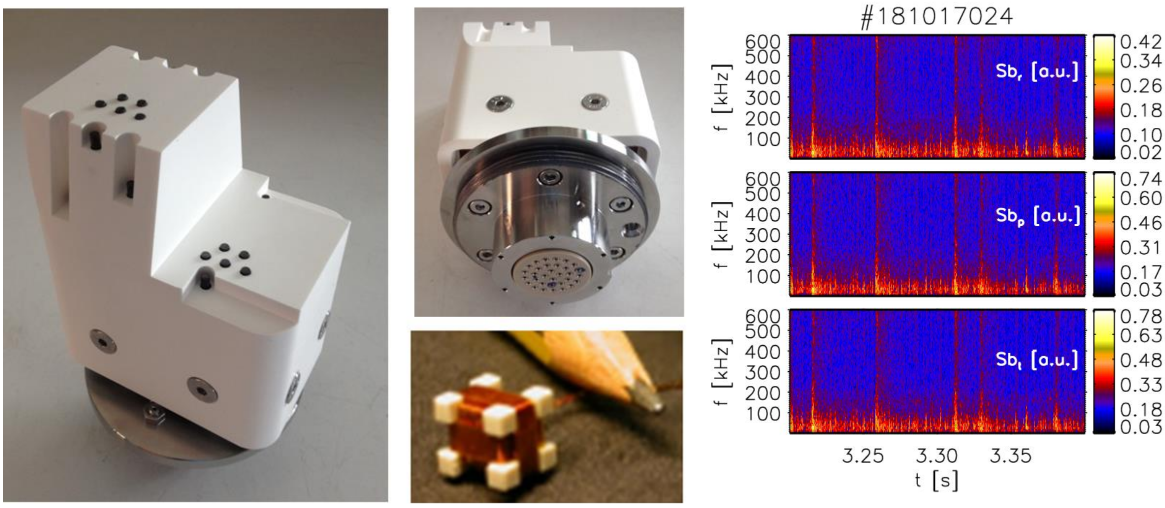

Fig. 3.35 Left: HRP probe, different views of the probe head: 4 Mach probes radially distributed, 2 set of 5-pins triple probe (2 radial positions), 3 set of 3-axial magnetic coils (2D array). Right: Example of br, bp and bt magnetic fluctuation spectrograms measured in the W7-X SOL, during OP1.2b experimental campaign.

3.3. *ITER NBI Physics activities and accompanying program*

3.3.1. *Introduction*

Aimed to train the personnel and to complement the ITER NBI activities at Consorzio RFX by investigating research lines not included in the main program, during 2018 the accompanying activity to the ITER NBI program have been carried out by operating the experiment NIO1, by realizing and operating the alternative ion source ATHENIS and by developing new numerical tools to tackle the controllability of a NBI system . In the following the main activities on NIO1 and ATHENIS are presented.

3.3.2. *NIO1 Experiment*

The operation of the NIO1 experiment in 2018 was devoted to improve the performances of the negative ion source in pure volume operation. The aim was to increase the accelerated current, to reduce the fraction of co-extracted electrons and improve the voltage holding capability of the acceleration system. This was pursued by exploiting the flexibility of the machine, mainly by changing the magnetic configurations of the Extraction Grid (EG), of the front magnet multipole.

The phases of the operation of NIO1 throughout 2018 are described here below.

At the beginning of the year, NIO1 operated in the magnetic configuration with the vertical field given by the only current flowing in the Plasma Grid (PG) and with an horizontal field in front of the plasma grid of 15 mT.. The extraction grid was equipped with Asymmetric Deflection Compensation Magnets (ADCM), to minimize the beam deflection. The profiles of magnetic field in vertical (x axis) and horizontal (y axis) direction along the source axis (z) are plotted for configuration *d* in Fig. 3.36. where z=0 corresponds to the knife edge of the PG apertures. From the operation it resulted that the EG field, which penetrates in the source volume, was insufficient to limit the co-extraction of electrons.

From 01/03/2018 to 24/04/2018 a shutdown of the machine took place, to substitute the EG

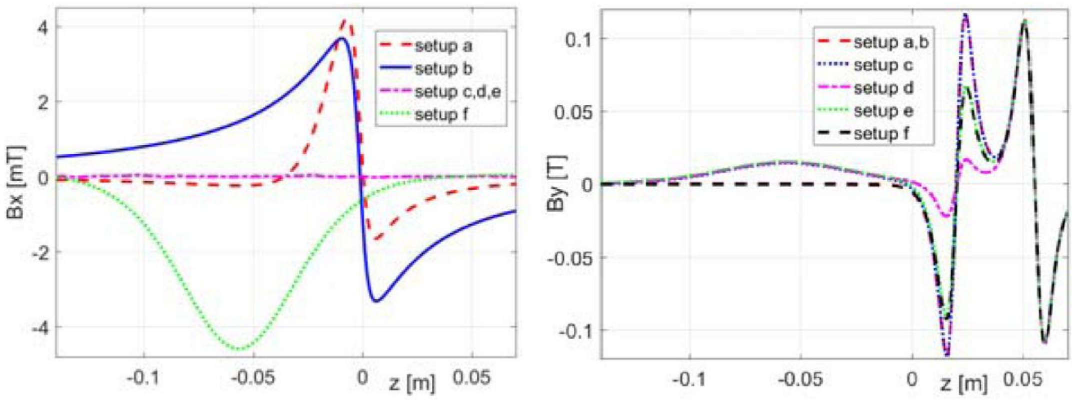

Fig. 3.36 Vertical (Bx) and horizontal (By) profile of the permanent magnetic filter field in NIO1[3].

magnets in order to produce a stronger filter field. The pyrex cylinder which separates the source volume from the RF coil was substituted.

From 24/04/2018 to 16/07/2018 the source resumed operation .

From 16/07/2018 to 26/07/2018 another shutdown took place, to change the magnetic configuration: the extraction grid was left unaltered, while the front multipole was modified in order to create a vertical, downwards magnetic field of 5 mT (3 times lower than the previous one). The (vertical) magnetic filter field created by the plasma grid current (max 3 mT @ 400 A) was found capable of modifying the total field more effectively.

From 26/07/2018 to 09/11/2018 the source resumed operation. The operative capabilities of the source were limited by an internal short circuit on the bias plate, which prevented it from being polarized. Moreover, the plasma became more evidently affected by some transient behaviors, characterized by a rapid (~1÷2 min.) drop in plasma luminosity, correlated to a dramatic increase (up to a factor 10) of the accelerated current. Each phenomenon was then followed by a regrowth of plasma luminosity and by a corresponding decrease of the accelerated current.

From 09/11/2018 to 21/11/2018 a shutdown was performed to solve the bias plate short circuit, and to modify the PG electric circuit in order to easily switch the current direction, and so the produced magnetic field.

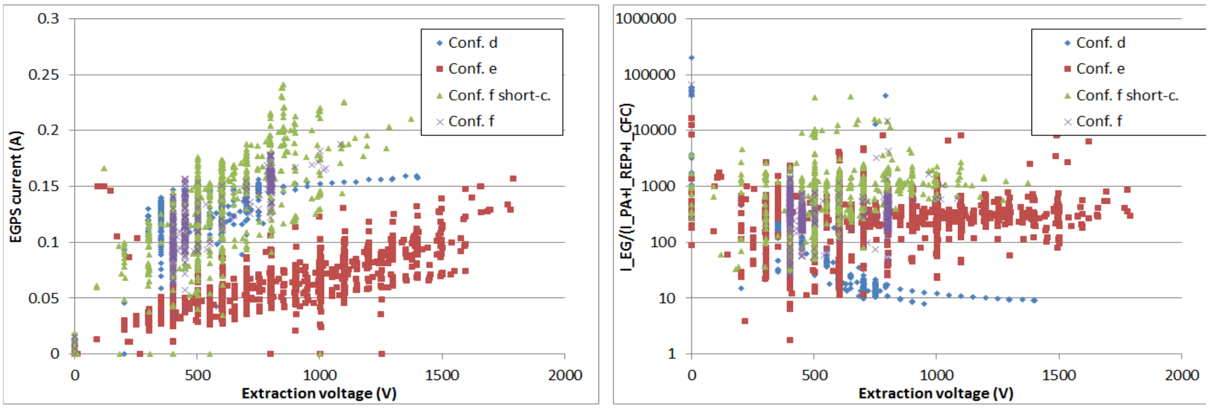

Fig. 3.37 EG current and fraction of coextracted electrons, plotted for each data point collected in 2018, as function of the extraction voltage.

From 21/11/2018 the source resumed operation with the bias plate now operative. It has been found that the temperature of the pyrex cylinder is strongly affecting the plasma conditions. The investigation on this phenomenon is ongoing.

The performances of the source in the 3 magnetic configurations adopted in 2018 can be compared in Fig. 3.37. The plots in the figure show the EG current, which can be assumed as the coextracted electron current, and the fraction of co-extracted electrons, calculated as the EG current over the sum of the currents collected on the other grids (PA and repeller) and on the CFC tile. The modeling activity on negative ion beam acceleration for NIO1 was improved by considering the effect of the secondary particles produced in the beam gas-interaction.by the code IbSimu. In particular, the stripping of the primary beam, the ionization of the background gas and the secondary emission of electrons due to the beam-grids interactions has been now considered.

The results on the beam-gas and beam-grids interaction were successfully compared to those obtained by the code EAMCC. The agreement with the experimental from the visible cameras in the drift region was consistently enhanced and is now quite satisfactory, as

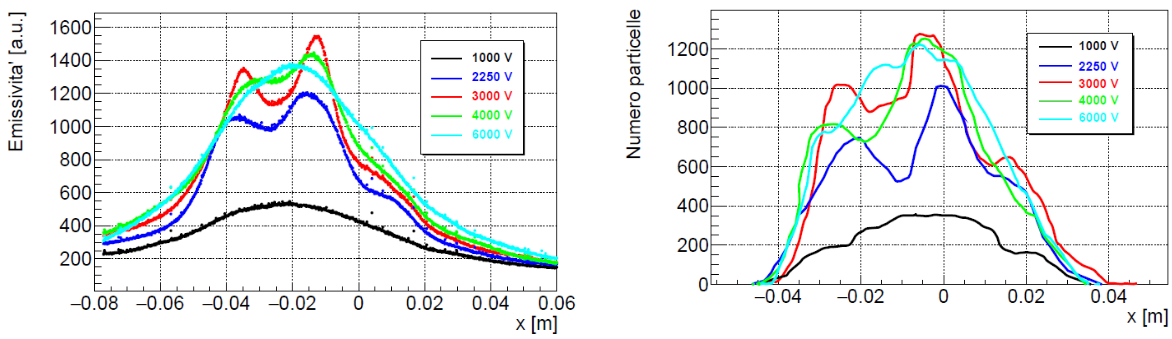

(a) (b)

Fig. 3.38 (a) Emissivity from beam-gas interaction in the horizontal direction measured by a visible camera at about 400 mm downstream the accelerator. (b) Beam profile along the horizontal direction at 400 mm downstream the accelerator calculated by IbSimu.

shown in Fig. 3.38

In order to analyze the space charge compensation (SCC) phenomenon in NIO1, a single Langmuir probe was installed in the diagnostic tube downstream the accelerator. Data have been collecting varying the beam current, the beam energy and the pressure in the vacuum vessel. The latter was varied by switching on and off the NIO1 cryopump. The effect on the I-V characteristic is given in

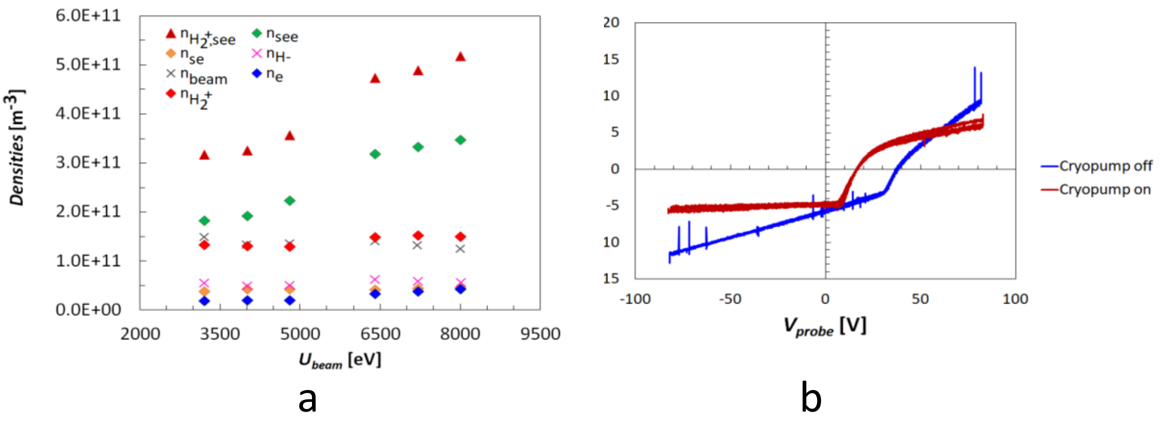

Fig. 3.39 a. The different contributions affect different portions of the I-V characteristic and may be determined by a multi-variable fit. The dependence of the different contributions on the beam energy is instead given

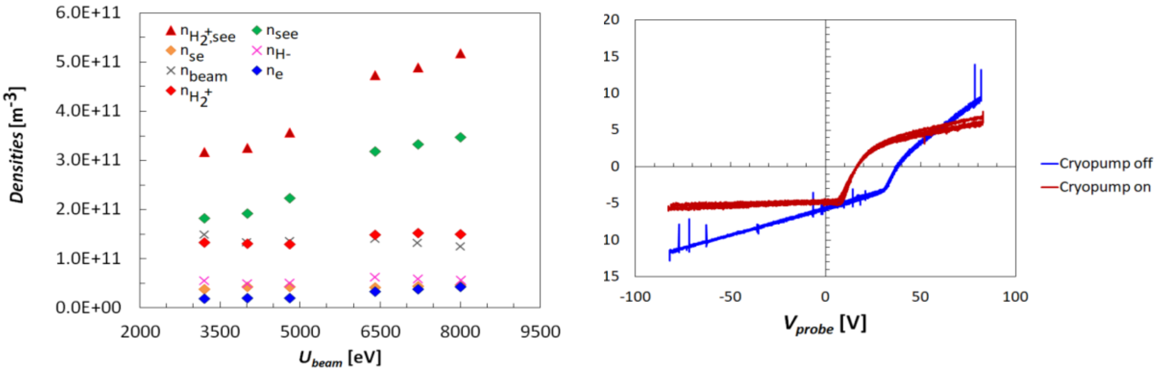

a b

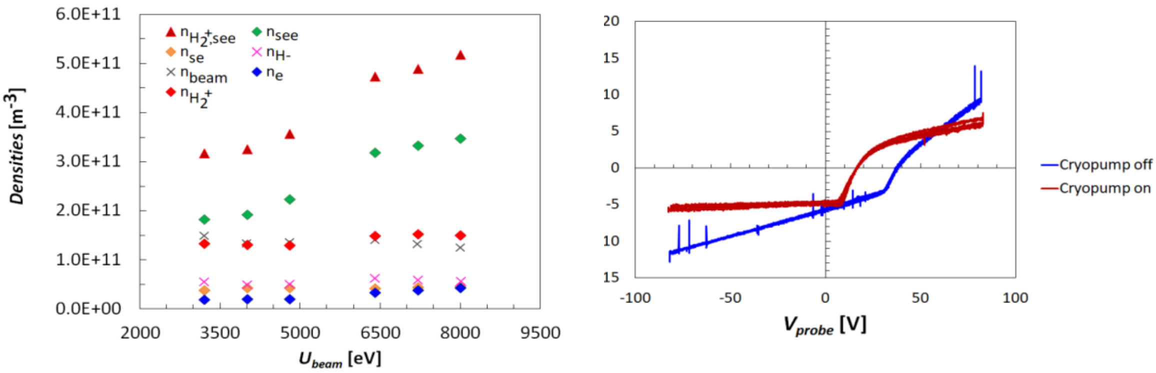

a b

Fig. 3.39 (a) Effect of cryopumping on the probe I-V characteristic. (b) Densities of different species derived from fitting of the characteristic, no cryopump.

Fig. 3.39 b. In particular it was found that :the secondary emission and electron stripping contribution is non-negligible, also when the cryopump is operating; the positive ion density is about one order of magnitude larger than plasma electron density and increases with the beam energy It is worth highlighting as the improvement of the NIO1 performance will enable to minimize the perturbation due to the probe itself.

NIO1 is provided with many diagnostics which allows to completely characterize the source and the extracted negative ion beam. In particular, the diagnostics available to characterize the NIO1 beam are the Beam Emission Spectroscopy (BES), three CMOS cameras, two electrostatic probes, a Retarding Field Analyzer and a LANGMUIR probe. In addition to these, the current hitting the grids of the NIO1 accelerator and the CFC tile which is used as a calorimeter are also measured. A comprehensive description of the negative ion beam is given using the data collected by the BES, the currents measured on the various components and the images collected by the cameras.

Beam emission spectroscopy is based on the study of the radiations produced by the interaction of the energetic ions with the molecules in the vacuum chamber, downstream of the ion source grids. It enables to measure the beamlet divergence, uniformity and direction of propagation. The beam divergence depends on both the acceleration and extraction voltage as shown in

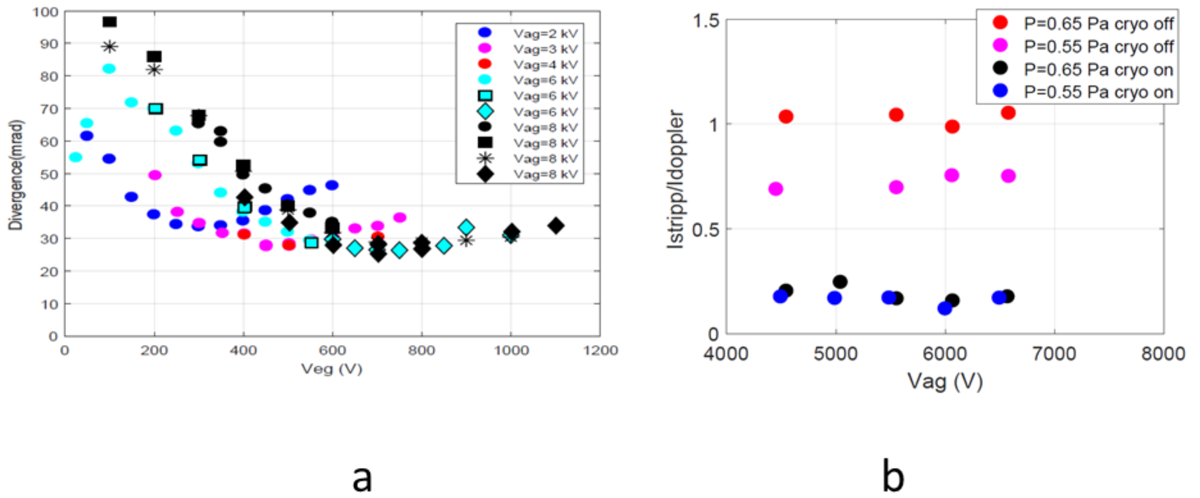

Fig. 3.40a, where the minimum of beam divergence in the *d configuration* shifts towards higher extraction voltage value as the acceleration voltage increases.

From April 2018, three telescopes are used to monitor the beam evolution. Such telescopes are installed at different vertical positions in order to characterize also the vertical properties of the beam. The beamlet divergence obtained is comparable with the beamlet divergence measured by the single telescope (around 45 mrad as mean value).

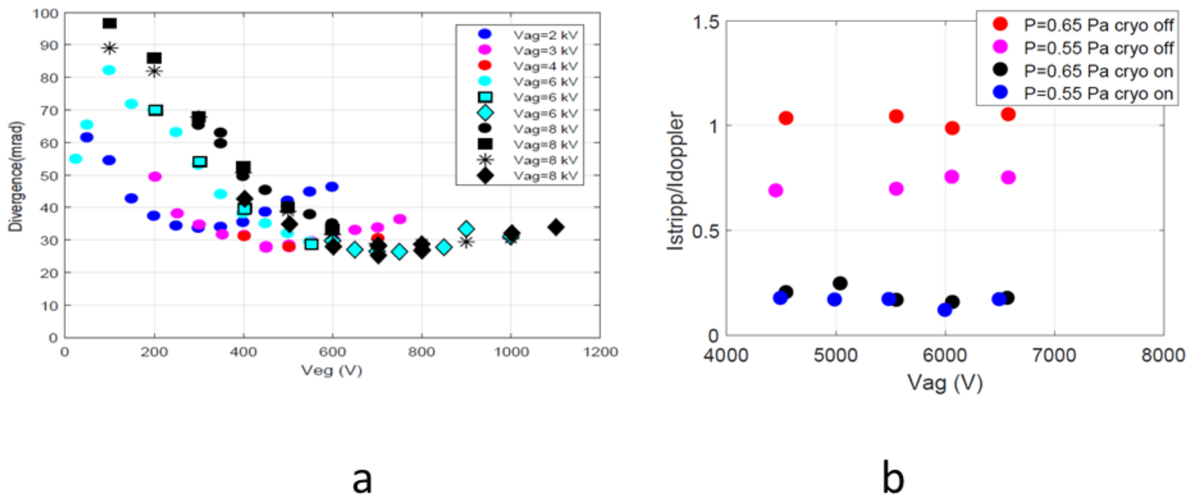

Fig. 3.40 (a) Beam divergence evolution as a function of extraction voltage at different acceleration voltages. (b) $I_{stripp}/I_{doppler}$ as a function of the acceleration voltage at different pressures and with/without cryopump.

The beam emission spectroscopy allows also the measurement of the stripping integral and emphasize the effect of the cryogenic pumps, with a decrease in the ratio $I_{stripp}/I_{doppler}$

larger than a factor 2.5 (

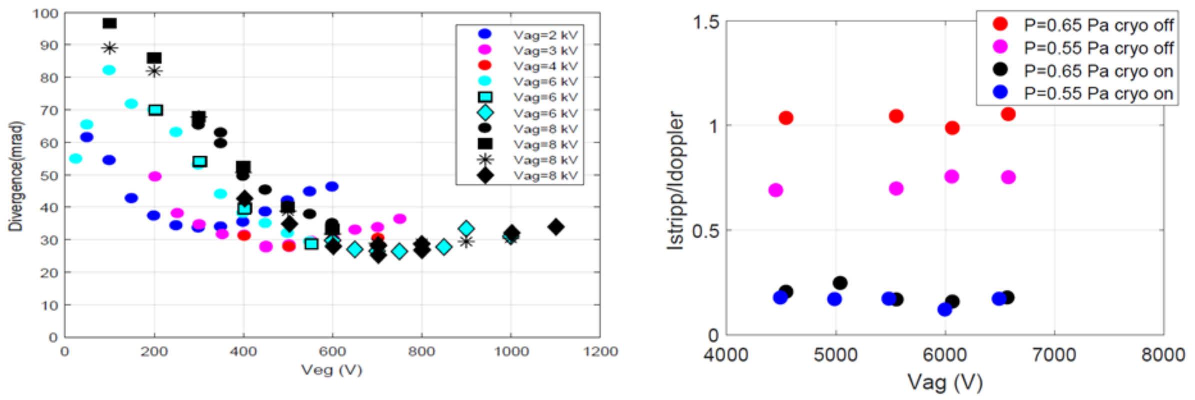

a b

Fig. 3.40b).

Visible tomography. Tomography aims at measuring the emission or the absorption of radiation through a large number of lines of sight (LOSs). Beam tomography aims at measuring beam spatial uniformity which is found to be one of the most difficult issue to solve.

NIO1 tomography system was composed by two visible CMOS cameras positioned at 90 degrees with respect each other. A third camera was installed in July 2018 in order to achieve a more complete beam reconstruction: using a mirror inside the NIO1 vacuum vessel, the third camera is able to see the beam at an angle of almost 80 degrees with respect the horizontal plane. By fitting the data with three Gaussians it has been possible to determine the horizontal displacement of the beamlets due to the effect of the filter current. -

3.3.3. *Alternative ion Source ATHENIS*

During 2018 ATHENIS (Alternative Thruster Hall Effect Negative Ion Source) has been completed and operated to test the plasma generated in the source. This alternative scheme is based on a Hall Effect Thruster (HET), and the HET is used as a plasma generator with tunable ion energy by means of the operational voltage. According to the project, the source will be complemented within the end of the year by an extraction system and by a system of grids to partially shield the plasma and highlight the contribution of the dissociated atoms.

Fig. 3.41 shows a scheme of ATHENIS: the inner diameter is 6mm, the outer diameter is 12.6mm and the length is 58.5mm. The magnetic field is generated by permanent magnet disks inserted in rings of aluminum (15 magnets for each ring).

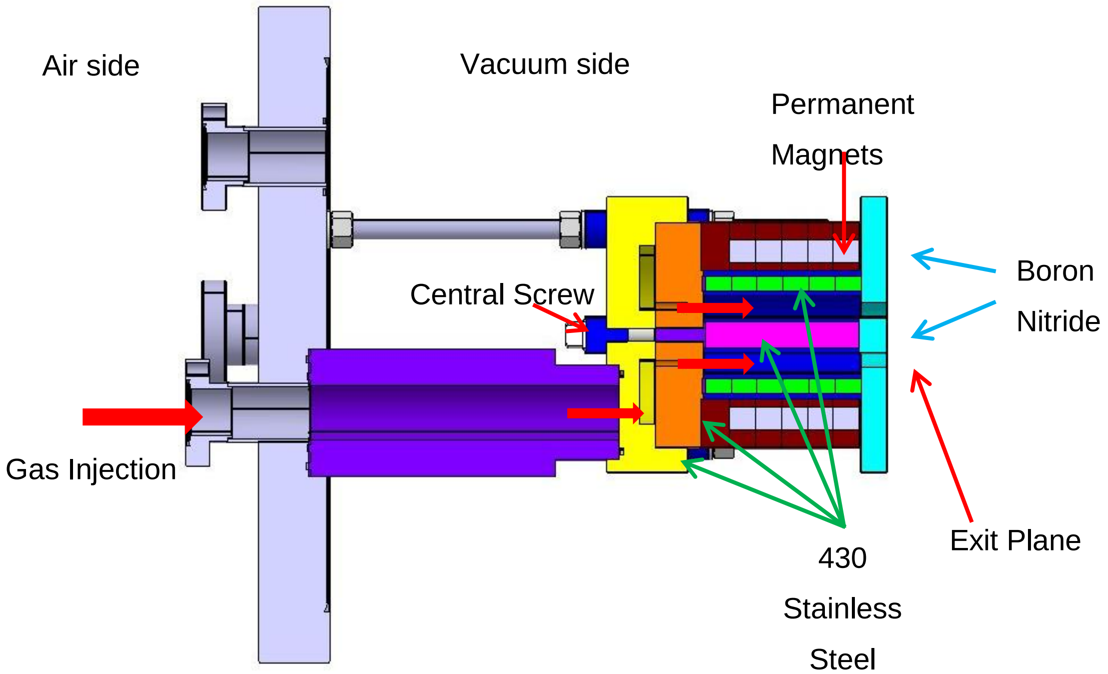

Fig. 3.41. Scheme of ATHENIS, a Hall Effect thruster operating at Consorzio RFX.

To ignite the plasma, a ring-shaped tungsten filament has been placed at 2.5 cm from the exit plane so that it works as an emissive cathode. The best position of the filament to let the emitted electrons enter the HET channel before the ignition has been obtained as the outcome of a numerical simulation of the trajectories of electrons leaving the cathode in every direction and subjected to the electric and magnetic field.

Figure 3.42(a) shows the experimental set-up hosting ATHENIS. The device is installed inside the small cubic chamber, while the larger vacuum chamber is necessary to keep the Hydrogen concentration within the safety requirements. Vacuum of the order of 10^{-6}mbar without gas injection, and of 10^{-2} mbar with gas injection, is regularly achieved by a 1000 l/s turbopump and a rotative pump of 60 m^3/s. The cathode is negatively biased with a maximum voltage of -90V, while the anode is positively biased to a maximum of 250V. The anode consists of all the metallic parts that delimit the channel of the device, i.e. the yellow, orange, purple, green, dark red and the permanent magnets shows the vacuum electric field, which is axial only at the exit plane. After the ignition, the plasma cannot close the circuit to the channel walls since they are made of quartz. The plasma is then forced to close the circuit at the bottom of the channel, where the gas injection occurs.

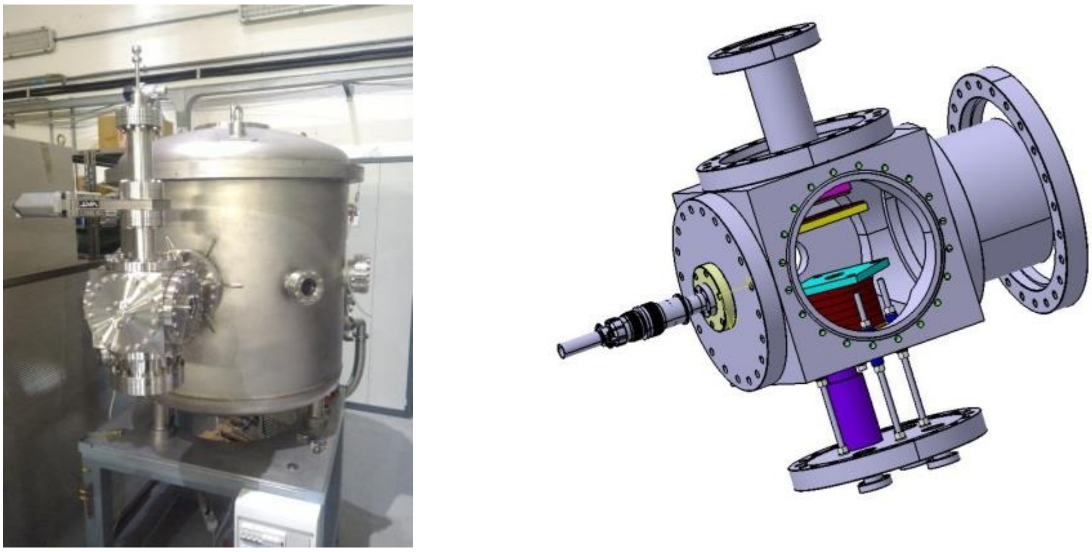

(a) (b)

Figure 3.42. (a) ATHENIS facility; (b) 3D drawing of ATHENIS assembled parts.

3.3.3.1. Langmuir probe measurements

In order to characterize the plasma generated by the device, a Langmuir probe has been installed on a z-shifter manipulator. The main results in Nitrogen are shown in Figure 3.43 and Figure 3.44. The temperature and density plots in the bulk plasma, spanning a distance of 4 cm from the ion source exit, show an almost constant temperature of the order of 3 eV except for the region near the cathode (see Figure 3.43). Figure 3.44 shows, that density and temperature values increase with the applied voltage and are uniform over the spatial range spanned by the probe. From these results it appears, that the voltage plasma discharge is the main drive of the plasma parameters. To control this parameter, both in Hydrogen and Nitrogen, it has been found that we have to decrease the cathode current. For operation in Nitrogen an optimum value of mass flow rate has been found at which plasma density and electronic temperature reach their maximum value. For the Hydrogen case, only low values of mass flow rate were considered in order to keep the pressure low enough to guarantee a mean free path of the H_0 atoms of the order of some cm so to allow them to hit the caesiated target. It has been found that the plasma parameters keep the same trend for both values of mass flow rate studied, even though a more stable behavior has been observed for the higher one.

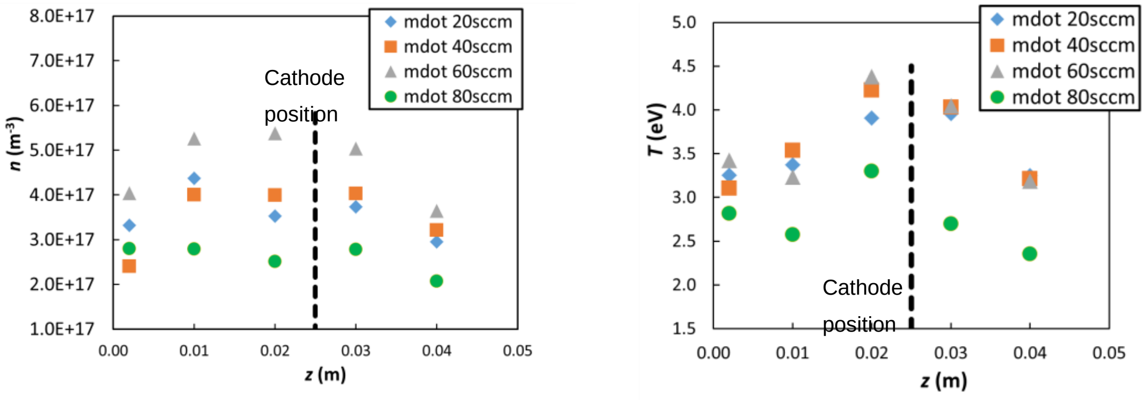

(a) (b)

Figure 3.43. (a) Plasma density axial profile for several N_2 mass flow rates. (b) Electron temperature axial profile for several N_2 mass flow rates. Plasma voltage discharge varies from 65V to 95V with a fixed cathode current of 6.3A. The position of the filament (the cathode) is also shown

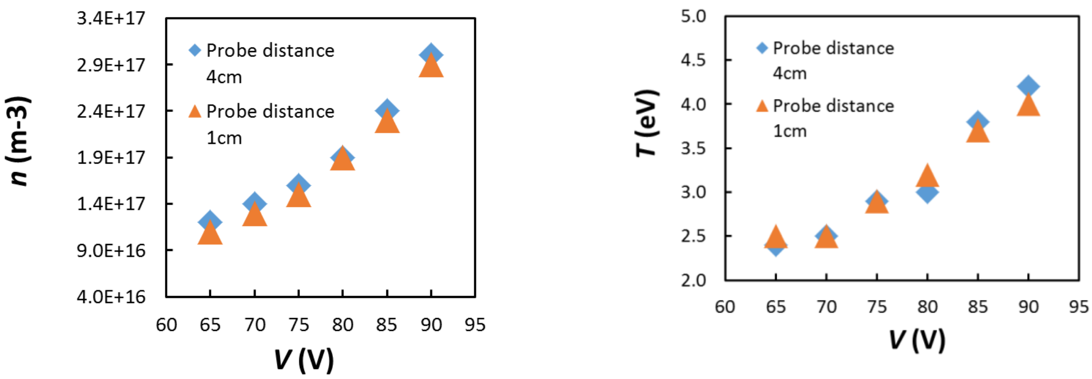

(a) (b)

Figure 3.44. (a) Plot of plasma density according to plasma voltage discharge. (b) Plot of electronic temperature according to plasma voltage discharge. Current plasma discharge varies from 0.4A (65V) to 1.2A (90V). Cathode current 5.8A.

Preliminary results from the experimental campaign in Hydrogen show (see Figure 3.45), that the plasma density is almost spatially uniform while the temperature tends to decrease with the distance from the HET exit.

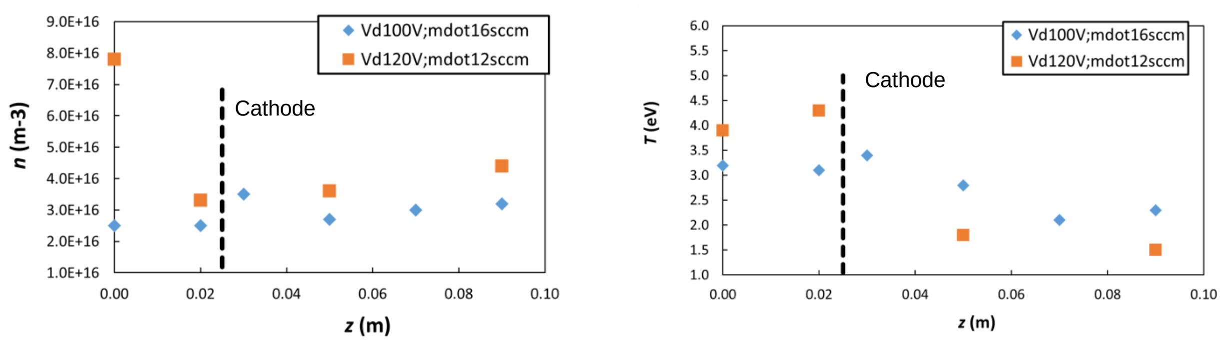

(a) (b)

Figure 3.45. (a) Plasma density axial profile with different voltage discharge and similar mass flow rate. (b) Electronic temperature axial profile with different voltage discharge and similar mass flow. Current plasma discharge 1.312A with cathode current 5.6/5.8A.

3.4. *PPPT Projects*

3.4.1. *WPHCD – Heating and Current Drive systems*

The injection of high energy neutral beams is one of the main tools to heat the DEMO plasma up to fusion conditions. A conceptual design of the Neutral Beam Injector (NBI) for the DEMO fusion reactor is currently being developed by Consorzio RFX in collaboration with other European research institutes. High injector efficiency and RAMI (Reliability, Availability, Maintainability and Inspectability), which are fundamental requirements for the success of DEMO, must be taken into special consideration for the DEMO NBI.

A novel design of the beam source for the DEMO NBI is being developed featuring multiple sub-sources, following a modular design concept, capable of increasing the reliability and availability of the DEMO NBI.

During 2018, the DEMO NBI conceptual design has been discussed with the interested working groups of EUROfusion, working on the main related issues (physics, integration, breeding blanket, remote maintenance, neutronics). Moreover, an External Design Review Panel has been organized in February 2018, which has given a feedback on the proposed design solutions, and meetings with industry were held in order to understand the industrial feasibility of some critical components.

Based on these discussions, the following activities were carried out in 2018 in collaboration with the EUROfusion groups working on the heating and current drive systems, on the breeding blanket and on the remote maintenance, the CCFE groups studying neutronics and remote handling, and the CIEMAT group designing the BB with the Dual Coolant Lithium Lead (DCLL) concept:

- RAMI (Reliability, Availability, Maintenability, Inspectability) analysis of the beam source
- Engineering design of design solution featuring a plasma neutralizer
- General improvement of conceptual CAD of the NBI injector
- Advancements in the design integration.

Photoneutralization is regarded as one of the most interesting alternatives to stripping neutralizers in NBI systems. R&D activity on photoneutralization at Consorzio RFX involves the construction and test of a non-resonant cavity for second laser harmonic trapping, fed by a pulsed Nd-Yag laser. During 2018, the cavity has been under operation and has demonstrated the possibility to achieve stable optical configurations, with a particular focus on the studies regarding the capability to maintain a continuous and constant second harmonic beam in an optical cavity using a pulsed laser source.

3.4.2. ***WPDC – Diagnostic and Control***

In 2018 WPDC underwent some modifications in order to focus the effort on the priority activities. The 2016/2017 RFX tasks were not considered among these and the RFX research group working on WPDC has been asked to modify the 2018 work proposal to meet the priority issue. In this context, in 2018 the activity concerned the support to IFP in Milan working on diagnostic design for MHD detection. In particular, the activity focused on the proposal (searching in the literature) for diagnostic systems alternative to the ECE systems (e.g. interferometer and polarimeter). For this activity the ppy allocation has been squeezed to 0.1 ppy.

A preliminary activity concerned also a more accurate definition of the diagnostic systems features to be used for MHD detection. As a part of 2019 activity, diagnostic signals will be simulated and the possible time/space resolution and S/N ratio will be investigated for the DEMO equilibria. However, the final decision on the 2019 activity will be agreed with respect to the WPDC priority.

3.4.3. ***WPFTV - Tritium, Fuelling and Vacuum Pumping Systems***

Consorzio RFX is involved in the development of new pumping systems within the WPTFV, with a dedicated research activity related to the development of Non Evaporable Getters as viable option for replacing cryogenic pumps in Neutral Beam Injectors.

The final design of the large-scale mockup pump was completed in July 2018 with a review meeting, after which the manufacturing activities could begin. In parallel to the manufacturing of the pump, the design and preparation of the power supplies and control system began. The requirements for the experimental tests, and therefore the upgrade requests for the TIMO facility where the tests will be carried out, were also defined.

The design activity of the large NEG pump mock-up has been finalized. The results of numerical simulations (thermal and gas distribution) and of experimental campaigns on intermedium size getter pumps (performed by SAES) have been used to define the best conceptual solution comparing 3 different configurations. The mock-up pump is based on the configuration which has a good compromise between engineering requirements and performance (see Fig. 3.46). It is composed by 9108 disks divided in 204 stacks with an overall size of 390x300x980 mm, with a total mass of getter of about 32 kg. This solution shows a good uniformity among different 6-stack modules and non-uniformities are limited within the module itself. Each module is provided of 4 heaters for redundancy, connected two by two in series. The cartridges have a plug-in system for the installation on the support frame.

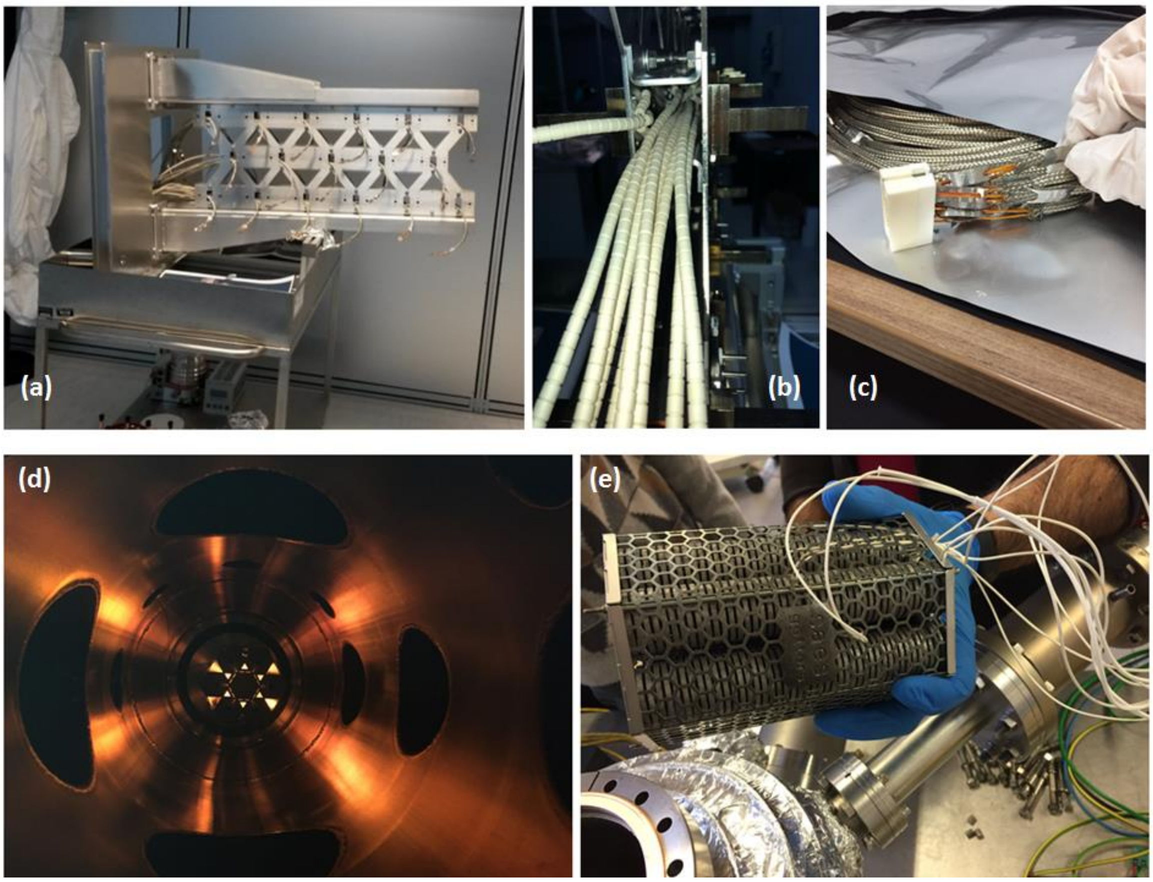

Fig. 3.46 Pictures of mockup assembly and tests on the protoype single cartridge: (a) support structure for the 34 getter cartridges during assembly (b) alumina bead insulated cables for powering cartridge heaters (c) in vacuum connectors and cables (d) prototype cartridge during regeneration (e) prototype cartrige wired with thermocouples

In December 2018 the construction of the pump cartridges and the support structure has been completed. The support structure was designed for the installation of the pump in TIMO facility (KIT laboratory) for the next tests to be carried out in the second half of 2019. The power supply of the heating system and the control software has been defined with SAES.

In the meanwhile, a prototype of one getter cartridge (about 258 sintered ZAO alloy disks), has been characterized in terms of thermal behavior, thus determining possible improvements of the heating system that are being investigated. A new version of the heating system is expected to be prepared before May 2019. In December an experimental campaign has begun in order to study the regeneration and the pumping performance of the NEG prototype cartridge.

3.4.4. ***WPMAG – Magnet System***

The studies on DEMO TF circuit topologies have continued this year. Four different topologies (called A, B, C and D) have been identified as possible candidate for the DEMO TF circuit, differing for the earthing system (ITER-like or JT-60SA like) and for the connection of the discharge resistors: in parallel to the FDU circuit breaker or to the coil.

Additional fault conditions have been identified which led to discard two of them, since in case of untimely intervention of one FDU only, the transient voltage peak applied to the coil could raise to very high values before the intervention of a backup circuit breaker. However, their relative merits could be kept in further mixed topologies, that could be studied in the future. The results of numerical simulations of the TF circuit operation for both the cases with 16 and 8 coil sectors and for A and B topologies have shown minor merits of one topology versus the other in terms of maximum values of voltage at the coil terminals, across the coils and i^2t in the coils during the discharge. Both of them could be adopted for DEMO: deeper analyses will be possible after having defined the technology of the FDU circuit breaker and at least a tentative layout to evaluate the stray impedances of the TF circuit connections so as to better estimate the transient voltage waveforms at the coil discharge and gain more arguments for the topology selection.

As for the reduction of the number of TF coil sectors to eight, the analyses suggest to maintain the present reference TF circuit topology with 16 sectors.

3.4.5. ***WPBOP PES – Plant Electrical System***

In 2018, the *Plant Electrical System* (PES) design activities, included in the WPPMI work package in the previous years, have become a sub-project of the Balance of Plant work package (WPBOP). The PES design covers the Electrical power generation system and the Power Supply (PS) systems necessary for feeding all the plant loads, including H&CD power supplies and fast converters for error field correction, plasma stability and MHD mode controls.

This year, the work has remained mainly concentrated on the DEMO SuperConducting (SC) Coil Power Supply (PS); the estimation of the reactive power demand has been concluded developing a comprehensive analytical model, assuming the voltage and current profiles provided by CREATE Consortium and a traditional design approach based on thyristor rectifiers. The model includes the same current control algorithm for the converter units and the sequential control of series connected units applied in ITER. Then, also the bypass control of series connected units has been implemented in the model.

The results of the estimations of active and reactive profiles to be required from the grid, showed in Fig. 3.47, proved to be far beyond limits generally fixed by the power grid operators. Since these limits are expected to become even more stringent in the future scenarios with weaker grids because of the extensive use of distributed renewable energy source, studies have started to explore innovative design solutions to supply the SC coils.

One of the two approaches explored this year s based on Active Front End (AFE) technology for the power converters to supply the SC coils. The suitability for DEMO has been verified with a dedicated numerical model also to investigate the impact in term of reactive power required to the grid. A preliminary design has been perfomed also with the aim to estimate the area occupancy of DEMO base converters using this technology in comparison with the ITER-like solution. This study will be expanded in the next year to investigate on possible issues related to the integration of AFE converters in the DEMO coil circuits.

Another design approach that seems very promising has been conceived this year; it consists in a new Magnetic Energy Storage and Transfer (MEST) system, whose scheme is shown in Fig. 3.48. The basic idea is to provide an additional Superconducting Magnetic Energy Storage coil (TC), pre-charged along with the coil to be supplied to the same current value and then to transfer step by step the energy from one to the other and viceversa during the different phases of the plasma pulse, via switched capacitor.

A model of the system has been developed and numerical simulations have been performed to reproduce its operation; the results have shown that the proposed scheme can effectively support the plasma ramp-up and sustainment with a smart interface with the electrical grid, since no high power peaks and reactive power are required, but only the active power to sustain for the plasma and compensate for the circuit losses. The application of this design approach to the DEMO CS magnet is in progress and will proceed during the next year.

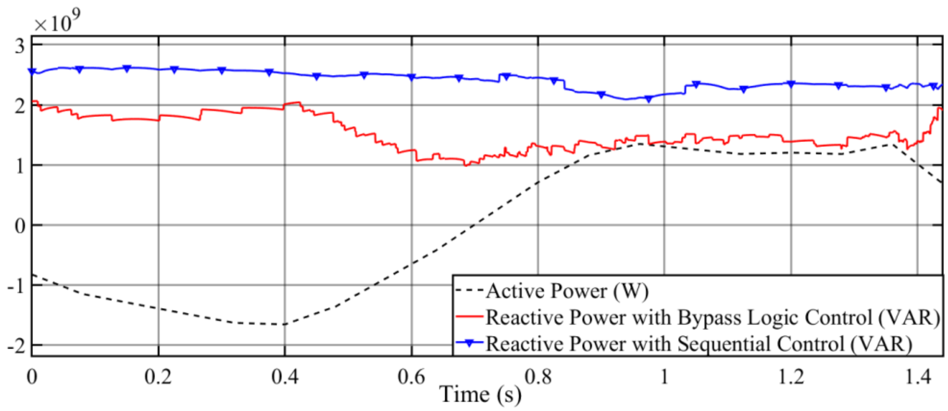

Fig. 3.47 Active and reactive power profiles for the DEMO plasma breakdown phase

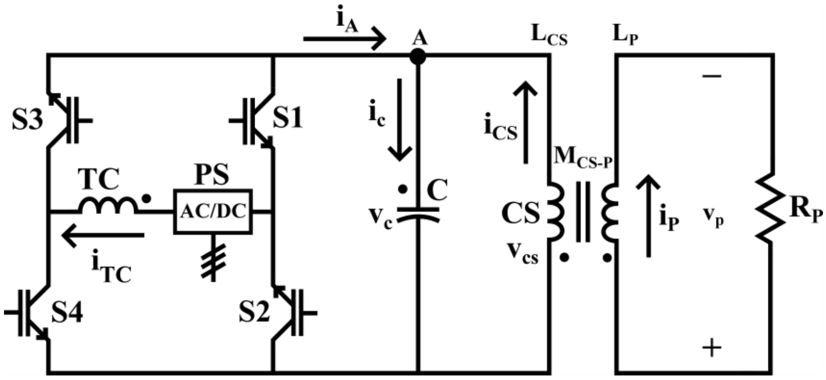

Fig. 3.48 equivalent scheme of CS magnet coupled with the plasma and PS for coil charge and losses compensation

3.5. *Socio Economic Studies (SES) and DEMO*

3.5.1. *Fusion power plant assessment studies*

The task under the EUROfusion Work Package PMI on cost sensitivity studies with PROCESS, originally planned for 2017, has been extended to 2018 with no additional resources. Sensitivity analyses have been carried out for the identification of the cost range of the most relevant components that increases the capital cost by no more than 10%. The outcomes of the study provide indications on where efforts should be addressed to reduce the overall costs of a DEMO power plant and, as a second step, a commercial power plant. The activities on the FRESCO code developments (upgrades for modelling Reversed Field Pinch reactors and Fusion-Fission hybrid reactors) have been postponed to 2019.

3.5.2. *The role of fusion in long term energy scenarios*

The resources allocated on the EUROfusion Work Package on Socio Economic Studies encompass both project management and research activities.

Within the research activities, Consorzio RFX contributed to the development of new scenarios for the estimation of the impact of external costs, that are the monetary quantification of socio-environmental damages/benefits due to the power plant construction and electricity generation, on the penetration of fusion power plants in the future global electricity system. Fig. 3.49 shows that the share of electricity from nuclear fusion increases when external costs are considered. Nevertheless, fusion penetration is higher in scenarios with high electrification and more stringent climate policies (Paternalism and Harmony scenarios). Therefore, even though externalities can help future fusion penetration, factors like investment costs, stringency of climate policies and electrification of the energy system seem to have greater influence.

Consorzio RFX gave support to ENEA and the Joint Research Centre (JRC) for the implementation of the dispatch model of a possible European energy system in 2060, based on the outcomes of the SES studies on energy scenarios. The first preliminary outcomes of the study show that moving towards a fully decarbonized European energy system, based on the available European renewable resources, could require more nuclear power capacity than today, to be installed even in countries that are now nuclear-free to ensure electricity generation and demand balancing.

In addition, a small contribute to the implementation of the Multi Region Input Output methodology to study the socioeconomic benefits of fusion power deployment at a global level was given.

Within EUROfusion activities, Consorzio RFX has been also involved in the design of a section of the new Fusion Expo. Specifically, indications on the scientific content of the "energy game" that will be based on the SES energy scenarios were given.

Besides, new studies have been carried out with the COMESE code (*COsto MEdio del Sistema Elettrico*) on European scale. Fig. 3.50 shows that in a carbon-free power generation mix, likely by year 2080 and beyond, fusion power plants would reduce the cost of electricity both in typical North-Europe and South-Europe scenarios, in comparison with 100%-RES scenarios. Sensitivity analyses demonstrate that this is true as long as the overnight cost of a fusion power plant will

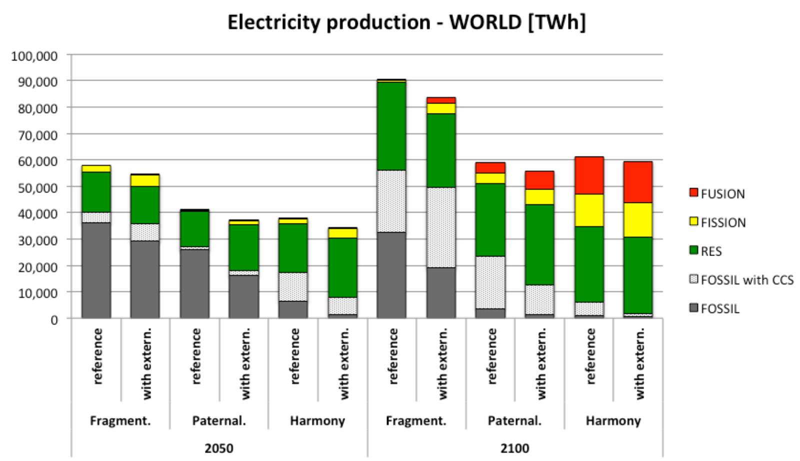

Fig. 3.49: Electricity generation by source in the EUROfusion scenarios Paternalism, Fragmentation and Harmony w/o externalities (SOFT 2018 conference)

be lower than 8500 Eur/kW in the North-Europe case and lower than 12500 Eur/kW in the South-Europe case. Studies on the economic impact of the electric grid expansion due to the increased share of electricity from renewables have been postponed to 2019.

3.5.3. *SES economic studies – dissemination and communication of results*

In 2018, dissemination and communication of the SES foresight activities started with the upgrade of the SES pages of the EUROfusion website. In particular, larger emphasis was put: a) on the presentation of the stakeholder consultation on storylines and scenarios carried out through a Delphi survey, to give reason for the interesting results collected from stakeholders' opinion; b) on the illustration of the first data obtained from the European Survey on public attitudes towards fusion energy and research carried out in 2018 by SES in view of their analysis in 2019.

3.6. *Education and Training*

In 2017 the Universities of Padua and Gent, on the basis of the successful experience in running two international leading programmes (the *Padua-Lisbon-Munich* and the *Erasmus Mundus Fusion Doctoral College*), have implemented a Joint Doctorate Programme in *Fusion Science and Engineering* aiming at the continued formation of a suitable number of doctoral students at the highest level of excellence. So far, 8 PhD students have been enrolled in academic year 2017/18 (XXIII cycle) and 2018/19 (XXIV cycle).

Moreover, in academic year 2016/17 10 PhD students enrolled in the last cohort(XXXII cycle) of the previous Doctorate Programme in *Fusion Science and Engineering*, coordinated by Padua University under an international agreement between the Universities of Padua, Lisbon and Naples "Federico II".

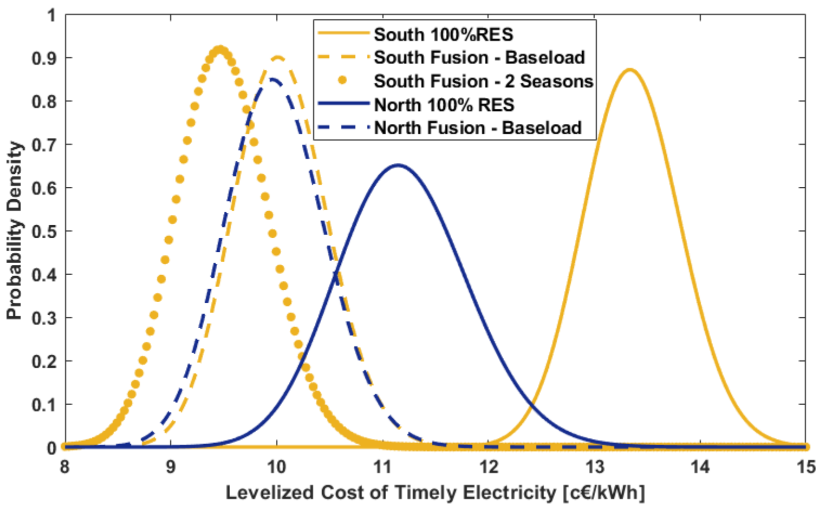

Fig. 3.50: Probability density distribution of the LCOTE generated with the COMESE code (SOFT 2018)

Overall, in 2019 18 PhD students will operate at Consorzio RFX and partners' premises, under the tutoring of members of the PhD Academic Council and RFX researchers.

The other educational and training actions carried out at Consorzio RFX have continued as usual, with tutoring of 24 Master/Bachelor students in Physics or Engineering , with internships of master students and with summer stages of high school students.

One master student in Physics has carried out a thesis project in the field of fusion at the Eindhoven Technical University, under an Erasmus student exchange program coordinated by the Physics and Astronomy Department of Padova University.

Moreover the following 7 regular courses on Plasma Physics, Fusion Technology and Industrial Applications of Plasmas were held by teachers from Consorzio RFX at Padua University:

- Basic principles of Plasma Physics (6 ECTS, 1st Level Degree, Physics)
- Physics of Nuclear Fusion and Applications of Plasmas (6 ECTS, 2nd Level Degree, Physics)
- Fluid and Plasmas Physics (6 ECTS, 2nd Level Degree, Physics)
- Fission and Fusion Nuclear Plants (9 ECTS, 2nd Level Degree, Engineering)
- Energy Technology and Economics (9 ECTS, 2nd Level Degree, Engineering)

In addition a national prize of the Consorzio RFX for the best thesis project in the field of controlled fusion has been awarded to 4 master studentes, 2 in Physics and 2 in Engineering.

3.7. *Communication and outreach*

- The information activity carried out in 2018 at Consorzio RFX developed, in collaboration with ITER IO and F4E communication offices and Eurofusion Public Information network, along two main lines of activities:
- production of information content;
- outreach and communication initiatives;
- Informative material (brochures and posters), multimedia content and production (photos, videos) and press kits were regularly produced on the occasion of events and initiatives, the most significant are listed below.
- The first months of 2018 were dedicated to the preparation of the ceremony of SPIDER Inauguration, which took place on 11 June 2018. Weekly video-conference discussions among IO, F4E and RFX communicators were regularly organized to agree on shared approaches and schedule of the event. About 360 people attended

the ceremony in the presence of ITER and its stakeholders. During the ceremony, plasma was generated in the beam ion source for the first time and the event was seen in streaming worldwide.

In order to prepare the Italian press to report on it and increase the media interest on fusion research and ITER NBI research, a course for Italian journalists was held on 6 June 2018 at NBTF premises in collaboration with the Order of the Journalists of the Veneto. The event was attended by 26 journalists, some of them wrote articles covering the Spider event.

The preparation of the European Night of Researchers (28 September 2018) started soon after, with the realization of an education game on the optimization of negative beam production in SPIDER and with the organization of the exhibition at the University of Padua, guided by a team of about 10 researchers from Consorzio RFX. Within the activities of the European Night of Researchers, a promo video on SPIDER-NBTF was realized in parallel; it was shown at Porto Astra Multiplex, a large cinema in Padova, before each shows in all the movie theatres, free of charge, for a couple of weeks, thus reaching a large audience. An evaluation of the feedback could not be taken from the audience, since no questionnaire could be prepared in time; still really positive comments arrived from Porto Astra, who could monitor the public reaction, and from personal contacts.

In August, Consorzio RFX presented the NBTF project at the 75 Mostra Internazionale di Arte Cinematografica of Venice during an event organized by the Veneto Region at Hotel Excelsior. The presentation focused on how fusion and plasma heating can be seen through the video camera. The event sow the participation of industrialists and representatives of the Veneto Region and of the author of some videos produced at Consorzio RFX. The event was successful and led to a new interest from the Region towards the research.

During the summer, Topolino, the Italian version of the Walt Disney production, could finalize the story "Topolino e il padrone del buio" ("Mickey Mouse and the owner of the dark"). It'll be published and the beginning of 2019.

Two other important events were organized towards the end of the year: in late October about 50 industrialists from the Salone di Impresa Organization visited the Consorzio RFX laboratories; on 19 November the Urban Sketcher Claudio Patanè organized a workshop of Science Sketching at Consorzio RFX in collaboration with Accatagliato Association, Observa and the City of Padua.

In parallel to the above described events, as in the last years, a strong commitment continued to be devoted to a programme of tours and visits to the facilities with a significant public participation and a large presence of secondary school students, thus confirming the tradition of a fruitful dialogue between the laboratory and the school.

The chart in Fig. 3.51 shows the number of visitors in the last twelve years. In 2018 we had a total of 1749 visitors, 1409 of them directly under scientific guide responsibility.

Concerning the RFX-mod activity, a significant contribution was provided for the communication of the MIAIVO Project with actions (informative material, interviews and multimedia production) in parallel to all the communication activities of Consorzio RFX.

4. Broader Approach

4.1. *Power supplies for in-vessel sector coils for RWM control*

During this year the activities for the procurement of the Power Supply system for RWM control (RWM-PS) have been completed up to the delivery of the system in Japan, at the end of September, as scheduled

It is recalled that this power supply system is devoted to control a set of plasma instabilities called Resistive Wall Modes (RWM). RWM-PS is composed of an ac disconnector, a step-down transformer, an ac/dc conversion system and 18 power amplifiers, feeding as many in-vessel sector coils of JT-60SA. The power amplifiers (300 A, 240 V each) constitute the most innovative part; their final design, based on hybrid Si-SiC IGBTs (Isolated Gate Bipolar Transistors), was the result of an R&D task aimed at proving the feasibility of the fulfilment of stringent dynamic requirements (bandwidth of 3 kHz and latency between output voltage and

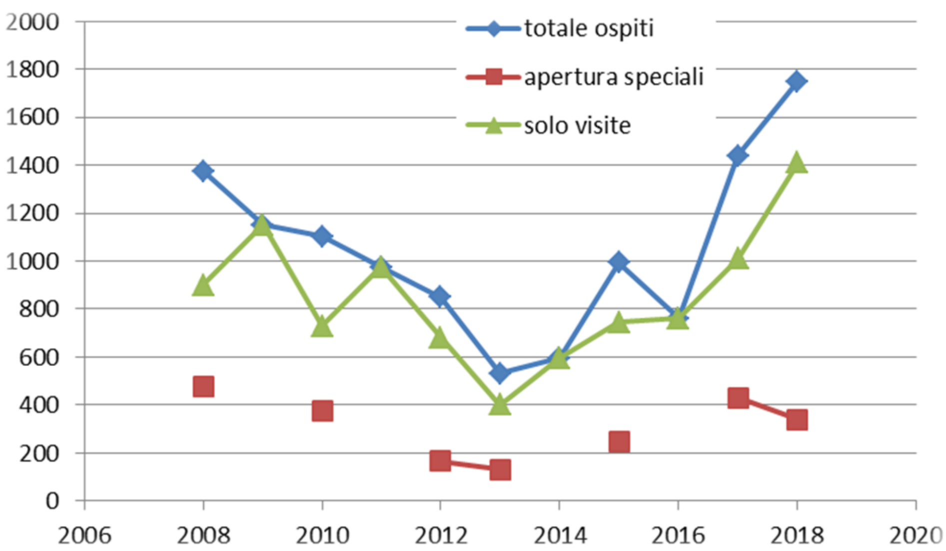

Fig. 3.51 Trend of visits during the last 12 years

reference lower than 50 μs), which were beyond the standard industrial performances, adopting a simple H-bridge topology.

The contract for the procurement of the whole system was placed at the beginning of 2016. After the completion of the detailed design and the development and test of the prototype completed in June 2017, the system manufacturing was completed this year, in late spring.

The factory tests and final integrated tests with the whole system, connected like in the final conditions on Site, fully confirmed the expected performance. For each power amplifier connected to the dummy load, the dynamic performance in terms of bandwith and latency were verified; the test results confirmed the fullfilment of the requirements with significant margin. Other key features were verified too, like the compensation of the non-linearities due to the dead-time to be introduced in the power switches commands to prevent the simultaneous conduction of two switches in the same leg of the fast inverter H-bridge, the effectiveness of the differential output filter to reduce the resonances on the long output cable, and of the common mode filter to smooth the Common Mode voltage oscillations at the load. The correct operation of a dynamic voltage clamp circuit provided in parallel to the dc-link so as to enhance the protection capability for the possible overvoltages induced in case of plasma fast terminations, was also successfully verified. Fig. 4.1 shows the whole RWM-PS system in the final test arrangement.

Fig. 4.1 - Arrangement of the whole RWM-PS system for the final integrated tests

Unfortunately, during the unpacking of the components in Naka, it has been realized that a cabinet including 9 inverters (PCC-B) sustained severe damages during the transportation. The reason and the time when the damages occurred are not yet been clarified. A clarification process among the insurance companies (of the companies in charge fro the packaging, the sea transportation and the ground transportation in Japan) is in progress.

5. Industrial and non-fusion related collaborations

5.1. *Electrostatic design of Vacuum Interrupters using the Voltage Holding Prediction Model*

In 2018 the activity has been almost stopped in absence of an official Agreement with Siemens. Anyhow, in the last quarter of the year discussion with Siemens has taken place to finalize the content of a new agreement. To this purpose, at the Dept. of Electrical Engineering, Padova University a Lightning Impulse Voltage Waveform (LIVW) pulse generator has been set up - see Fig. 5.1 - to perform preliminary tests on two samples of Vacuum Interrupters sent by Siemens Berlin.

A new procedure of voltage application has been implemented, that proved to be more effective in producing Weibull voltage breakdown distribution. The agreement is presently under signature in Berlin

5.2. *Biomedical plasma applications*

As in previous years, a substantial effort has been devoted to the improvement of the array of plasma sources available for the research on biomedical plasma applications. In the past, all the activities were performed using a radiofrequency (RF) plasma source for indirect

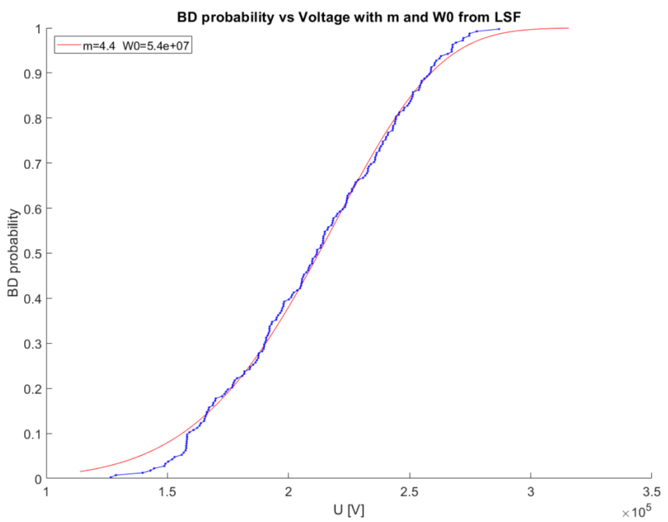

Fig. 5.1 LIVW generator arranged to produce a 300 kV pulse. Inside the transparent tank is visible the VI under test. On the right, the voltage breakdown distribution (8 mm contact gap), and its Weibull distribution fit

treatments, originally developed for disinfection within the context of corneal keratitis. During the course of 2’17, a new plasma source based on the principle of the Dielectric Barrier Discharge (DBD) plasma jet has been developed and tested. The prototype has been improved in 2018, with a 3D-printed final version realized towards the end of the year which has shown remarkable properties of robustness and reliability. The source hosts a high voltage electrode and a grounded electrode, separated by a dielectric layer, required to prevent the onset of an electric arc. The high voltage electrode is driven by a specifically developed power supply, creating a voltage waveform with an amplitude of 6-8 kV and a frequency of the order of 10 kHz. The power supply unit uses an Arduino Leonardo microcontroller to drive a coil mounted on the source head, which produces the required high voltage. As shown in Fig. 5.2, a plasma jet having a length of the order of 2 cm is produced, having a gas temperature low enough to allow a direct non-damaging treatment of living tissues. The source can use He or Ar as work gases. The development was carried out in the framework of the 3-year research project which Consorzio RFX is carrying out in collaboration with University *Magna Graecia* of Catanzaro and AIST-Tsukuba, on the topic of non-thermal plasma driven blood coagulation, with funding from *Fondazione con il Sud*.

The project on non-thermal coagulation mentioned above, meanwhile, has continued to produce results. The plasma treatment has been found to accelrate coagulation on blood samples from patients following an anticoagulant therapy even for treatment duration shorter than one minute. The histological analysis performed on blood smear after tretament showed both platelet aggregation and fibrin polymerization. Prothrombin levels were found to decrease with the treatment, while an increase was observed for thrombin, in agreement with expectations from the standard coagulation cascade. Superoxide dismutase 1 analysis evidenced the increase in the reactive oxygen species level in blood cells. A 90’’ treatment was found to signifcantly reduce bleeding from femoral artery in rats, enhancing *in situ* blood coagulation. The same result was found inn another model based on rat paw cutting. Bacteria viability reduction was also observed following the

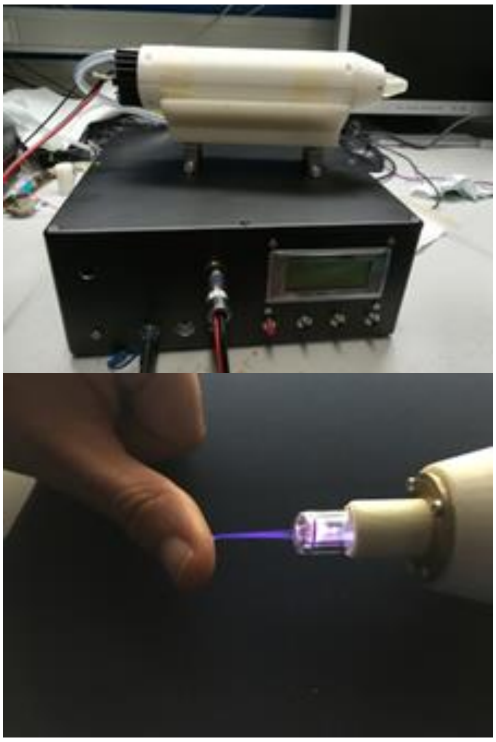

Fig. 5.2 Top: Last version of the DBD plasma jet, including the power supply; Bottom: example of plasma plume produced by the source using helium.

plasma treatment, confirming that coagulation induction is accompanyied by a sterlizing effect.

Concerning the RF source developed at Consorzio RFX, a detailed characterization of the physical and chemical properties of the produced plasma was carried out, with techniques including electrical measurements, Schlieren imaging, emission spectroscopy and fomration of reactive oxygen and nitrogen species in the liquid phase through water treatment. In particular, the dissipated power over the plasma was evaluated to be 0.4 W, a plasma density of 10^{20} m^{-3} and an electron temperature of 0.18 eV were evaluated. Rotational and vibrational temperatures were derived from N2 and OH spectral lines. It was found that rotational temperature is a good estimator of the translational one and the vibrational temperature is consistent with the electron temperature. The total UV emission in the range 200–315 nm was estimated through an absolute calibration of the UV part of the spectrum, and found to be below safety EU prescriptions for treatment times shorter than 6 min. The study on the liquid phase indicates that OH radicals are formed very efficiently in treated water and may thus be the prevailing species responsible for the observed effects in previous applications.

The disinfectant effect of the RF source was also studied in detail. In particular, it was found that the plasma treatment induces a membrane permeabilization in both the outer and inner membrane of Gram-negative bacteria, and also a depolarization of the membrane. The disrtuption of the cytoplasmic (inner) membrane prevents the generation of antibiotic-resistant forms, as was demonstrated thrugh repeated exposure to the plasma effect. Moreover, the plasma was found to synergistically cooperated with common antimicrobial drugs to maximize antibacterial activity, likely by facilitating penetration of antimicrobial drugs through damage of bacterial layers. The antibacterial activity was found to be independent of the cell wall thickness and structure, thus confirming the plasma treatment as and effective inactivation strategy for the treatment of polymicrobial infections in living tissues.

Details on the ongoing activities were communicated to the scientific community in invited talks at the International Confernce on Plasma Medicine (ICPM-7) in Philadelphia, at the ISPlasma conference in Nagoya and at the ISNTP-11 conference in Montegrotto Terme.

5.3. *Plasma study for GALILEO Passive Hydrogen Maser*

Anomalous operation is occasionally affecting the space Passive Hydrogen Maser (PHM), the master clock on the Galileo navigation payload manufactured by Leonardo-Finmeccanica and SpectraTime. This anomaly is attributed to malfunctioning of the Hydrogen Dissociator, with reduced dissociation efficiency and consequent reduced flux of atomic Hydrogen from the Dissociator to the Maser cavity. The physics of the Dissociator has some important analogies with that of the RF source for ITER NBTF. In late 2017 Leonardo has signed a contract with Consorzio RFX and with Nanotech-Bari for a characterization of the Dissociator, aiming at the identification of possible causes of malfunctioning. The contact foresees three phase: preliminary joint analysis of the available documentation, modeling the Dissociator by Nanotech, experimental investigation of an available module using spectroscopic techniques by Consorzio RFX. In 2018 the first phase has been completed. Consorzio RFX has prepared and actively contributed to a failure investigation review meeting with Leonardo, ESA and other project parties and eventually produced a report with the analysis of available measurements and a literature survey relevant to the understanding of the dissociator operation and possible failure routes: capacitive-to-inductive coupling hysteresis and the hyodroxylation kinetics on the bulb surface were considered the most relevant candidates and will therefore constitute the focus of the simulation.